Electron Transfer and Other Reactions Using Atomic Metal Anions

Jeffery Michael Butson

Thesis submitted to the
Faculty of Graduate & Postdoctoral Studies
University of Ottawa
in partial fulfillment of the requirements for the
M.Sc. degree in the

Ottawa-Carleton Chemistry Institute

Thèse soumise à
Faculté des études supérieures et postdoctorales
Université d'Ottawa
en vue de l'obtention de la maîtrise ès sciences à

L'Institut de chimie d'Ottawa-Carleton

Abstract

The atomic metal anions Rb^-, Cs^-, Cu^-, Ag^- and Fe^- have been generated in the gas phase and reacted with various neutral reactants in a triple quadrupole mass spectrometer. The metal anions were formed via electrospray ionization of the metal-oxalate solutions and form in gas phase between the capillary and the first quadrupole. Neutral gas phase reactants investigated include NO, NO_2, SO_2, C_6F_5OH, $C_6F_5NH_2$, C_6F_6, E-octafluoro-butene and 1,2,3/1,2,4/1,3,5 trifluoro-benzene. When possible, CBS-4M methods were used to suggest the lowest energy products based on relative energy. Observed reactions of atomic metal anions with the aforementioned neutral species include electron transfer and dissociative electron transfer to the neutral gas phase reactants. In addition, hydrogen abstraction and fluorine abstraction forming a neutral metal hydride or fluoride as well as the formation of multiply substituted metal-oxide/fluoride anions was also observed. Metal-complex anions observed from the gas phase reactions include CuF^-, CuF_2^-, CuO^-, CuO_2^-, FeF^-, FeF_2^-, FeF_3^-, FeO^-, FeO_2^-, FeO_3^-, CsF^- and CsF_2^-.

Acknowledgements

I would like to acknowledge first Dr. Jean-Francois Couture, Dr. Wendy Pell and Dr. Gabriel Guillet for writing the reference letters with which I applied to Graduate school.

I would like to thank Dr. John Holmes and Dr. Alain St.-Amant for the advice and lessons learned while taking their courses.

Jaleh Halvachizadeh, Jenna Hamilton and Melanie Oulette were always there with a shoulder, or meal, when I was in need.

The efforts of Joe Su should also be mentioned. Joe performed experiments on some fluorinated compounds and was in general a pleasure to be around and an excellent summer student.

Further mention should be given to Sharon Curtis who taught me much of what I know and suggested trying to collide atomic metal anions with the molecules NO, NO_2 and SO_2. This direction proved very fruitful.

Without the instruments I would be unable to do research, therefore I would like to thank Dr. Sander Mommer's for his technical expertise regarding the upkeep of the triple quadrupole mass spectrometer.

Brandi West and Justin Renaud deserve acknowledgement. Brandi for her help with analysis and Justin for his 'soft handed' guidance to think outside the box (or in this case, the triple quad).

Many thanks are owed to Nick "The Zinc Standard" Zinck. He knows why.

I need to thank my family, Allan, Robin, Nick and Dylan Butson, who were always there with a supportive shoulder.

I feel that my supervisor, Dr. Paul Mayer, is deserving of my utmost gratitude. With nothing but a handshake I began my journey in the ocean that is graduate school. His steady-hand and calm demeanor have helped me through the hard times and have had a profoundly life-altering effect within my psyche that will play out for years to come.

Thanks Paul.

Table of Contents

List of figures and tables

List of Abbreviations

AMA	Atomic metal anion
LPES	Laser photodetachment electron epectroscopy
FTM	Fourier transform mass spectrometer
CID	Collision induced dissociation
RF	Radio frequency
DC	Direct current
HF	*Ab initio* model chemistry using Hartree Fock theory
UHF	*Ab initio* model chemistry using Unrestricted Hartree-Fock theory
MP2	*Ab initio* model chemistry using Moller Plesset perturbation theory
MP4SDQ	*Ab initio* model chemistry using Moller Plesset perturbation theory
3-21G(*)	Basis set utilized for various model chemistries
6-31G	Basis set utilized for various model chemistries
6-31+D**	Basis set utilized for various model chemistries
CBS1B1	Basis set utilized in CBS-4M model chemistry

Chapter 1 – Introduction

Our discussion begins with a comparison of the general characteristics of anions relative to neutral atoms and cations.

1.1 The Ground State of Atomic Anions

Most atoms are able to attach an electron to the ground state electron configuration.[1] This extra electron is bound in the anionic ground state by a short-range potential on the order of r^{-4} where 'r' refers to the distance between the extra electron and the nucleus.[1] This is in contrast with cations and neutral atoms, whose electrons are bound in a long range Coulomb potential.[1] The strength of the Coulomb barrier decays on the order of r^{-1}.[1] This strong potential associated with the Coulomb field results in the outermost electrons 'seeing' a positively charged ion core, thus their motion will be dominated by the long range Coulomb interaction.[2] The Coulomb potential is able to support an infinite number of bound states, converting to a Rydberg series at the threshold of ionization, while anions cannot.[1] Qualitatively, a negative ion may be considered in terms of the stationary states of an electron in an attractive field of force falling off rapidly with distance compared to the Coulomb field.[3] In such a field, the number of stationary states is finite.[3] This difference results in the increased importance of correlation energy in the formation of anions.[2] The short range potential associated with correlation energy is unable to support an infinite number of bound states, instead being able to bind the extra electron in the ground state of the anion only, or in the case of several possible states, the lowest energy one.[1] Thus correlation energy is one of the most important factors when calculating neutral atomic/molecular electron affinity or atomic/molecular anion electron binding energy.

1.2 Electronically Excited States of Atomic Anions

Electronically excited states of atomic anions are typically higher in energy than their ground state parent neutrals.[1] Thus most excited atomic anions are metastable, decaying via shape or Feshbach resonance depending on the length of time the decay occurs (10^{-11} – 10^{-16}).[1] Shape resonances are very short lived resonant states and could be considered a one electron phenomena.[1] The classical scattering description of this process requires the incoming electron tunneling through a potential energy barrier, remaining within the barrier for a finite time limit (typically that of the resonance) and then tunneling out again.[2] It can also be described as a resonance where an electron is experiencing a region of attractive potential surrounded by that of a repulsive potential.[4] As the electron attempts to leave the attractive potential, it will be hindered by the repulsive potential, resulting in the electron becoming temporarily bound to the target atom/molecule.[4] A Feshbach resonance involves the electron transferring some of its energy into some internal degree of freedom of the target, thereby trapping it until the electron acquires enough energy to escape.[2] Feshbach resonances differ from shape resonances in that the incident electron loses energy by exciting the target molecule, creating a temporary bound state of the electron while the target remains in the excited state, or the electron reabsorbs enough energy from the target to be re-emitted.[4] Thus Feshbach resonances keep the extra electron bound for a much longer time, a characteristic attributed to the reorganization of the atomic core which allows the electron to become part of the outer electron shell.[1]

It should be noted that excited atomic anions that lie energetically below the ground state of their neutral parent molecule would be stable as the anion would be unable to decay via electron autodetachment processes. This was recently proven by Bilodeau et al. via their

LPES study of Os^-.[5] In their study they observe two resonances, one at 3.52 meV and the other at 11.48 meV above the groundstate threshold of the Os atom.[5] Analysis of the 11.48 meV resonance suggests it is resultant from a ground $^4F^e_{9/2}$ state of Os^- while the 3.52 meV resonance is resultant from an excited $^4F^e_{7/2}$ state of Os^-.[5] They were able to determine that both states lie energetically below the neutral Os atom, the ground $^4F^e_{9/2}$ state of Os^- possessing an electron binding energy of 1.07780 eV and the excited $^4F^e_{7/2}$ state of Os^- an electron binding energy of 0.553 eV.[5] Thus they were able to deduce that Os^- is the first anion discovered possessing a bound excited state.[5]

1.3 Electron Affinity

The electron affinity (EA) of an atom A is defined as the difference between the total energies (E_{tot}) of the ground state of A and it's negative ion A^-

$$EA(A) = E_{tot}(A) - E_{tot}(A^-)$$

by ground state, one refers to the lowest energy hyperfine structure level of A and A^-, respectively. The quantity EA(A) is positive for stable anions A^-.[6] The total energy can be written as:

$$E_{tot} = E_{HF} + E_C + E_{SO} + \delta$$

where E_{HF} corresponds to the (restricted) Hartree-Fock energy, E_C is the non-relativistic correlation energy describing the deviation of the many-electron system from the Hartree-Fock self-consistent-field model, E_{SO} is the spin-orbit energy for states with non-zero orbital angular momentum and spin, and δ comprises correction terms including hyper-fine structure, mass polarization and radiative effects.[6] Correlation energy plays a decisive role in

determining the stability of many atomic negative ions,[6] and in some instances the task of calculating electron affinities is essentially that of obtaining an accurate number for the correlation energy difference, $E_c(A) - E_c(A^-)$.[7]

1.4 Experimental Determination of Electron Affinities – Photodetachment

The main parameter utilized to characterize negative ions is represented by the electron binding energy of the anion, or electron affinity of the corresponding neutral. Experimental photodetachment of electrons from atomic anions and molecules is one method used to measure electron affinities in a reliable manner and represents one of the most accurate methods for EA determination.[8,9] The method is used to measure the minimum photon energy necessary for photodetachment from a negative ion or for the production of ions during the dissociation of a molecule, which can then be used to determine the electron binding energy of the negative ion.[8] Most electron affinities listed in this study were determined via photodetachment of electrons from negative atoms in a beam or calculated using quantum calculations (see '2.3 Computation Methods' for details).

1.5 Production of Atomic Anions

To measure the electron binding energy of negative ions via photodetachment, a beam of negative ions is required. As noted by Andersen et al., there are three main techniques used for the production of negative ions.[1] They include utilizing charge exchange of an initially positive beam in a gas or a metal vapour, direct extraction of negative ions from a Penning/plasma-type source and via a caesium sputtering source.[1] Further information regarding the first two negative ion sources as well as caesium sputtering can be found in the review articles by Dawton[10] and Middleton[11] respectively.

1.6 Study of Negative Atomic Metal Anions (AMA)

While there is a significant body of study of regarding negative ions, most of these studies have focused on the more easily produced anions, such as the halogens. This is likely due to the fact that these species can be generated easily by a number of ionization methods relative to their positive ion counterparts.[12] For example, a Penning type source can generate an atomic Cl^- beam at 100% intensity relative to its positive counterpart.[13] Other anions, such as the AMAs Li^-, Cs^- and Rb^- cannot.[13] Compared to their positive counterparts, Li^- was produced at an intensity equal to 1.83% of the positive ion, Cs^- an intensity equal to 4.25% and Rb^- at an intensity equal to 1.25%.[13] As a result of these significant difficulties with flux, very few studies have been accomplished on AMAs

1.7 Characteristics of Selected Atomic Metal Anions

1.7.1 Rubidium and Caesium Anions

Rb^- and Cs^- exist as $5s^2\ S_0$ and $6s^2\ S_0$ ground state anions respectively, as measured via tunable laser photodetachment emission spectroscopy (LPES) threshold experiments.[6] Resonance structures were noted in the photodetachment spectra of Rb^- and Cs^- when it was noted that the photodetachment cross sections were significantly diminished over a small wavelength range just below the first excited state thresholds.[14,15] These diminished cross sections could be explained by the existence of a resonance in the ^1P channel just below the respective excited state thresholds.[1] Electron scattering experiments have shown that resonances above the first excited neutral atom states can also be observed.[2]. Scheer et al. were successful in localizing the Cs^- ($6s6p\ ^3P_J$) states just above the ground state of Cs using a storage ring experiment.[16] Since the transition from the Cs^- ($6s^2\ ^1S$) ground state to the

excited 6s6p ^3P_l is forbidden in the LS coupling scheme (LS refers to the interaction between electron spin and angular momentum), the photo excitation becomes very sensitive to the spin-orbit interaction.[1] The Cs^- (6s6p $^3P_1$) resonance was observed in the photodetachment spectrum, while the Cs^- (6s6p $^3P_0$) was not. However, the J=0 state was calculated to exist 3.5 meV below the J=1 state,[17] therefore it should also be observable. In 2003 Khuskivadze et al. performed a theoretical study of the static electric-field effects on the photodetachment cross section at the ^3P resonance region.[18] They suggested that more favourable experimental conditions for the observation of the $^3P_0$ resonance could be achieved by studying the near-threshold photodetachment cross section of Cs^- in the presence of a DC electric field.[18]

1.7.2 Iron

Fe^- exists as a $3d^7 4s^2\ ^4F_{9/2}$ ground state anion as measured via LPES.[1] No data is available regarding excited states of Fe^-, likely due to the more complicated atomic structures associated with open d-shells.[1]

1.7.3 Copper and Silver

Cu^- and Ag^- exist as $3d^{10}4s^2\ ^1S_0$ and $4d^{10}5s^2\ ^1S_0$ ground state anions respectively, as measured via tunable LPES threshold experiments.[1] The negative ions of the elements Cu and Ag only possess one bound state (^1S), which originates from the $nd^{10}(n + 1)s^2$ configurations with n being 3 for Cu.[1] Scheibner et al. performed calculations predicting an excited state of Cu^- would exist as a $3d^{10}4s4p\ ^1P$ shape resonance located about 1.7 eV above the ground state of Cu^-.[19] Experiments performed by Balling et al. confirmed this shape resonance, but suggested that the shape resonance should be shifted to higher energies.[20] Further theoretical analysis accomplished by Ivanov et al. has also suggested that the shape

resonance should be shifted higher due to sensitivity of the shape resonance to the polarization interaction between the outgoing electron and core electrons.[21]

While there are experimental photodetachment spectra for Cu^- above threshold, only theoretical calculations have been accomplished regarding Ag^- for the energy region above threshold.[22] Calculations performed by Amusia et al. suggest that the 4d subshell is quite close to the outer 5s subshell.[22] Thus the inner shell correlations manifest themselves, resulting in two predicted maxima occurring in the theoretical photodetachment cross section.[22]

1.8 Production of Atomic Metal Anions

Pioneering work to produce a significant flux of AMAs was performed by Sallans et. al. in 1983. They reported that atomic metal transition-metal anions can be produced in good yields in a Fourier transform mass spectrometer (FTMS) utilizing collision-induced dissociation (CID) of anionic metal carbonyl complexes and argon.[23] Their initial experiments utilized $Cr(CO)_5^-$ formed by a 12.9 eV, 150-ms electron beam pulse on $Cr(CO)_6$ at approximate pressures of 5×10^{-8} torr. After another 100 ms, an 18.5 eV CID pulse was applied for 0.100 ms, and a 100-ms CID interaction time was used against Ar at 6×10^{-6} torr.[23] Following this, all other ions were ejected from the FTMS except Cr^-, allowing subsequent reactions of Cr^- with neutral substrates via leak valves[23]. The sequential loss of CO ligands from a metal anion complex produces the atomic metal anion as per the following general scheme:

$$M(CO)_x + e^- \rightarrow M(CO)_x^- \rightarrow M^- + X(CO)$$

where M is the metal center and X is the number of CO ligands. In this manner, Sallans et al. were able to generate the atomic transition-metal anions V^-, Cr^-, Fe^-, Co^-, Mo^-, and W^- via CID of the corresponding metal carbonyl negative ions in a FTMS.[24] In this manner, the production of AMAs via the CID of the negatively charged metal complexes was made possible, allowing further analysis of AMAs and their reactions with neutral substrates.

The electron affinity of CO is 1.32 eV,[8] meaning that the production of atomic metal anions via CID of metal carbonyl anions is likely endothermic. Thus a lower electron affinity of the ligand should improve the flux of AMAs and enable their efficient production. This propensity was noted by Curtis et al. after observing the decomposition of metal-oxalate complexes in the gas phase.[25] Curtis et al. performed CID of K and Ag oxalate anion complexes in the gas and were able to produce atomic metal anions via the loss of neutral CO_2 using an electrospray ionization source in a triple quadrupole mass spectrometer.[25] The process can be generalized as follows:

$$M(CO_2)_x + e^- \rightarrow M(CO_2)_x^- \rightarrow M^- + X(CO_2)$$

where e^- is an electron, M is the metal center and X is the number of CO_2 ligands. It is theorized by Curtis et al. that the high production of AMAs is enabled largely via the negative electron affinity of CO_2 (-0.6 eV),[26] but is also affected by the electron affinity of the metal, the size of the metal, and the strength of the bond between the carbon and metal within the complex.[25,27]

In addition to metal-oxalate complexes, other dicarboxylic acid salts such as maleate, fumarate and succinate were observed to produce AMAs such as Na^-, K^-, Cs^-, Ag^- via CID at ambient temperatures using an ESI source.[28]

1.9 Reactions of Atomic Metal Anions

Sallans et al. probed the reactions of neutral substrates with the atomic metal anions V^-, Cr^-, Fe^-, Co^-, Mo^- and W^- produced via CID of the parent carbonyl complexes in a FTMS.[24] The details of their experimental setup were described in detail by Burnier et al.[29] Due to the experimental method used, the parent metal complexes were always present in the system as a background pressure, enabling extensive characterisation of their reactions with the AMAs.[24] The neutral parent carbonyl complexes used to produce and subsequently react with the AMAs were $V(CO)_6$, $Cr(CO)_6$, $Fe(CO)_5$, $Co_2(CO)_8$, and $W(CO)_6$ (though no reactions were accomplished with neutral $W(CO)_6$ due to insufficient flux of W^- anions).[24] Each AMA was able to react with the respective parent metal carbonyl by dissociative electron transfer to produce mono and di-nuclear metal carbonyl anions from which one or more CO ligands are expelled.[24] Further details regarding exact product anion identities and relative intensities of the aforementioned reactions of AMAs with their parent metal carbonyl complexes can be found in their paper, referenced herein.[24]

Sallans et al. were able to assemble an impressive list of neutral reactants with which to obtain quantitative estimates of atomic metal anion basicities based on proton abstraction from 10 acids with well established acidities ranging from ~336-347.3 kcal/mol.[24] The acids studied include; CH_3CH_2COOH, HCOOH, $CH_3COCH_2COCH_3$, p-$H_2NC_6H_4COOH$, $C_6H_5COCH_2COCH_3$, 5,5-dimethylcyclohexane-1,3-dione, C_6H_5SH, m-HOC_6H_4COOH and $CH_2(CN)_2$. The underlying assumptions associated with their calculations were that the occurrence or non-occurrence of a reaction is controlled by thermodynamics (rather than kinetic factors) and that the diatomic hydride is the only neutral metal product formed according to the following equation:

$$M^- + AH \rightarrow MH + A^-$$

where M^- refers to the AMA, AH the neutral acid, MH the metal hydride and A^- the acid anion.[24] In this manner they were able to determine the metal hydride gas phase acidities and homolytic bond dissociation energies using the known gas phase acidities of the neutral acids and electron affinities of the metal anions (V^-, Cr^-, Fe^-, Co^- and Mo^-) and acids tested.[24]

Sallans et al. also examined the reactions of simple thiols, sulfides and disulfides with Fe^- and Co^-.[30] The suite of reactants tested is expansive, the primary product anions observed for the reactions of Fe^- and Co^- with thiols being MS^-, MSH^-, MSH_2^-.[30] The reactions of Fe^- and Co^- with sulfides and disulfides resulted in a large and complex suite of product anions, with reactions generally involving cleavage of the carbon-sulfur bond as well as retention of the charge by the metal bearing species.[30] V^-, Cr^- and Mo^- were also reacted with various organosulfides. The reactions observed were much slower than the reactions of Fe^- and Co^- and resulted in a complex suite of product anions.[30]

Miller et al. continued the study of metal anions by looking at the reactions and kinetics Fe^- with the acids $CH_3C(O)CH_2C(O)CH_3$, HCO_2H, CH_3CO_2H, $CH_3CH_2CO_2H$, and H_2S using a selected-ion flow drift tube (SIFT).[31] They were able to measure the electron detachment rate of Fe^- with the various neutral reactants by monitoring the total ion current collected on the ion-sampling aperture plate as a function of reactant concentration.[31,32] Electron detachment from Fe^- was observed for all neutral reactants tested and was the only reaction channel observed for HCO_2H, CH_3CO_2H and $CH_3C(O)CH_2C(O)CH_3$.[31] Reactions of Fe^- with H_2S produced FeS^- while reactions with HCO_2H produced FeH_2^-, HCO_2^- and $Fe(HCO_2H)^-$.[31] Using the reaction observed with Fe^- and HCO_2H, the authors were able to

calculate the hydride strength of FeH, ΔH_{acid} 35.1 +/- 4.3 kcal/mol, which was within experimental error of the value calculated previously by Sallans et al. (29.6 +/- 3 kcal/mol).[24]

Miller et al. also studied the reactions of Fe^- with CH_3-X (X= F, Cl, Br, I) using a SIFT apparatus.[32,33] Reaction products suggested that X^- formation only occurred when the calculated reaction enthalpy of $Fe^- + CH3\text{-}X \rightarrow X^- + Fe\text{-}CH_3$ was exothermic or near threshold.[33] Reactions with CH_3-F produced no reaction and posessed a theoretical enthalpy of 1.64 - D_0 eV, whereas reactions with CH_3-Cl, CH_3-Br and CH_3-I were observed, each with a calculated enthalpy of 0.16 - D_0 eV, 0.15 - D_0 eV and -0.45 - D_0 eV where D_0 refers to the unknown bond energy of Fe-CH_3.[33]

In 2011 Curtis et al. studied the reactions of gaseous AMAs with neutral molecules in a Micromass Quattro-LC triple-quadrupole mass spectrometer equipped with a Z-spray ESI source.[34] The AMAs were produced by CID occurring in the ESI source and then isolated using the 1st triple quadrupole as a filter.[34] The atomic metal anions tested were K^-, Rb^-, Cs^-, Fe^-, Co^-, Ni^-, Cu^- and Ag^-.[34] The suite of neutral compounds tested included CH_3Br, CH_3Cl, CH_3CH_2Cl, CH_3NO_2 and CH_3CN.[34] K^- and Rb^- were observed to react with the suite of neutral compounds to produce Cl^-/Br^-, NO_2^- and CN^-. Cu^- and Ag^- were observed to produce Cl^-/Br^{--} with reactions of halo-alkanes, NO_2^- and $CH_2NO_2^-$ with nitromethane, and CH_2CN^- and CN^- with acetonitrile.[34] Fe^-, Co^- and Ni^- were observed to produce $CH_2O_2^-$ and NO_2^- from reactions with neutral nitromethane, while Fe- was observed to also produce $CH_3NO_2^-$ as well.[34] Reactions of these AMAs were able to produce Cl^- from reactions with neutral CH_3Cl.[34] Fe^- and Ni^- were able to produce CH_2CN^- and CN^- while Co^- was unable to produce CN^- but was the only AMA able to transfer an electron to this molecule.[34] The conclusions of the study found that AMAs produced by filling s-orbital shells tend to react closely

according to the electron affinity and acidity of the corresponding neutral metal and metal hydride.[34] Metal anions produced by placing an extra electron in an open valence shell were able to access reactions not based on thermochemistry alone.[34] The authors state that the metal anion can insert into bonds containing first row elements in an oxidative addition/reductive elimination reaction.[34] In addition, proton abstraction was found to occur via a harpoon mechanism rather than insertion into the C-H bond itself and electron transfer is able to occur spontaneously only when the electron affinity of the metal is lower than that of the neutral molecule.[34]

1.10 Research Objectives

The Mayer group is interested in experimentally and computationally characterizing the role of AMAs in electron transfer, dissociative electron transfer and ion-molecule reactions such as gas-phase oxidative addition/reductive elimination reactions. The focus of this work has been on further characterization of the reactions of AMAs with small environmental contaminants, NO, NO_2 and SO_2. Further work has been accomplished on pentafluoroaniline and pentafluorophenol with a view to explore dissociative electron transfer. Finally, experiments further characterizing the reactions of AMAs with various aromatic, saturated and unsaturated fluorinated derivatives will be discussed.

Chapter 2 – Experimental Methods

2.1 Electrospray Ionization & Generation of Metal Anions

Electrospray ionization was first introduced by Dole et al. in 1966 at the International Symposium on Macromolecular Chemistry in Tokyo[35] and was published by Dole and his colleagues in 1968.[36] However, it was John Fenn who would go on to improve the technique 'for the development of methods for identification and structure analyses of biological macromolecules', for which he and Koichi Tanaka jointly won ½ of the Nobel Prize in Chemistry in 2002 for 'their development of soft desorption ionisation methods for mass spectrometric analyses of biological macromolecules'.[37] In his Nobel laureate speech, Fenn states that Dole 'clearly recognized the need to disperse the charged droplets in a gas at relatively high (atmospheric) pressure. Such gas would provide the enthalpy required to vaporize solvent from those highly charged droplets. Moreover, collisions of the ions with molecules of that gas would reduce their initially high kinetic energies to those of the ambient neutral gas molecules, thereby avoiding the need for mass analyzers capable of accommodating high energy ions, e.g. magnetic sector instruments'.[35]

Dole's research had touched on an effect first noted by Lord Rayleigh in 1882. Rayleigh had mathematically analyzed the behaviour of highly charged droplets and found that for a given potential, an inherent instability existed between the electric potential and the capillary force holding the droplet together.[38] A limit would arise where a given electromotive force present in a liquid droplet would overcome the stability produced by the cohesive tension holding the droplet together, causing the droplet to split.[38] Thus, as solvent evaporated the density of charges on the droplet surface would increase to a critical value,

now known as the "Rayleigh Limit".[35] John Zeleny would later prove this model correct, in pioneering experimental studies on the production and behaviour of charged droplets passed through a needle maintained at a high potential relative to an electrode of opposite current.[39] He observed the break-up of the liquid droplets as the solvent evaporated, resulting in a fine spray, just as predicted by Rayleigh (Figure 1) .[39] The conical form of the spray is called a 'Taylor Cone' as it was predicted theoretically in 1964 by G. I. Taylor in his paper.[40]

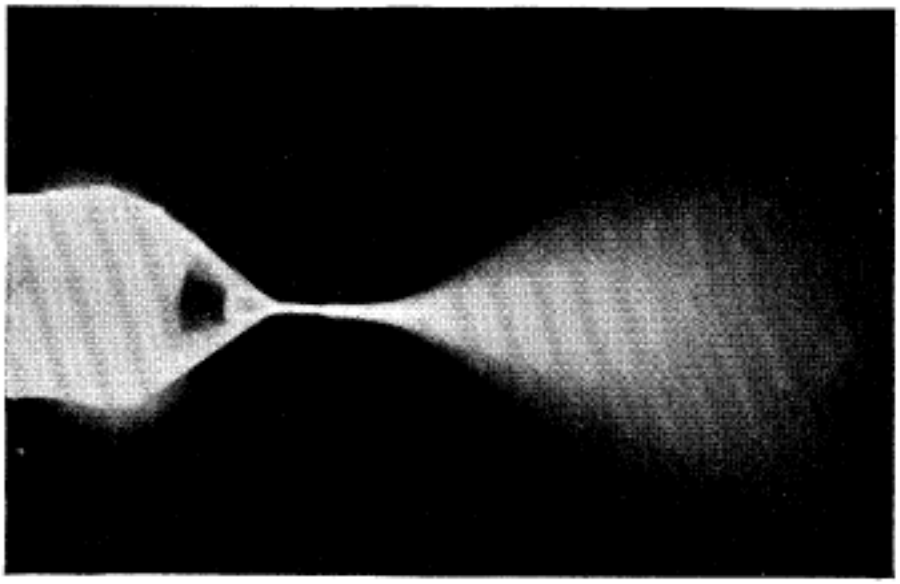

Figure 1. Image of a "Taylor Cone" taken from 'Instability of Electrified Liquid Surfaces' by John Zeleny. Image was captured after an exposure of 30 seconds with light concentrated upon the object from an arc lamp placed at the side. The potential of the drop was 5,000 volts. Reproduced from Zeleny, J. *Physical Review* 1917, *10*, 1.[39]

In his 'Principles of the Experiment' section, Dole's 'charge residue model' as it is now referred assumes that droplets formed from the Taylor Cone continuously break up into smaller and smaller droplets as solvent evaporates due to continuously reaching the 'Rayleigh' limit (Figure 2, A).[36]

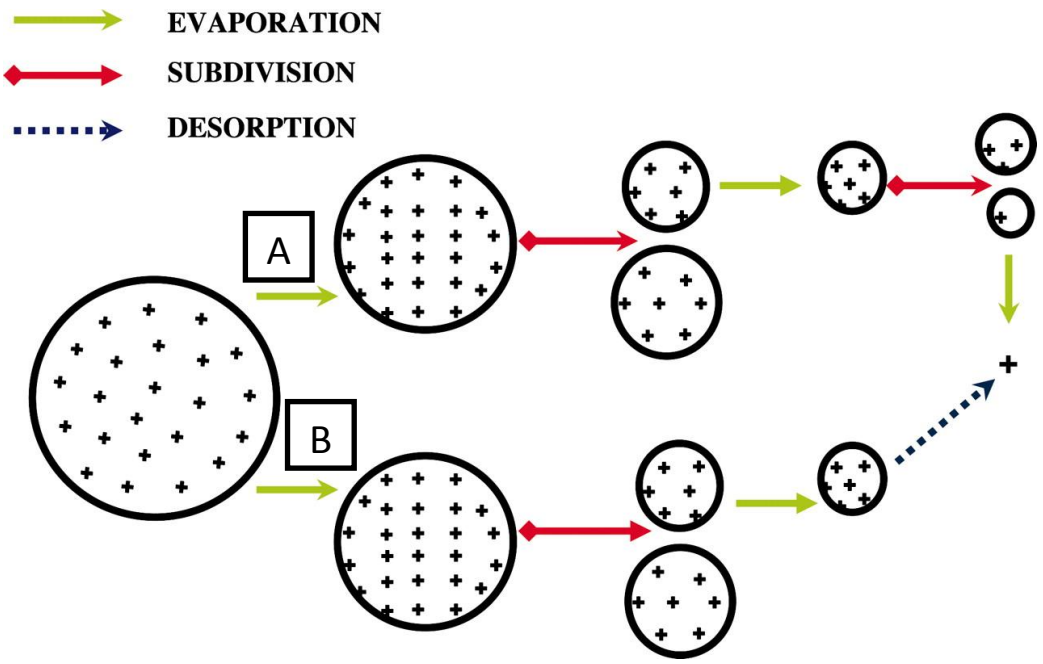

Figure 2. A graphic depiction of the two possible ion formation mechanisms produced from ESI. A) Dole's charge residue model.[36] B) Iribarne and Thomson's ion evaporation mechanism.[41] Reproduced from Nguyen, S.; Fenn, J. B. *Proceedings of the National Academy of Sciences* 2007, *104*, 1111.[42]

Since then, a competing theory has been put forward by Iribarne and Thomson called the 'ion evaporation mechanism' (Figure 2, B).[35] The theoretical model produced by Iribarne and Thomson takes into account both enthalpic and kinetic terms, suggesting that small ions separate or "evaporate" from droplets carrying electrical charges in addition to Rayleigh instability.[41] They suggest that the Rayleigh limit, the solute limit, and the evaporation limit

play a role in this process.[41] They go on further to say that ion evaporation from charged droplets can occur if; the electrostatic energy becomes large enough, the size radius of the evaporating charged particle is larger than the radius of the droplet left behind, and is larger than the Rayleigh limit of instability.[41]

The aforementioned production of atomic metal anions by Curtis et al. and Attygale et al. make use of these physical processes in the gas phase to produce atomic metal anions in the area between the ESI source and triple quadrupole mass spectrometer used in our studies.[25,28]

2.2 Triple Quadrupole Mass Spectrometer

As mentioned in Fenn's Nobel Laureate speech, one of the component processes of ESI is that the high energy ions are slowed by collisions with gas at atmospheric pressures, eliminating the need of mass analyzers capable of accommodating high energy ions.[35] This allows ESI to be coupled to other lower energy instruments, such as quadrupole mass spectrometers.

A triple quadrupole mass analyzer uses radio frequencies (RF) and direct current (DC) voltages to guide a beam of ions to a detector.[43] The structure is composed of four hyperbolic rods located at 90° angles to each other. The quadrupole electrodes located angles along the *x* or *y* axis will always possess the same polarity, either $+\phi_o$ or $-\phi_o$ (Figure 3).[43,44]

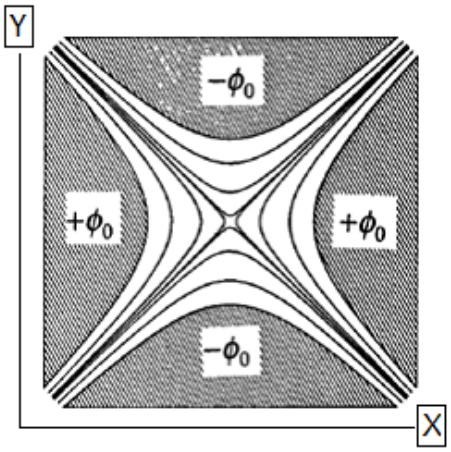

Figure 3. A schematic diagram of a linear quadrupole. Quadrupole electrodes are shown with applied potentials, $+\phi_o$ or $-\phi_o$. Reproduced from Douglas, D. J. *Mass Spectrometry Reviews* 2009, *28*, 937.[44]

Balanced potentials between opposite rods (in either the *x* or *y* directions) create a net '0' potential, represented by equipotential lines in Figure 3.[44] An RF frequency applied to the rods will allow a broad range of masses to pass through, while a DC voltage will allow none, as the ions will simply discharge on the rods of opposite polarity.[43] Applying a specific DC voltage and RF frequency will allow only ions of a specific mass to charge ratio to pass through the quadrupole, with all others discharging on poles of opposite polarity.[43] In this way, a quadrupole will act as a mass filter for a linear beam of ions.[43]

2.3 Sample Preparation and Mass Spectrum Measurement

This mass selection ability of a quadrupole is what defines its usefulness. In our experimental method, AMAs that are produced between the source and the 1st quadrupole are mass selected. The AMAs are then allowed to react in a hexapole collision cell (kept at a constant RF frequency, allowing all masses to pass through). Product anions are then

analyzed by ramping specific RF frequencies and DC voltages in the final quadrupole, producing a mass spectrum for analysis when coupled with a detector (Figure 4).

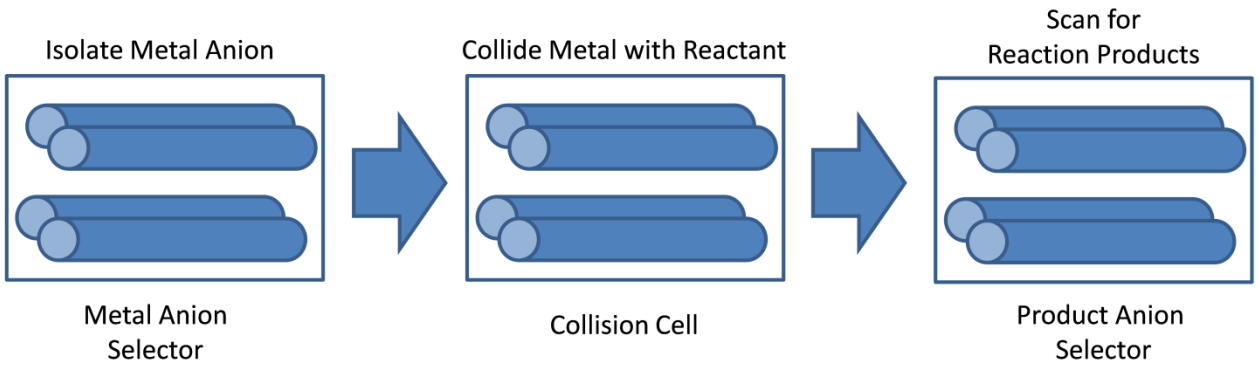

Figure 4. Experimental set-up of the triple quadrupole mass spectrometer utilized for the study of gaseous atomic metal anions and neutral reactants

Electrospray ionization mass spectrometry experiments were accomplished with a Micromass Quattro-LC triple-quadrupole mass spectrometer utilizing a Z-spray source while running the MassLynx 3.5 operating system. Metal oxalate solutions were prepared by combining 2mols of aqueous oxalic acid to 1 mol of a metal salt solution at concentrations on the order of 10^{-1} mol/L in methanol. Solutions were subsequently placed on a Daiger Vortex-Genie 2 shaker, at 0 speed setting, and allowed to shake for approximately 30 minutes before being diluted to a final working concentration of 10^{-4} mol/L or lower. Solutions containing iron typically require a 3:1 ratio for best results, likely due to the binding of two oxalic acid molecules to the 3+ oxidation state of the iron salt used, rather than one required of other 1+ oxidation state metals. A flow rate of 50 μl/min were used with the capillary voltage set to 2.96 kV, cone voltage set to 42 V and the extractor voltage at 7 V. The source temperature was set to 80°C in order to limit clustering.[45] The ion beam was focused using an RF lens set to 0.5 eV. The metal anion m/z is first selected with the

first quadrupole. The purity of the metal anion beam is tested via collisions with argon at 8 x 10^{-4} bar, using lab frame collision energies up to 75 eV. Entrance and exit voltages of the hexapole collision cell are always set to 50 eV, collision energy remains variable. Impurities at the set m/z will dissociate at these collision energies and result in fragment ions, while the pure atomic metal anion will not. If pure, metal anion is then allowed to undergo reactions with neutral substrates in the hexapole collision cell in the absence of argon. Entrance and exit voltages of the hexapole collision cell are always set to 50V, with the exception of reactions of Cs^- with pentafluorophenol. Collision energy remains variable throughout the gas phase experiments of AMAs with neutral reactants. Pressures of a neutral collision gas partner are kept constant throughout an experiment, though some decreases do occur as the neutral gas reactants are 'pulsed' into the collision cell.

Specific m/z signals are discriminated against using an in house program. The median intensity of the signals present in a spectrum is first computed to estimate the background present. Only m/z signals possessing intensity larger than 2X the median intensity are used for further analysis.

2.4 Computational Methods

Reaction energies were computed with the Complete Basis Set 4M level of theory[46,47] using the Gaussian 09 suite of programs.[48] In this approach, geometries are optimized using UHF/3-21G(*). Frequencies are then calculated at the optimized geometry using HF/3-21G(*). A series of zero point energies are then calculated using first MP4SDQ/6-31G followed by MP2/6-31+D** using the minimal population localization method analysis and finally by HF/CBSB1. The errors associated with CBS-4M are comparable to other methods (mean absolute deviation of 3.26 kcal/mol on the G2/97 test

set) but can be applied to much larger systems[47] making it ideal for the study of metal anions and their reactivity with neutral molecules. The energies and electron affinities calculated in this document should be used for relative comparison of various potential neutral partners for a given product ion. Thus they should be taken as qualitative, their purpose being to determine chemical formulas and reaction pathways based on the lowest energies of the possible reaction pathways. K^- was used as a stand-in for calculating relative energies of potential reaction pathways involving Rb^- and Cs^- due to limitations within the CBS-4M method's treatment of inner core electrons. Given the similarity in the EA of K, Cs and Rb, this is not expected to result in significant error as long as reaction intermediates are not probed.

Chapter 3 – Electron Transfer to Small Molecules

3.1 Electron Attachment

Electron attachment processes are most significant at low electron energies, approximately 15 eV and below.[49] The process of attaching electrons to neutral molecules is usually described in terms of the resonance model, where a neutral molecule (AB) captures an incoming electron to form an excited state (AB^{*-}) (Figure 5, A).[3,4,8,50] This attachment can result in two different 'trapping mechanisms' with which the electron is attached, and are referred to as shape or Feshbach resonances (see Section 1.2 for details).[4] Once an electron is attached to a molecule, elastic/inelastic scattering as well as dissociative/non-dissociative processes can occur.[4] Dissociative attachment occurs when there exists a

resonant state of the correct asymptotic form that prevents electron emission and allows dissociation to occur (Figure 5, B).

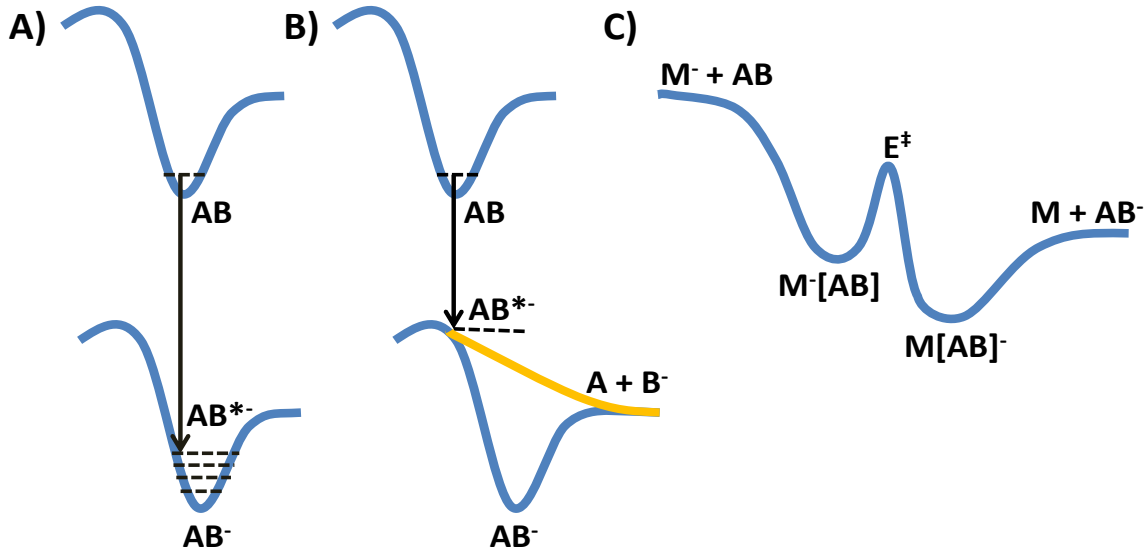

Figure 5. (A) Potential energy diagram of the theoretical molecule AB undergoing vertical electron attachment to an excited anion state AB^{*-}. (B) Potential energy diagram of the theoretical molecule AB undergoing dissociative electron attachment producing A + B^-. (C) Potential energy diagram of the theoretical molecule AB colliding with an atomic anion M^- to produce M and AB^-

3.2 Dissociative Electron Attachment to NO, NO_2 and SO_2

Numerous electron attachment studies of these molecules have demonstrated that these neutral molecules dissociate into various fragments under electron impact at low electron kinetic energies in the gas phase. Fragments associated with the NO anion were first detected by Tate et al. in 1932.[51] They inferred that electron attachment had occurred by measuring the atomic anion currents associated with O^- formation from NO.[51] This assessment was confirmed by a number of authors as mentioned by Sambe et al. in their paper.[52] O^- is observed around electron resonance energies of 8-9 eV, as well as a Feshbach resonance associated with N^-.[52] Of note is the study performed by Chantry et al. where the

kinetic-energy distribution of the O^- ions demonstrated that the dissociative electron attachment process in NO lead exclusively to the production of O^- and an excited N atom.[53] Electron attachment to NO_2 yields O^- at resonance energies of 1.4, 3.1 and 8.3 eV.[54] The authors also observe NO^- and O_2^- anions, similar to the results reported by Aboua et al.[54,55] Electron attachment to SO_2 yields O^-, S^- and SO^- as observed in an electron attachment study reported by Spyrou et al.[56] In the study, they report onset energies of 4.55 and 7.3 eV for the formation of O^-, 4.2 and 7.24 eV for the formation of S^- and 4.85 eV for the formation of SO^-,[56] within experimental error of two similar studies reporting such values.[57,58] Interestingly, the relative energies of the dissociation fragments produced from electron attachment to NO, NO_2 and SO_2 lie well above the ground state of the intact product anion (Figure 6).

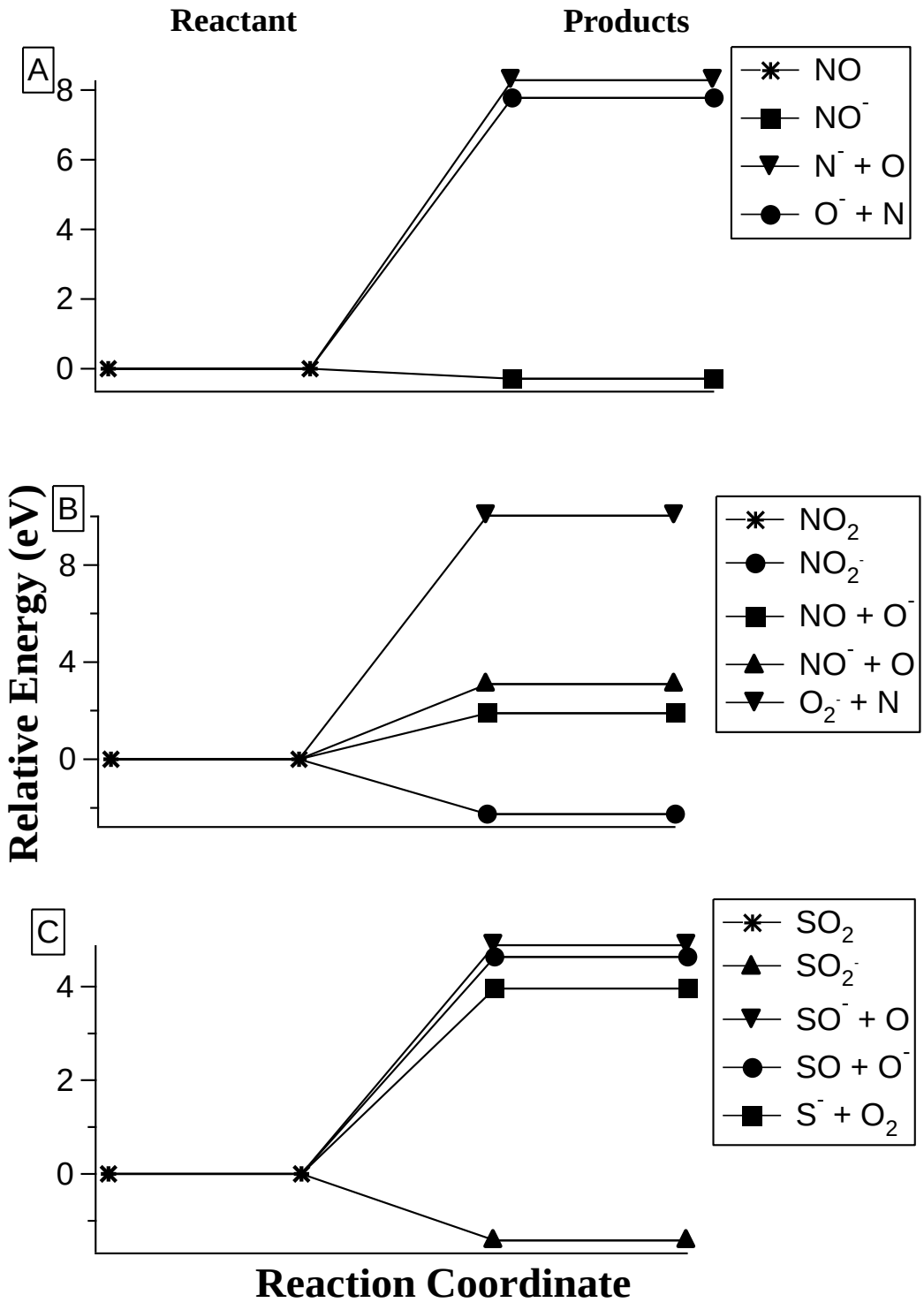

Figure 6. (A) Relative energies of the fragments produced from electron attachment to NO. (B) Relative energies of the fragments produced from electron attachment to NO_2. (C) Relative energies of the fragments produced from electron attachment to SO_2. All energies were calculated using CBS-4M methods, see section 2.4 'Computational Methods' for details.

The fact that only fragmentation occurs stems from the nature by which the electrons approach the neutral molecule. Electronic transitions are rapid on the nuclear time scale, in the Franck-Condon region.[59,60] Due to this, the nuclear geometry associated with the ground state of the neutral molecule will not be immediately altered from an electronic transition creating an anion.[59,60] The resultant anion could be formed in an energy level above the ground state of the intact molecular anion (Figure 5, A).[59,60] If the electronic transition corresponds to a high enough vibrational energy level, the anion can then follow a dissociative energy surface.[59,60] This is the case for NO, NO_2 and SO_2, where the difference in bond length and bond angles (Table 1) are such that the molecule would rather follow a dissociative pathway (Figure 5, B). One method to avoid this transition would be to excite the vibrational states of the molecule prior to electron attachment,[8] or transfer an electron via another atom/molecule (Figure 5, C).[9] Atomic anions, including AMAs, have been shown to transfer electrons to neutral reactants in the gas phase and will be further discussed in the following sections.

Table 1. CBS-4M geometry optimized bond lengths and angles of neutral NO, NO_2 and SO_2 and their anions.

	Bond Length[1] (Å)			**Bond Angle[2]**		
	Neutral	Anion	Δ Bond Length	Neutral Bond Angle	Anion	Δ Bond Angle
SO_2	1.419	1.502	0.083	118.71°	116.14°	-2.57°
NO_2	1.204	1.286	0.082	136.22°	116.40°	-19.82°
NO	1.202	1.312	0.111	n/a	n/a	n/a

1. As measured via S-O or N-O bond length
2. As measured from oxygen to oxygen

3.3 Electron Transfer Reactions via Atomic Anions

Electron transfer reactions are similar to electron attachment in that the transfer from one molecule/atom to the next occurs according to the Franck-Condon condition, i.e. at constant atomic coordinates.[9] Present theory suggests that the reactions are governed by the following relation;

$$M^- + AB \underset{k_b}{\overset{k_c}{\rightleftharpoons}} M^-[AB] \xrightarrow{k_p} E^{\ddagger} \longrightarrow M[AB]^- \longrightarrow M + AB^-$$

where M^- is the molecular/atomic anion, AB is the initial neutral molecule and $M^-[AB]/M[AB]^-$ represent the two encounter complexes before and after the electron transfer within the encounter complex,[9] similar to charge transfer mechanisms between gas-phase cations and neutral molecules.[61] The reaction constants k_c/k_b represent the initial formation/dissociation of the encounter complex while k_p represents the kinetic bottleneck that can occur when an internal energy barrier for electron transfer is present due to the geometries of $M^-[AB]$ differing from $M[AB]^-$ [Figure 5, C].[9,61,62] When the chemical barrier to electron transfer ($E^{\ddagger}$) is low, $k_p > > k_b$ and formation of the encounter complex is rate limiting and proceeds at near collision rates as predicted by the Langevin ADO model of gaseous molecular ion reactions with other gaseous molecules.[63,64] Since formation of the encounter complex is nearly independent of temperature, these reactions will proceed with little to no temperature dependence.[63,64] In situations where the internal energy barrier is large, $k_p < < k_c/k_b$, passage over this barrier becomes rate limiting and a positive temperature dependence should be associated with the reaction rate.[65-68]

As noted from electron attachment to NO, NO_2 and SO_2, even small changes in geometry between the neutral and product anions can prevent the formation of the intact product anion (Table 1). The use of atomic anions to transfer electrons to molecules alters this time scale significantly, allowing the correct geometries to be achieved through the formation of an initial encounter complex, such that the only product anions that are observed are the intact product anions.[69,70]

Atomic metals have some of the lowest electron affinities of the periodic table.[8] Due to this, they have the potential to transfer electrons to neutral reactants at high relative intensities. As aforementioned, issues of flux have prevented the study of these reactions.[13] However, the process used by the Mayer group has enabled a large enough flux of these anions in a bench top triple quadrupole mass spectrometer to enable their study.[25,34]

3.4 Electron Transfer Reactions via Atomic Metal Anions

3.4.1 Collisions with NO

Reactions of AMAs yielded anionic/neutral products resulting from electron transfer, adduct formation and atom abstraction. Reactions of Ag- and Cu- were confirmed for both isotopes. Figure 7 displays typical product anions of AMAs and NO collisions typically used for analysis. Figure 8 details the relative intensities of product anions resulting from electron transfer AMAs with NO at various centre of mass collision energies. Reactions with NO and atomic Cs^-, Fe^- and Cu^- yielded electron transfer to NO. Electron transfer from Cs^- and Cu^- to NO required 0.92 eV and 0.6 eV respectively, while Fe^- required no onset energy and Ag^-

did not react. Maximum relative intensities for electron transfer from Fe^-, Cs^-, Cu^- and Ag^- to NO were 56.4%, 18.4%, 3.3% and 0% respectively.

Figure 9, panels A and B illustrate potential three body reactions producing NO_2^- resulting from Cs^- and Cu^-. However, the presence of NO_2^- is most likely a result of a small amount of NO_2 present in our NO gas. High relative intensities are due to the high efficiency with which electron transfer occurs between gaseous AMAs and NO_2, discussed in detail in 3.4.3 'Collisions with NO_2'. Cs^- was also observed to produce O_2^-, m/z 89 as well as m/z 183 (Figure 9, A). The identities of m/z signals 89/183 could not be deduced with a high degree of confidence. Both atomic Cu^- and Ag^- produced oxide anions CuO^- and AgO^- resulting from oxygen abstraction (Figure 9, B and C).

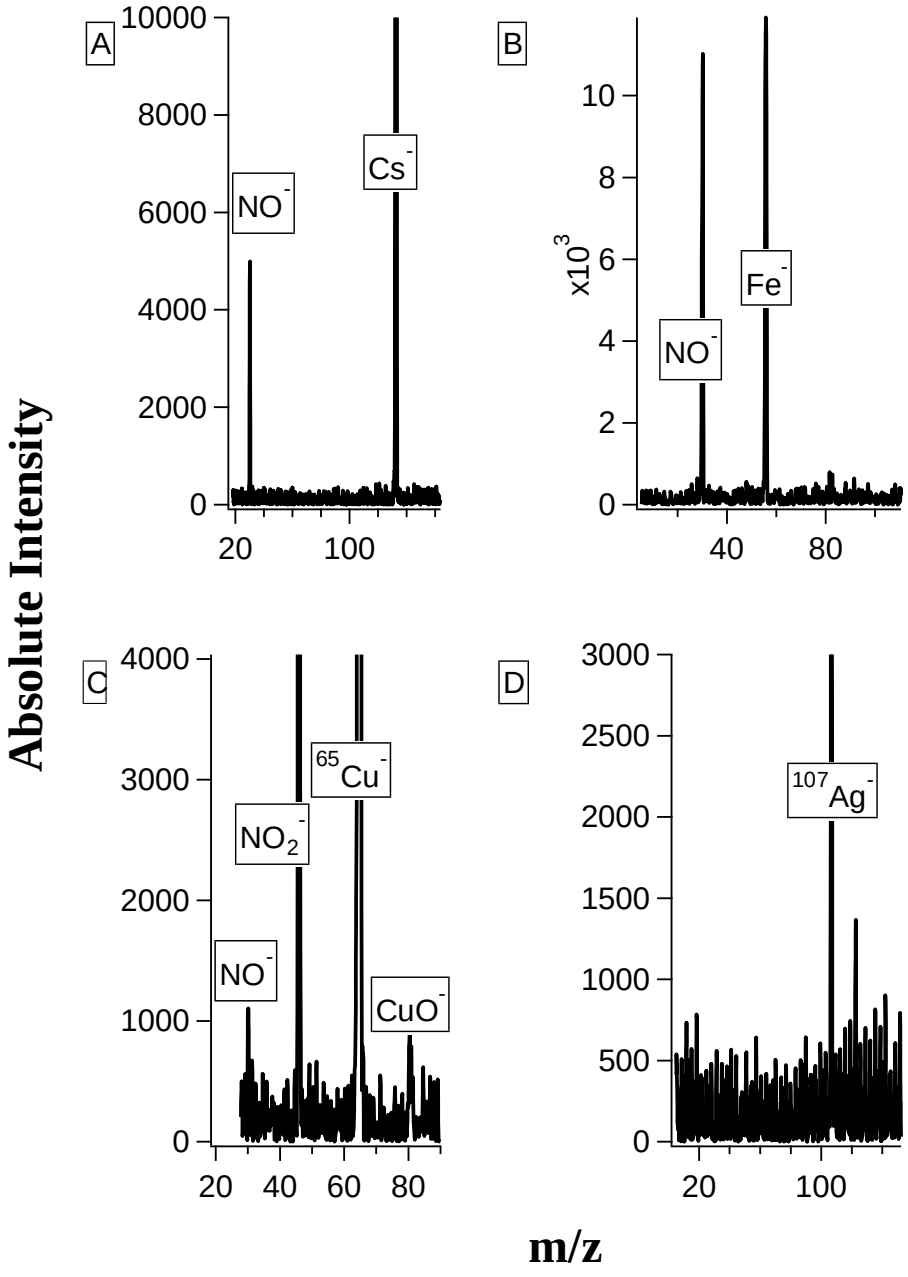

Figure 7. Characteristic mass spectra of (A) Cs^- (B) Fe^-, (C) $^{65}Cu^-$ and (D)$^{107}Ag^-$ reactions with neutral NO gas. The Y axis represents total ion abundance (absolute intensity) while the X axis represents mass to charge ratio (m/z). Pressures of NO gas range from; (A) 2.2 x 10^{-4}, (B) 1.5 x 10^{-4}, (C) 1.6 x 10^{-4} and (D) 3.5 x 10^{-4} torr. Centre of mass collision energy was set to (A) 0.92 eV, (B) 0 eV, (C) 0.95 eV and (D) 0 eV.

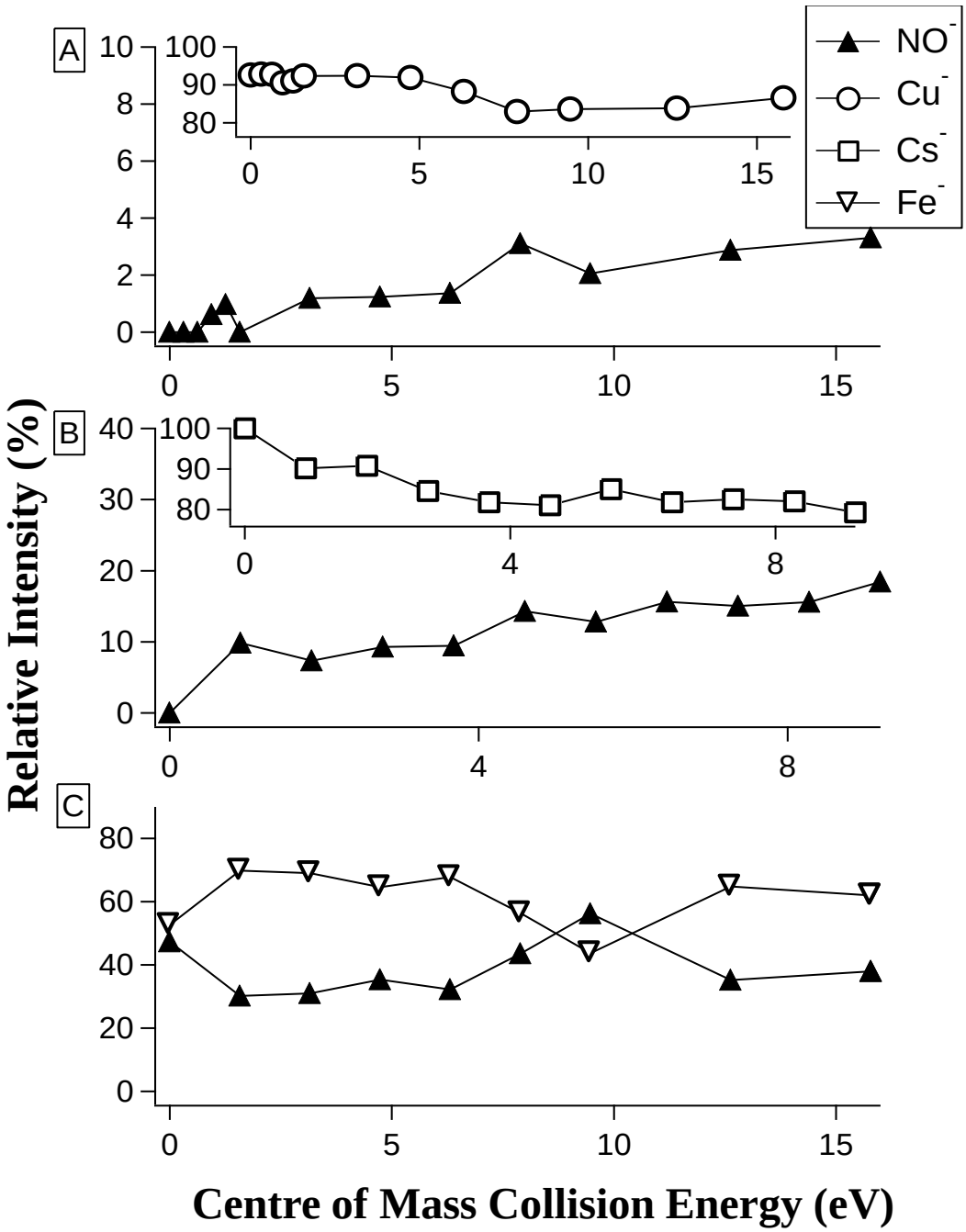

Figure 8. Relative intensities of (A) $^{65}Cu^-$, (B) Cs^- and (C) Fe^- with NO^-. The Y axis represents relative intensity (%) while the X axis represents centre of mass collision energy (eV). Pressures of NO gas range from; (A) 1.6 x 10^{-4}, (B) 2.2 x 10^{-4} and (C) 1.5 x 10^{-4} torr.

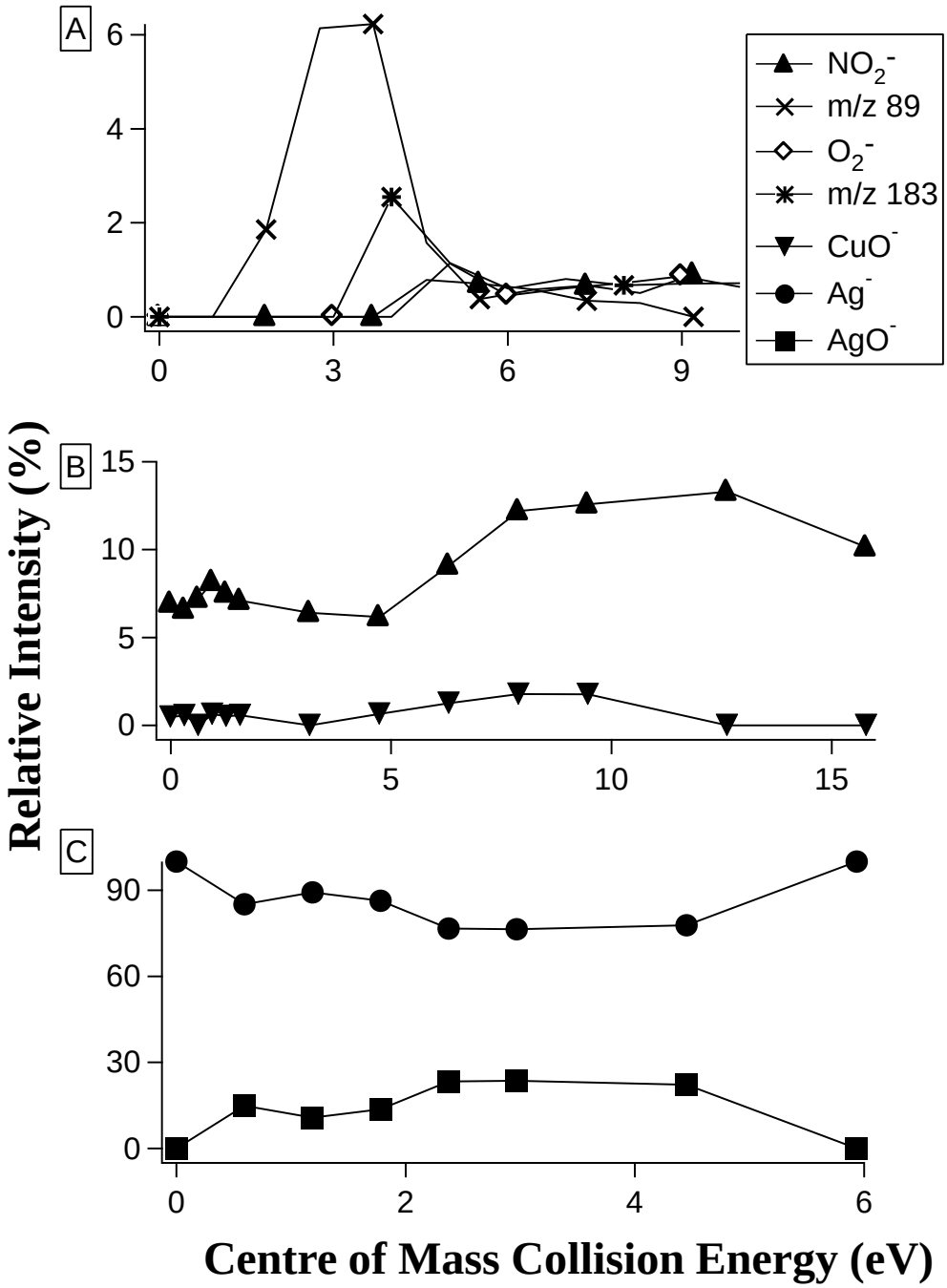

Figure 9. Relative intensities of various fragments from reactions with (A) Cs^-, (B) $^{65}Cu^-$ and (C) $^{109}Ag^-$. The Y axis represents relative intensity (%) while the X axis represents centre of mass collision energy (eV). Pressures of NO gas range from; (A) 2.2 x 10^{-4}, (B) 1.6 x 10^{-4} and (C) 3.5 x 10^{-4} torr.

3.4.2 Collisions with SO_2

Collisions of AMAs with SO_2 produced product anions indicative of electron transfer. Figure 10 shows selected spectra of typical product anions resulting from collisions between gaseous AMAs and SO_2. Reactions of Cu^- and Ag^- were confirmed for both isotopes. Onset energies for all electron transfer reactions were 0 eV for all AMA reacted. Figure 11 displays the relative intensities of AMAs and SO_2. Maximum relative intensities for electron transfer to SO_2 producing SO_2^- from Fe^-, Cs^-, Cu^- and Ag^- were 45%, 66%, 49% and 24% respectively. Figure 12 displays product anions thought to be the result of O_2 contamination in the case of Cs^- and Fe^- and m/z 153 produced from reactions of SO_2 and Cs^-. The identity of m/z 153 could not be deduced with a high degree of confidence. Possible options include oxalic acid contamination in the Cs^- anion beam, forming an adduct with SO_2 to produce $[C_2SO_4]^-$. However, this is unlikely, as tests of oxalic acid within the Cs^- beam yielded no breakdown products, and oxalic acid contaminations would be of the molecular formula $[C_3O_6]^-$ in order to equal m/z 133. Therefore the observed loss would likely be 44 mass units, producing m/z 89 in the spectrum. No m/z 89 was observed during tests of the Cs^- beam. For information regarding the confirmation of anion beam purity, refer to section 2.3 ‘Sample Preperation and Mass Spectrum Measurment.

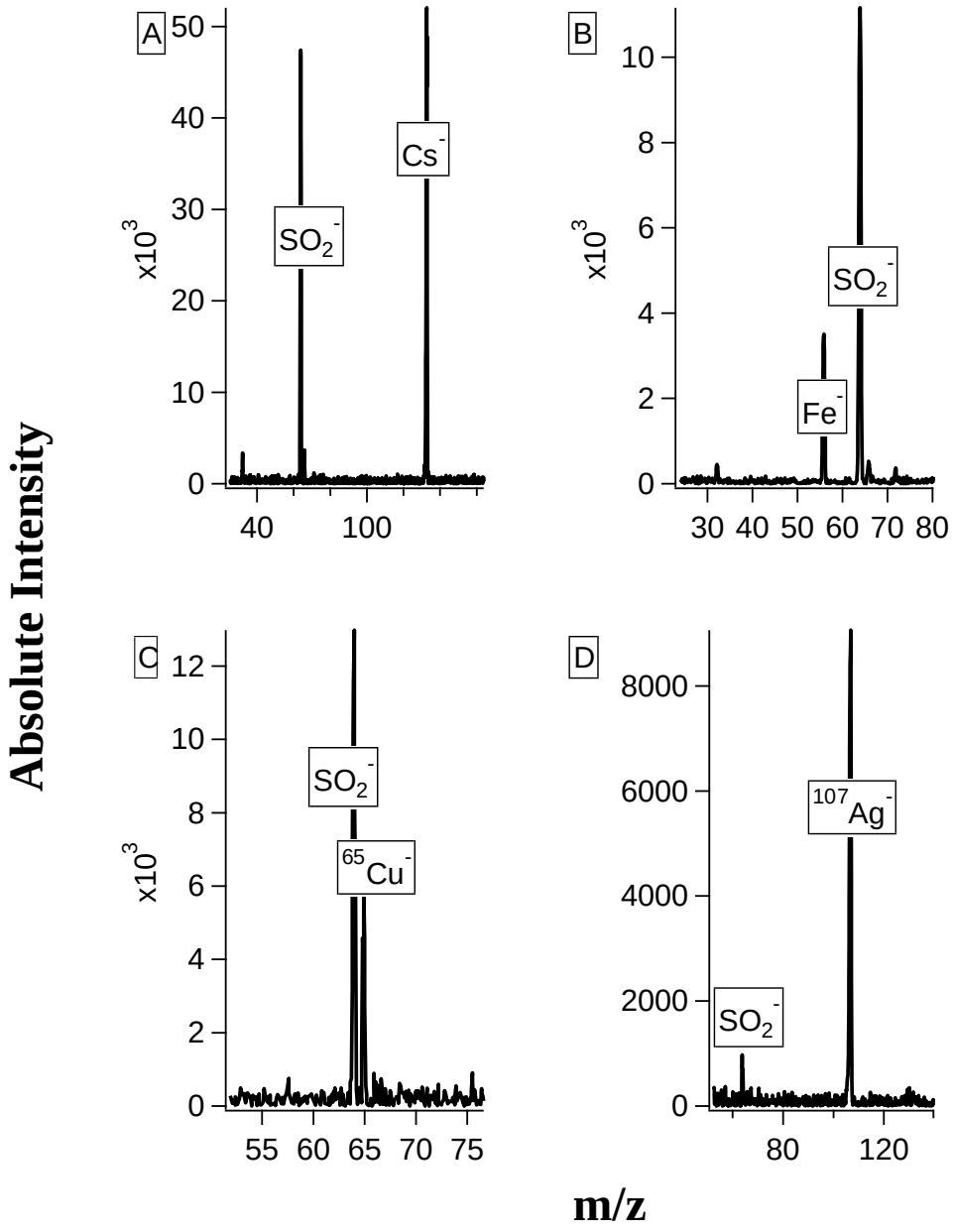

Figure 10. Characteristic mass spectra of (A) Cs^- (B) Fe^-, (C) $^{65}Cu^-$ and (D)$^{107}Ag^-$ reactions with neutral SO_2 gas. The Y axis represents total ion abundance (absolute intensity) while the X axis represents mass to charge ratio (m/z). Pressures of SO_2 gas range from; (A) 1.2 x 10^{-4}, (B) 1.4 x 10^{-4}, (C) 1.3 x 10^{-4} and (D) 1.8 x 10^{-4} torr. Centre of mass collision energy was set to (A) 1.92 eV, (B) 0 eV, (C) 0 eV and (D) 3.75 eV.

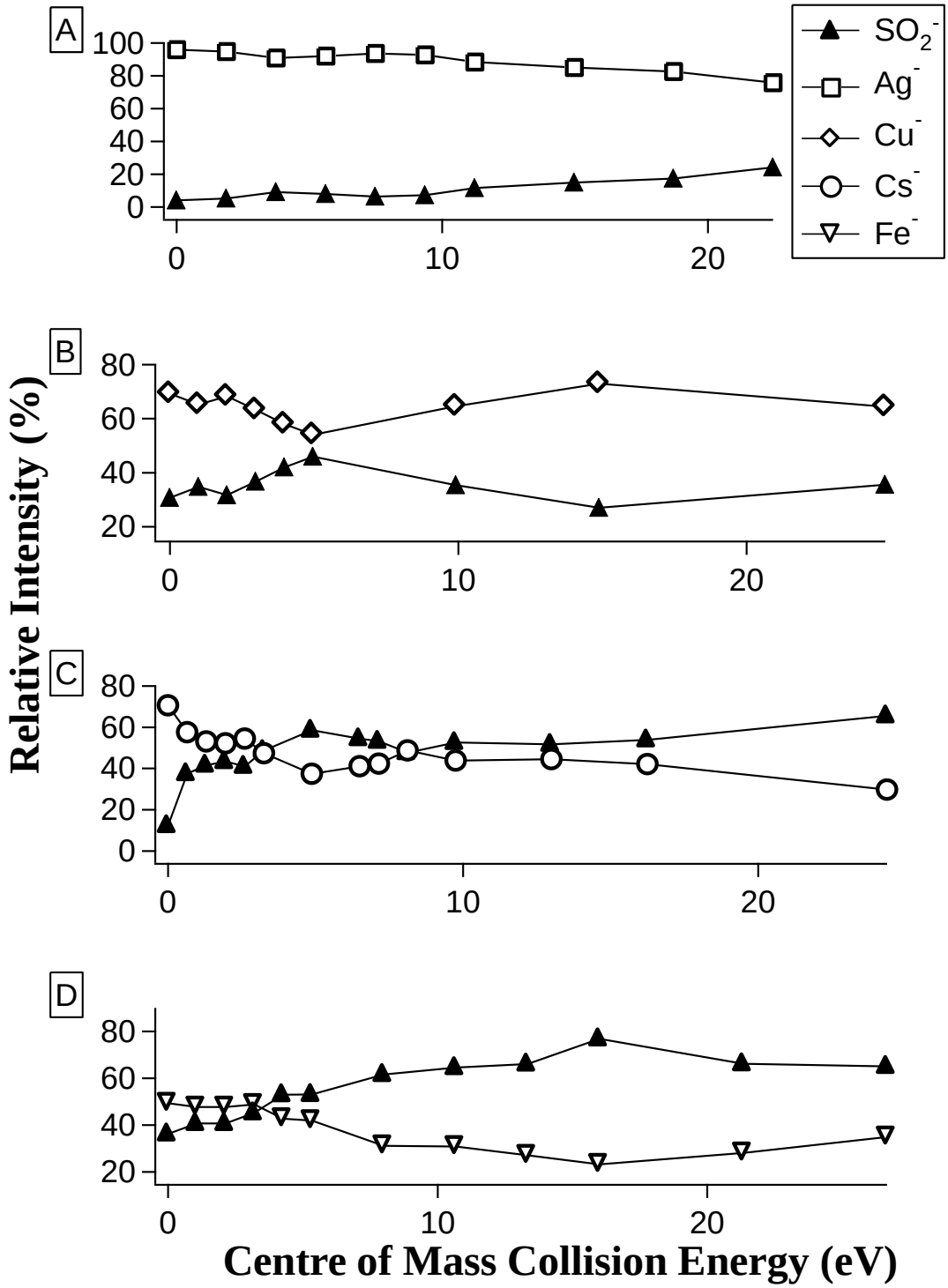

Figure 11. Relative intensities of (A) $^{107}Ag^-$, (B) $^{65}Cu^-$, (C) Cs^- and (D) Fe^- with SO_2^-. The Y axis represents relative intensity (%) while the X axis represents centre of mass collision energy (eV). Pressures of SO_2 gas range from; (A) 1.8 x 10^{-4}, (B) 1.3 x 10^{-4}, (C) 1.4 x 10^{-4} and (D) 1.2 x 10^{-4} torr.

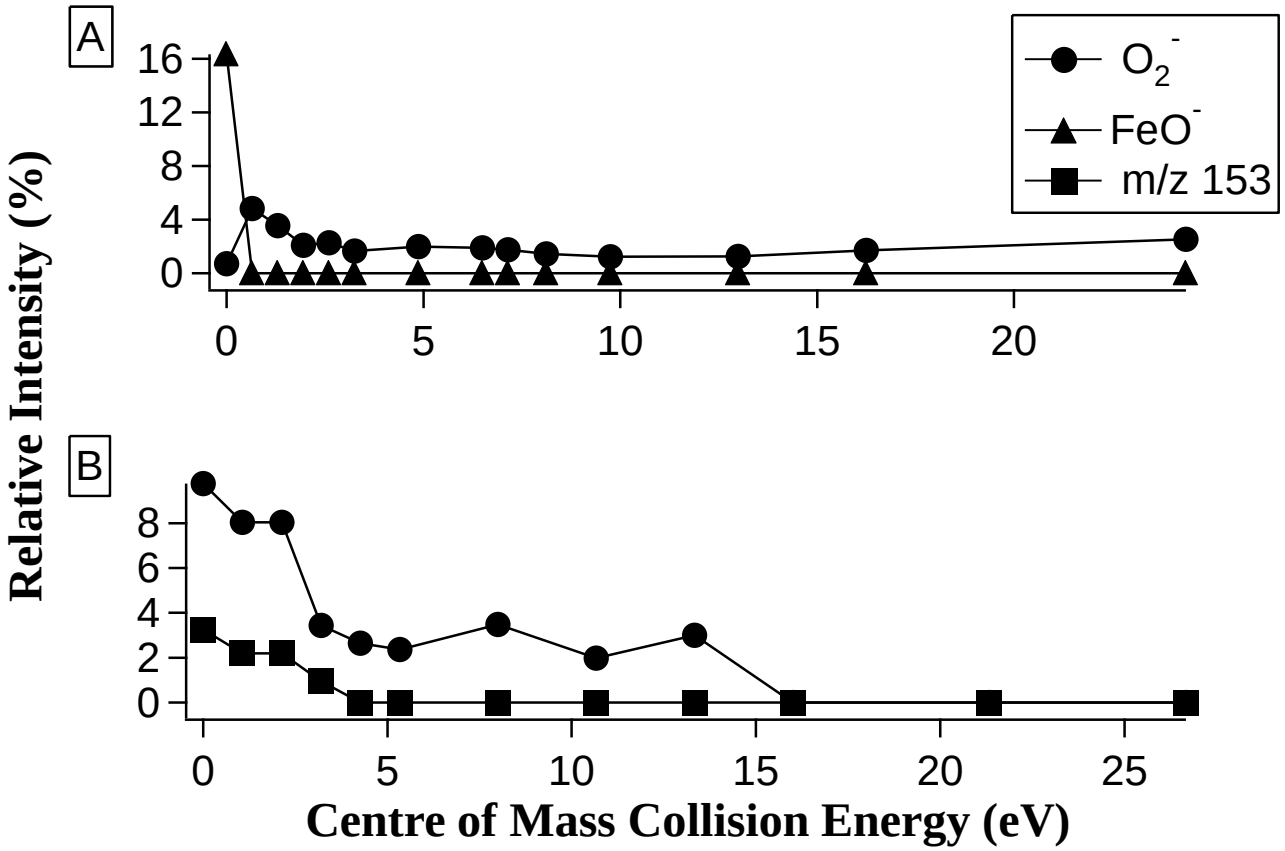

Figure 12. Relative intensities of various fragments from reactions with (A) Fe^-, (B) Cs^-. Pressures of SO_2 gas range from (A) 1.4 x 10^{-4} and (B) 1.2 x 10^{-4} torr.

3.4.3 Collisions with NO_2

Collisions of AMAs with NO_2 resulted in electron transfer as well as atom abstraction. Figure 13 exhibits typical product anions resulting from collisions between gaseous AMAs and NO_2 used for analysis. Similar to reactions with SO_2, onset energies for all electron transfer reactions were 0 eV. Reactions of Cu^- and Ag^- were confirmed for both isotopes. Figure 14 displays the relative intensity of electron transfer at various centre of mass collision energies with NO_2. Reactions of AMAs with NO_2 generated high relative intensities of electron transfer. Maximum relative intensities for electron transfer from Fe^-,

Cs^-, Cu^- and Ag^- to produce NO_2^- were 84%, 100%, 100% and 97% respectively. Figure 15 illustrates the noted abstraction products of Cu^- (CuO^-, CuO_2^-) and Fe- (FeO^-, FeO_2^-, FeO_3^-) and their relative intensities at various centre of mass collision energies.

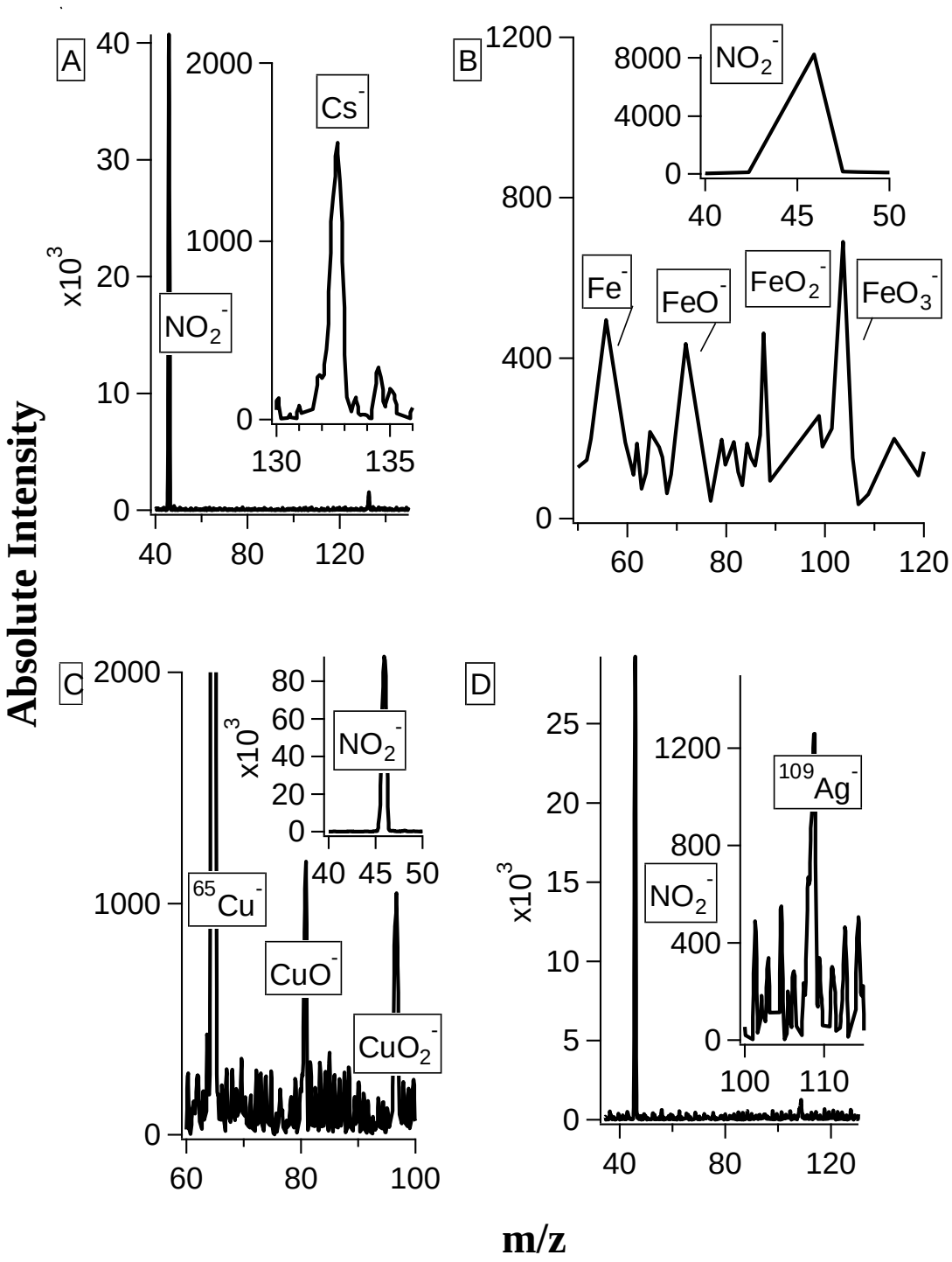

Figure 13. Characteristic mass spectra of (A) Cs^- (B) Fe^-, (C) $^{65}Cu^-$ and (D)$^{109}Ag^-$ reactions with neutral NO_2 gas. The Y axis represents total ion abundance (absolute intensity) while the X axis represents mass to charge ratio (m/z).Pressures of NO_2 gas range from; (A) 2.8 x 10^{-4}, (B) 2.0 x 10^{-4}, (C) 1.1 x 10^{-4} and (D) 1.4 x 10^{-4} torr. All centre of mass collision energies were set to 0 eV.

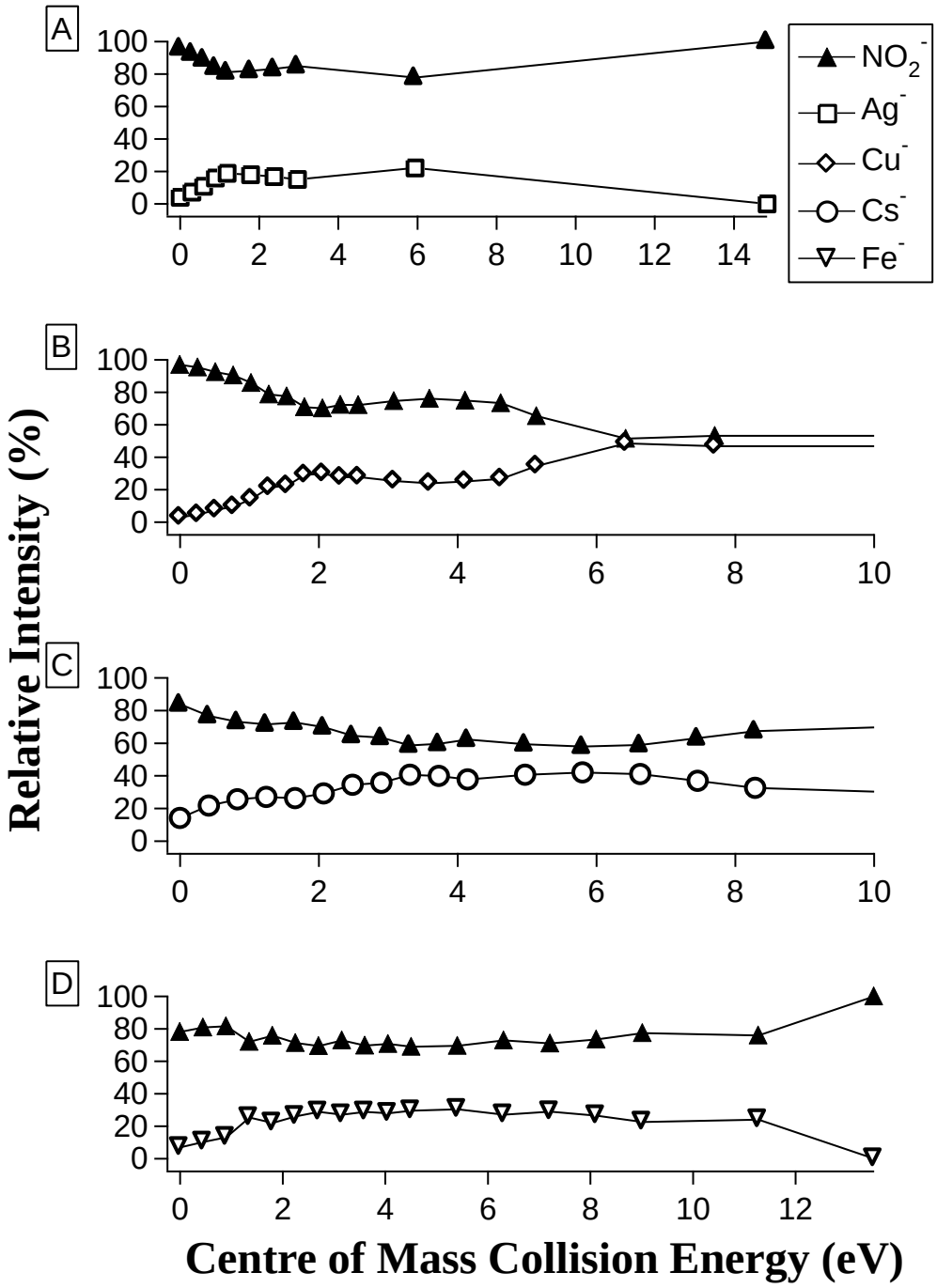

Figure 14. Relative intensities of (A) $^{109}Ag^-$, (B) $^{65}Cu^-$, (C) Cs^- and (D) Fe^- with NO_2^-. The Y axis represents relative intensity (%) while the X axis represents centre of mass collision energy (eV). Pressures of NO_2 gas range from (A) 3.5 x 10^{-4}, (B) 1.1 x 10^{-4}, (C) 2.0 x 10^{-4} and (D) 1.4 x 10^{-4} torr

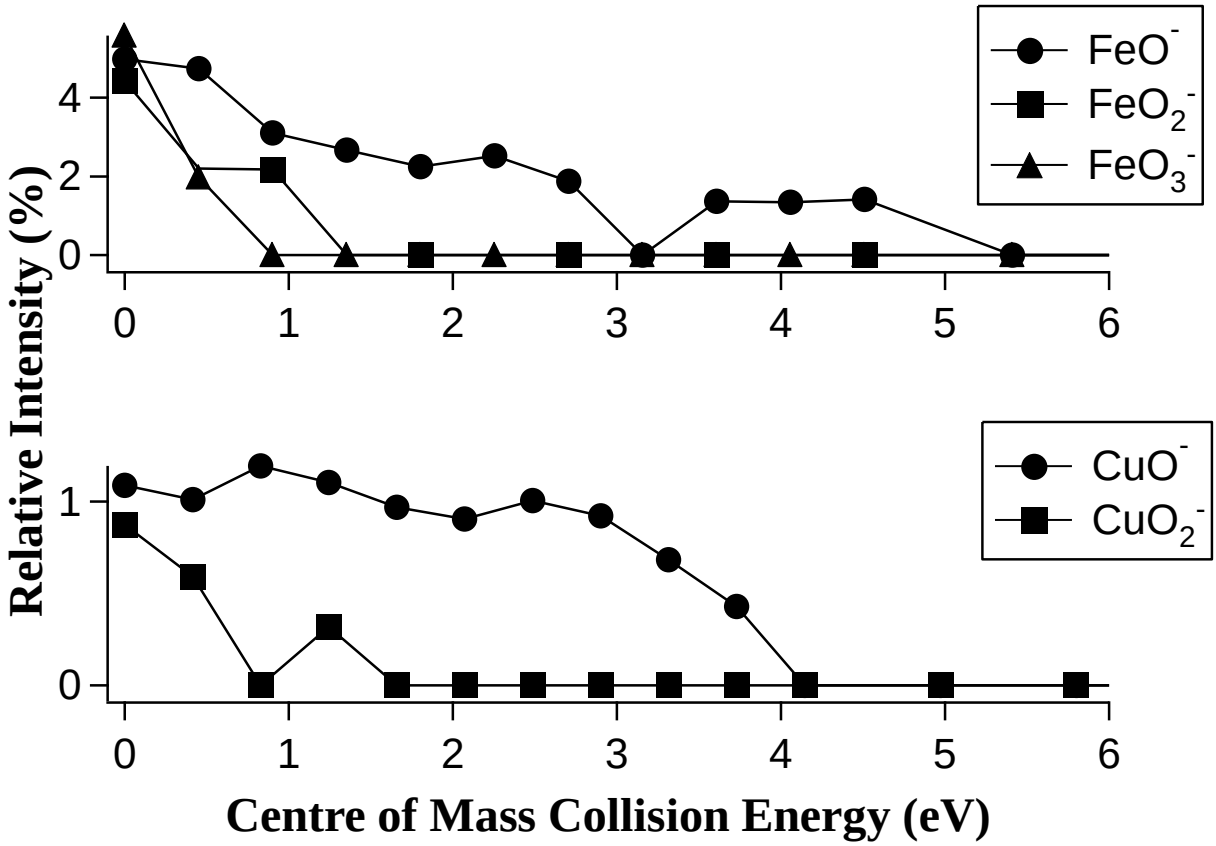

Figure 15. Relative intensities of (A) Fe^-, (B) ^{65}Cu adducts from reactions with NO_2^-. The Y axis represents relative intensity (%) while the X axis represents centre of mass collision energy (eV). Pressures of NO_2 gas range from (A) 1.4 x 10^{-4} and (B) 1.1 x 10^{-4} torr.

3.5 Adduct Formation of Cu^- and Fe^-

3.5.1 FeO^-, FeO_2^- & FeO_3^-

The formation of FeO^-, FeO_2^- and FeO_3^- from collisions with NO_2 implies a multiple collision reaction mechanism of Fe^- with NO_2 or the presence of an at least triply oxygenated neutral species, such as N_2O_4(Figure 15). Due to limitations of the experimental method, the

identity of the neutral partner is likely to remain ambiguous. Therefore, the focus of this section will be on the energetics of FeO^-, FeO_2^- and FeO_3^- formation.

A study of FeO^-, FeO_2^- and FeO_3^- using photoelectron spectroscopy revealed that each sequential addition of oxygen increases the electron affinity of the molecule.[71] The electron affinities of the ground states of FeO, FeO_2, and FeO_3 were found to be 1.50, 2.36 and 3.26 eV.[71] Semi-empirical calculations suggest that FeO_2^- is of the form $[O\text{-}Fe\text{-}O]^-$ rather than $Fe(O_2)^-$.[72] In addition, the authors of the photodetachment study suggest that the relatively high experimentally derived electron affinity of FeO_2 is inconsistent low electron affinities associated with Fe and O_2 and therefore a side bonded $Fe(O_2)$ (I) or a linear/bent Fe-O-O (II) type of structure.[73] They go on to suggest that the removal of a non-bonding d electron from a linear FeO_2^- molecule of the form of $O^{2-}\text{-}Fe^{3+}\text{-}O^{2-}$ would result in the high electron affinity measured experimentally, due to the stability of the d_5 configuration associated with a Fe^{3+} oxidation state.[73] Furthermore, based on laser ablation studies performed by Andrews et al., the most stable form of FeO_2^- was determined to be the $[O\text{-}Fe\text{-}O]^-$ with a bond angle of about 141 degrees.[74] This result was consistent with an FeO_2^- spectrum that produced two broad bending modes, consistent with this structure.[71] The photoelectron spectrum of FeO_3^- obtained by Wu et al. suggests a highly symmetric trigonal planar structure of FeO_3^-, similar to that of D_{3h} FeO_3.[71]

As previously mentioned, the electron affinities of the ground states of FeO, FeO_2, and FeO_3 were found to be 1.50, 2.36 and 3.26 eV.[71] Therefore, the addition of oxygen to an Fe anion or oxygenated derivative anion is exothermic and results in a thermodynamically favoured reaction from a collision with NO_2 or N_2O_4 contaminant. Interestingly, the electron affinity of FeO_4 does not increase in the same manner as FeO, FeO_2 and FeO_3.[71] Wu et al.

suggest that the reason for this is that the FeO_3 contains the maximum known oxidation state of the Fe atom (+6). As such, any additional oxygen will not further oxidize the Fe centre, clearly illustrated by the levelling off of the electron affinity of FeO_4.[71] This lack of a further increase in electron affinity explains why the FeO_4^- is never observed within this experiment and the highest Fe adduct observed is FeO_3^-. Thus the formation of FeO^-, FeO_2^- and FeO_3^- is thermodynamically favoured until the FeO_3^- is formed. Additionally, increasing centre of mass collision energy favours the formation of FeO^- over FeO_2^-, while both are favoured over FeO_3^-.

3.5.2 CuO^- & CuO_2^-

Collisions of Cu^- with NO_2 produced CuO^- and CuO_2^- (Figure 15). The formation of CuO_2^- in non-statistical equivalence to CuO^- suggests that it is either produced during a single collision with NO_2, leaving a neutral N atom or via a collision with a N_2O_4 contaminant.

The CuO_2^- anion could be of the form $[O\text{-}Cu\text{-}O]^-$ or $Cu(O_2)^-$. A previous study using LPES to probe electron affinities found that of the two isomers, $Cu(O_2)$ had an electron affinity of 1.50 eV, while $[O\text{-}Cu\text{-}O]^-$ had an electron affinity of 3.46 eV.[75] CuO possesses an electron affinity of 1.77 eV as measured via LPES.[76] NO possesses an electron affinity of 0.024 as measured via LPES.[8] The electron affinity of atomic N has never been determined experimentally, but quantum calculations suggest a ground state electron affinity of -0.07 eV.[7] Comparison of the electron affinities of CuO and NO compared to CuO_2 and N could explain the relatively high abundances of CuO_2^- compared to CuO^-. The higher electron

affinity of CuO_2 relative to CuO and lower electron affinity of N relative to NO suggest that the formation of the reaction pair CuO_2^-/N is thermodynamically preferred relative to CuO^-/NO. The formation of CuO_2^- may also be the result of increasingly favourable thermodynamics of the addition of O to CuO^- resulting in the formation of CuO_2^- at higher relative intensities than CuO^- similar to Fe^- becoming increasingly stable with sequential addition of O atoms, and thus thermodynamically favoured. Increasing the energy of these collisions favours the formation of CuO^- over CuO_2^- (Figure 15). It should be noted that the formation of CuO^- and CuO_2^- are clearly less favourable than electron transfer, occupying at maximum ~2% of the observed relative intensities (Figure 15).

3.6 Conclusions

When contrasted with the relative intensities of product anions produced from AMAs with higher electron affinities, an obvious trend emerges from the results of electron transfer to NO, SO_2 and NO_2 from Cs^-, Fe^-, Cu^- and Ag^- (Table 2). Within the results, increasing electron affinity of the neutral molecule and/or decreasing the electron affinity of the AMA increases the relative intensities of NO^-, NO_2^- and SO_2^- produced from collisions with the respective AMA.

Furthermore, some knowledge of the relative energy barrier of these reactions can be gleaned from their behaviour with regard to increasing internal energy. Increasing the centre of mass collision energy has the effect of increasing the translational energy of the collision partners. [77] Some of that translational energy is converted into internal energy of both the atomic anions and neutral reactants, in effect 'warming up' the reactants.[77] Numerous studies have shown that if an internal energy barrier exists in an electron transfer reaction, then there should be a 'positive temperature dependence' associated with the reaction channel. [61,63-68]

If there is no internal energy barrier with regard to electron transfer, then there should be little to no temperature dependence.[61,63-68] Therefore increasing the centre of mass collision energy should increase the relative intensities of the electron transfer products if there is an internal energy barrier, and should have no or a negative effect (due to additional scattering[77]/electron detaching processes[8]) if there is none. Therefore, the positive dependence of an electron transfer reaction (i.e. increase in the relative intensity of a product anion) in relation to the centre of mass collision energy is indicative of an energy barrier for the transfer of said electron.

The reactions of Cs^- and Cu^- with NO show a positive dependence on the centre of mass collision energy, while Fe^- shows little to no change in reactivity while increasing the centre of mass collision energy (Figure 8). This suggests that an internal energy barrier exists for the reactions of Cs^- and Cu^- with NO, while none exists for the electron transfer from Fe^- to NO. Ag^- did not react with NO at all, suggesting an insurmountable energy barrier for these reactants. All metal anions show a positive dependence on the centre of mass collision energy when transferring electrons to SO_2 (Figure 11), suggesting the presence of an internal energy barrier. Interestingly, all metal anions show negative temperature dependence or no temperature dependence (for the case of Fe^-) when reacting with NO_2 (Figure 14). This is suggestive of no internal energy barrier within this reaction channel, and the possibility of a competing reaction channel at higher internal energies, such as additional scattering or the formation of an excited state of NO_2^-, resulting in auto detachment of the electron via shape of Feshbach resonances and a drop in relative intensity of NO_2^-.

Table 2. Maximum relative intensities of NO^-, SO_2^- and NO_2^- resulting from collisions with various incident anions.

Neutral Reactant/Product Anion	Incident Anion (M^-)	Electron Affinity (M) (eV)	Maximum Relative Intensity (%)
NO/NO^-	Fe^-	0.15	47
	Cs^-	0.47	10
	Cu^-	1.22	0.6
	Ag^-	1.3	n/a
SO_2/SO_2^-	Fe^-	0.15	45
	Cs^-	0.47	66
	Cu^-	1.22	49
	Ag^-	1.3	24
NO_2/NO_2^-	Fe^-	0.15	84
	Cs^-	0.47	100
	Cu^-	1.22	100
	Ag^-	1.3	97

Chapter 4 – Dissociative Electron Attachment to Pentafluorophenol and Pentafluoroaniline

In 2012, Omarsson et al. published a study of the direct attachment of electrons ranging from 0 –14 eV in energy to neutral pentafluorophenol (PFP) and pentafluoroaniline (PFA) in the gas phase.[78,79] Omarsson et al. found that electron attachment to PFP produced dissociation fragments of m/z 184, 183, 165, 164, 145, 136, 117 and 19. Electron attachment to PFA produced dissociation fragments of m/z 183, 182, 163, 143, 124, 74, 26 and 19. In their studies, Omarsson et al. found that low energy electron attachment can be induced via dissociative channels, allowing high attachment cross sections of the anions formed from said dissociation. Furthermore, they found that intramolecular hydrogen bonding played a pivotal role in the dissociative electron attachment resulting in the formation of HF from either PFP or PFA.[78,79]

Their study provides us with a unique ability to directly compare dissociative electron transfer reactions using atomic metal anions with those employing isolated electrons. It is the goal of this chapter to connect and explain the reactions that are known to be driven by electron transfer versus those that involve the metal anion chemically interacting with the reactant.

Throughout the discussion, the words ‘relative energy’ will be used to discuss the various neutral/anion product energies relative to the starting neutral/anion reactants. The identity of neutral product fragments were determined on the basis of relative energies calculated at the CBS-4M level and evidence found in the literature. Electron affinities of all product ions/neutral partner fragments can be found in Table 3. Reactions of Cs^-

and Rb^- with PFP and PFA will be discussed. Reactions of Fe^- with PFP will also be discussed.

Figure 16/17 display characteristic mass spectra from each combination of metal anion and neutral gas phase collision partner, PFP/PFA respectively. The main reactions products are the fragments pertaining to H/F abstraction for PFA and PFP respectively, as well as the fragment associated with HF loss for PFP and the parent anion of PFP.

Table 3. Calculated electron affinities (in eV) of all charged and neutral species presented in this study. Electron affinities were determined using energy values calculated using CBS-4M methods in Gaussian 09. See Computational Methods for further detail.

Neutral Molecule	Electron Affinity	Neutral Molecule	Electron Affinity
F	3.63	C_6F_5OH	0.25
HF	-2.05	C_6F_5O	3.44
F_2	3.28	C_6F_4OH	3.37
H_2	-2.91	C_6F_4O	3.89
FHF	5.45	C_6F_3O	4.20
K	0.68	$C_6F_5NH_2$	0.05
KH	0.45	C_6F_5NH	2.52
KF	0.45	$C_6F_4NH_2$	3.13
KFHF	0.53	C_6F_4NH	3.78
KFH	0.63	C_6F_3NH	2.51
Fe	0.11	C_6F_3NH	4.62
FeFH	5.13		

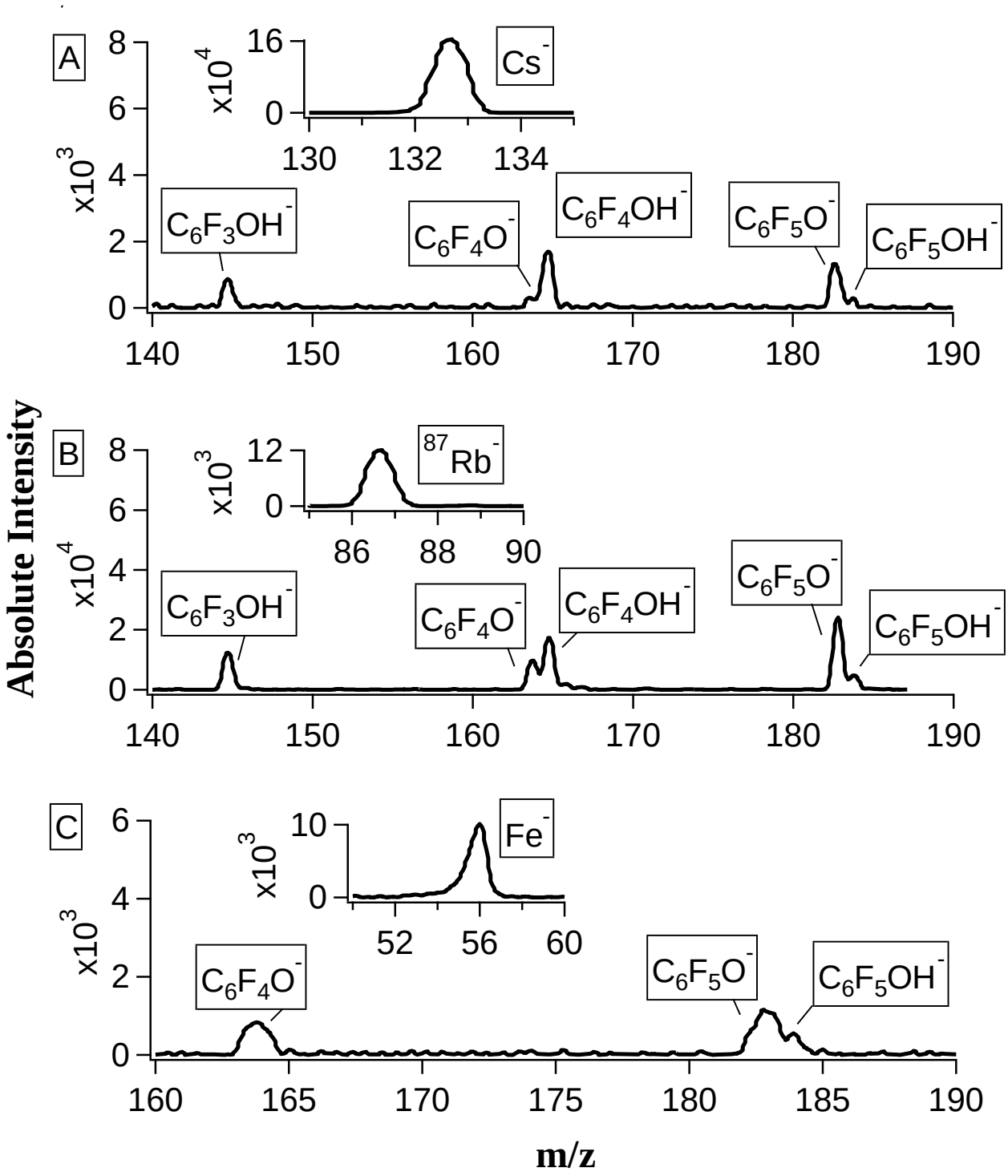

Figure 16. Characteristic mass spectra of (A) Cs^- (B) Rb^- and (C) Fe^- with pentafluurophenol (PFP). The Y axis represents total ion abundance (absolute intensity) while the X axis represents mass to charge ratio (m/z). Pressures of gaseous PFP range from; (A) 1.8 x 10^{-4}, (B) 1.1 x 10^{-4}, (C) 1.1 x 10^{-4} torr.

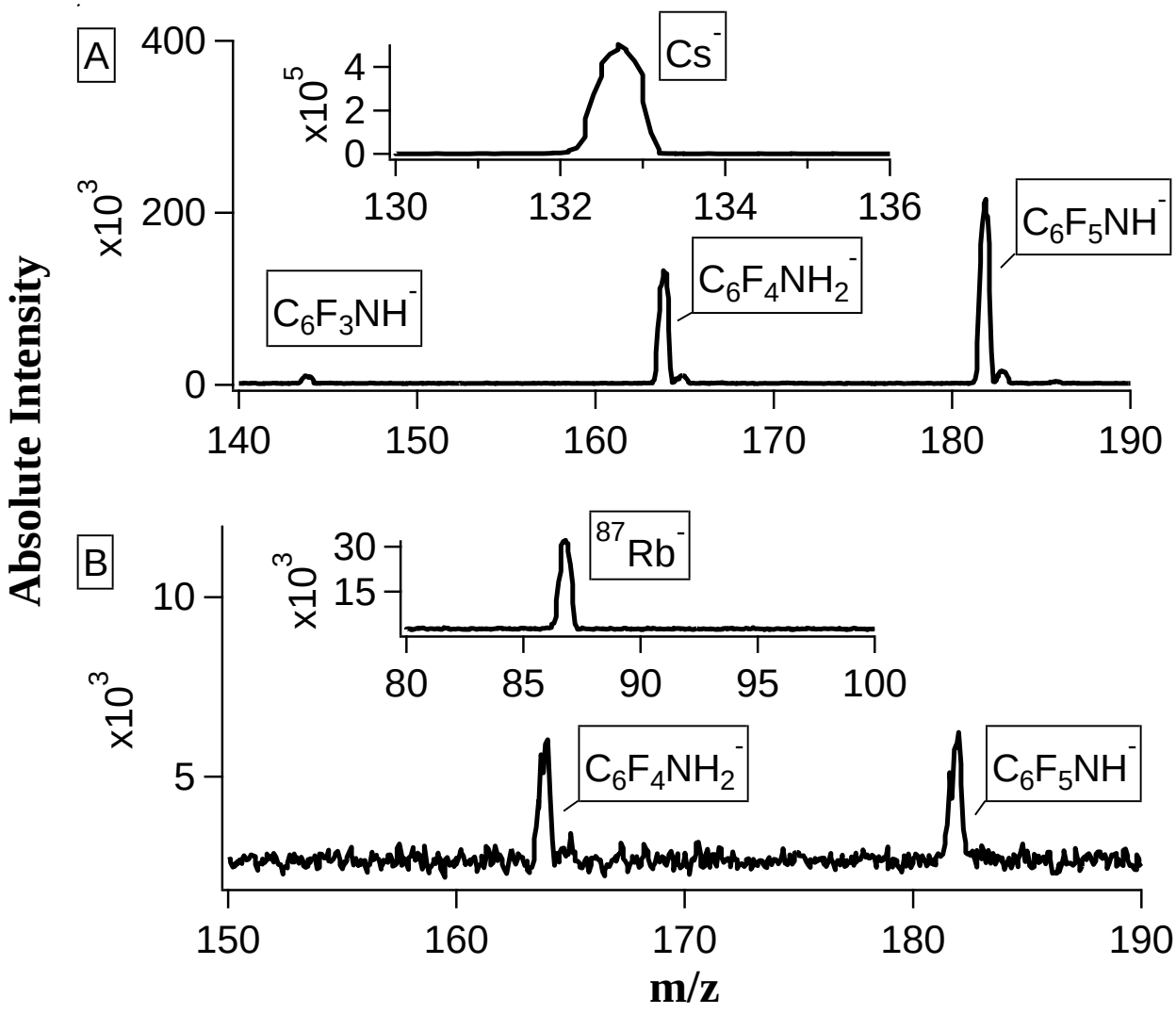

Figure 17. Characteristic mass spectra of (A) Cs^- and (B) Rb^- with pentafluuroaniline (PFA). The Y axis represents total ion abundance (absolute intensity) while the X axis represents mass to charge ratio (m/z). Pressures of gaseous PFA range from; (A) 2.2 x 10^{-4} and (B) 2.2 x 10^{-4} torr.

4.1 Formation of Parent Anion PFP/PFA from Cs^-, Rb^-, Fe^-

Calculations at the CBS-4M level using K^- as a stand in for Cs^-/Rb^- suggest a relative energy of 0.426 and 0.632 eV for the formation of $[PFP]^-$ and $[PFA]^-$ (Table 4, reaction 1 and 2). Fe^- has a calculated relative energy of -0.139 eV and 0.067 eV for PFP and PFA respectively (Table 4, reaction 1 and 2). Formation of PFP^- is evident through the presence of m/z 184 $[C_6F_5OH]^-$ produced via collisions with Cs^-, Rb^- and Fe^- in Figure 16. The intensity of the PFP anion produced from Rb^-/Cs^- is such that it is possible to rule out background contamination due to ^{13}C contributions from m/z 183($[C_6F_5O]^-$) . Fe^- was also observed to produce m/z 184 ($[C_6F_5OH]^-$) with intensity high enough to rule out ^{13}C contributions from the deprotonated product m/z 183. However, the m/z 183 ($[C_6F_5NH_2]^-$) intensity is not high enough to rule out background contamination due to ^{13}C contributions from m/z 182 ($[C_6F_5NH]^-$). See Table 5 for further details.

Table 4. Relative energies (in eV) of potential reaction channels of Fe^-, Rb^-, Cs^- (using K^- as a stand-in) with PFP and PFA calculated using CBS-4M methods in Gaussian 09. See computational methods for details.

#	Reaction	Fe^-
1	$M^- + C_6F_5OH \rightarrow M + [C_6F_5OH]^-$	-0.14
2	$M^- + C_6F_5NH_2 \rightarrow M + [C_6F_5NH_2]^-$	0.07
#	**Reaction**	**K^-**
1	$M^- + C_6F_5OH \rightarrow M + [C_6F_5OH]^-$	0.43
2	$M^- + C_6F_5NH_2 \rightarrow M + [C_6F_5NH_2]^-$	0.63

Table 5. Theoretical ^{13}C contributions to observed experimental m/z intensities and actual intensities of observed m/z ratios in spectra.

Pentafluorophenol[1]			
Atomic Metal Anion[3]	Experimental Intensity of m/z 183	^{13}C Contribution from m/z 183 to 184	Experimental Intensity of m/z 184
Cs^- (0 eV)	31470	2077	3655
Rb^- (0 eV)	1927	127	724
Fe^- (3 eV)	682	45.0	383
Pentafluoroaniline[2]			
Atomic Metal Anion[3]	Exp. Intensity of m/z 182	^{13}C Contribution from m/z 182 to 183	Exp. Intensity of m/z 183
Cs^- (0 eV)	120600	7960	8014
Rb^- (0 eV)	4966	328	323
Fe^- (3 eV)	n/a	n/a	n/a

1. M/z 184 refers to $[C_6F_5OH]^-$ and m/z 183 refers to $[C_6F_5O]^-$
2. M/z 183 refers to $[C_6F_5NH_2]^-$ and m/z 182 refers to $[C_6F_5NH]^-$
3. (# eV) refers to the centre of mass collision energy used to produce the experimental signal intensities of m/z 182,183 or 184 from the gaseous collisions of AMAs and PFP/PFP

4.2 Loss of H/F via formation of neutral MH/MF

The loss of hydrogen was observed as reaction product channels for Cs^-, Rb^- and Fe^- (Fe^- with PFP only). In the case of fluorine, only the alkali metals were observed to produce neutral fluorine loss from PFP/PFA. There are a number of possible pathways for these reactions (Table 6, reactions 1a-1d, 2a-2d).

The case for H/F abstraction to produce MH/MF based on relative energies is quite strong (Table 6, reactions 1c/1d and 2c/2d). However, the absence of fluorine abstraction in the iron spectrum, suggests that there may be other factors at play within that energy surface. Fluorine abstraction with PFP and Fe^- may have an insurmountable energy barrier within the thermodynamic regimes of a triple quadrupole, while Cs^- and Rb^- have comparably lower energy of activation for fluorine abstraction reactions. Based on the relative energies of neutral hydrogen and fluorine dissociation compared to fluorine abstraction, it is suggested that fluorine abstraction with Cs^- and Rb^- is occurring (Table 6, reactions 1d/2d). Further evidence supporting H/F abstraction is the relatively low abundances of neutral H dissociation in electron attachment experiments and no neutral F dissociation observed at all compared with the high abundances noted in the reactions with Cs^- and Rb^- (Figures 16 and 17).[78] This suggests that a novel process, not simply dissociative electron transfer, but the formation MH/MF via hydrogen or fluorine abstraction.

Table 6. Relative energies (in eV) of potential reaction channels of Fe^-, Rb^-, Cs^- (using K^- as a stand-in) with PFP and PFA calculated using CBS-4M methods in Gaussian 09. See computational methods for details.

#	Reaction	Fe^-
1a	$M^- + C_6F_5OH \rightarrow M + [C_6F_5OH]^- \rightarrow M + H + [C_6F_5O]^-$	0.52
1c	$M^- + C_6F_5OH \rightarrow MH + [C_6F_5OH]^-$	-1.63
#	**Reaction**	**K^-**
1a	$M^- + C_6F_5OH \rightarrow M + [C_6F_5OH]^- \rightarrow M + H + [C_6F_5O]^-$	1.08
1b	$M^- + C_6F_5OH \rightarrow M + [C_6F_4OH]^- \rightarrow M + F + [C_6F_5OH]^-$	2.62
1c	$M^- + C_6F_5OH \rightarrow MH + [C_6F_5OH]^-$	-0.63
1d	$M^- + C_6F_5OH \rightarrow MF + [C_6F_4OH]^-$	-2.33
2a	$M^- + C_6F_5NH_2 \rightarrow M + [C_6F_5NH_2]^- \rightarrow H + [C_6F_5NH]^-$	2.18
2b	$M^- + C_6F_5NH_2 \rightarrow M + [C_6F_5NH_2]^- \rightarrow F + [C_6F_4NH_2]^-$	2.97
2c	$M^- + C_6F_5NH_2 \rightarrow MH + [C_6F_5NH]^-$	0.46
2d	$M^- + C_6F_5NH_2 \rightarrow MF + [C_6F_4NH_2]^-$	-1.97

4.3 Loss of HF from PFP/PFA

Evidence from the mass spectrum of gaseous Rb^-, Cs^- and Fe^- colliding with neutral PFP/PFA (Fe^- with PFP only) indicate that loss of HF may result from a number of potential dissociative electron transfer/HF abstraction reaction pathways (Table 7, reactions 3a-3c and 4a-4b). Calculated reaction energies for both PFP and PFA suggest that electron transfer leading to HF dissociation is the least endothermic (Table 7, reactions 3a/4a). Further validation of the identity of the neutral fragments arises from comparison of the electron affinities of various neutral and charged partners involved in the potential reaction pathways. In the case of Fe^- and PFP, if HF abstraction was indeed occurring, we would likely see

FeFH as a product anion due to its much higher electron affinity than C_6F_4O (Table 3). $FeFH^-$ (m/z 76) is never observed. A similar case can be made for the reactions of Rb^- and Cs^- based on the test case of K^- by comparing the electron affinities of KFH and HF (Table 3). Reaction energies of HF abstraction compared to dissociation suggest that dissociation is more energetically favourable by ~ 0.2 eV. Thus both HF and KFH could be potential products based on relative energies alone. The electron affinities of C_6F_4O/C_6F_4NH are much higher than both of the potential neutral products, K + HF or KFH (Table 3). Therefore either neutral product could result based on comparison of electron affinities. However, the electron affinity of HF is much lower than neutral K and KFH suggesting that it would be the most stable product and would better fit the electron transfer and subsequent HF loss reaction pathway hypothesized for the reactions of Cs^- and Rb^-.

Experimental evidence from the appearance energies of the fragments associated with HF loss suggests this is molecular HF formation rather than some other metal based derivative stems from experiments with Fe^-, Cs^- and Rb^- with PFP (notably Fe^-). The appearance of $[C_6F_4O]^-$ corresponds with the appearance of $[C_6F_5OH]^-$. This suggests that dissociative electron transfer producing $[C_6F_4O]^-$ from $[C_6F_5OH]^-$, rather than HF abstraction, is occurring. Direct observation of PFA^- is not possible due to ^{13}C contributions, thus the onset energies of $[C_6F_4NH]^-$ and $[C_6F_5NH_2]^-$ corresponding to HF loss and parent anion formation from PFA cannot be compared, but must be inferred based on chemical similarity to PFP and evidence from the study by Omarsson et al. suggesting a dissociative electron transfer, rather than an abstraction process, is taking place.

Multi-collision reactions, involving both abstraction and dissociation, via the formation of MF + H, MH + F or MF + MH, were not explored due to the low collision

frequencies experienced within the collision cell of the triple quadrupole under the reaction pressures used.

Table 7. Relative energies (in eV) of potential reaction channels of, Rb^- and Cs^- (using K^- as a stand-in) with PFP and PFA calculated using CBS-4M methods in Gaussian 09. See computational methods for details.

#	Reaction	Fe^-
3a	$M^- + C_6F_5OH \rightarrow M + [C_6F_5OH]^- \rightarrow HF + [C_6F_4O]^-$	0.16
3b	$M^- + C_6F_5OH \rightarrow M + [C_6F_5OH]^- \rightarrow H + F + [C_6F_4O]^-$	6.06
3c	$M^- + [C_6F_5OH] \rightarrow MFH + [C_6F_5OH]^-$	3.82
#	**Reaction**	**K^-**
3a	$M^- + C_6F_5OH \rightarrow M + [C_6F_5OH]^- \rightarrow HF + [C_6F_4O]^-$	0.72
3b	$M^- + C_6F_5OH \rightarrow M + [C_6F_5OH]^- \rightarrow H + F + [C_6F_4O]^-$	6.63
3c	$M^- + [C_6F_5OH] \rightarrow MFH + [C_6F_5OH]^-$	0.94
4a	$M^- + C_6F_5NH_2 \rightarrow M + [C_6F_5NH_2]^- \rightarrow HF + [C_6F_4NH]^-$	0.61
4b	$M^- + C_6F_5NH_2 \rightarrow M + [C_6F_5NH_2]^- \rightarrow H + F + [C_6F_4NH]^-$	6.51
4c	$M^- + [C_6F_5NH_2] \rightarrow MFH + [C_6F_4NH]^-$	0.82

4.4 Loss of FHF from PFP/PFA

The final reaction channel to be discussed involving PFP involves the loss of FHF. This reaction channel could be the result of a number of possible dissociation/abstraction channels (Table 8, reactions 5a-5h, 6a-6h).

The two reaction channels with the lowest relative energies involve the concerted abstraction of FHF from neutral PFP/PFA or the abstraction of an F atom followed by the loss of HF (reactions 5d/5f and 6d/6f PFP and PFA respectively). The relative energies of these reactions are separated by ~ 1.20 eV, favouring the formation of M-FHF rather than the two step process required for the formation MF followed by the dissociation HF. FHF loss is observed in electron attachment experiments with PFP at electron energies of 8 eV and is not observed from electron attachment to PFA.[79] The loss of FHF is observed in metal anion collision experiments with PFP and PFA at 0 eV, suggesting that the metal plays a role in this neutral loss from PFP/PFA and further disqualifies electron transfer as the first step in this reaction channel.

Table 8. Relative energies (in eV) of potential reaction channels of, Rb^- and Cs^- (using K^- as a stand-in) with PFP and PFA calculated using CBS-4M methods in Gaussian 09. See computational methods for details.

#	Reaction	K^-
5a	$M^- + C_6F_5OH \rightarrow M + [C_6F_5OH]^- \rightarrow F_2 + H + [C_6F_3O]^-$	3.87
5b	$M^- + C_6F_5OH \rightarrow M + [C_6F_5OH]^- \rightarrow FH + F + [C_6F_3O]^-$	8.31
5c	$M^- + C_6F_5OH \rightarrow M + [C_6F_5OH]^- \rightarrow FHF + [C_6F_3O]^-$	3.82
5d	$M^- + C_6F_5OH \rightarrow MFHF + [C_6F_3O]^-$	-2.32
5e	$M^- + C_6F_5OH \rightarrow MFH + F + [C_6F_3O]^-$	4.04
5f	$M^- + C_6F_5OH \rightarrow MF + HF + [C_6F_3O]^-$	-1.13
5g	$M^- + C_6F_5OH \rightarrow MF_2 + H + [C_6F_3O]^-$	4.44
5h	$M^- + C_6F_5OH \rightarrow MH + F_2 + [C_6F_3O]^-$	6.59
6a	$M^- + C_6F_5NH_2 \rightarrow M + [C_6F_5NH_2]^- \rightarrow FHF + [C_6F_3NH]^-$	5.37
6b	$M^- + C_6F_5NH_2 \rightarrow M + [C_6F_5NH_2]^- \rightarrow FH + F + [C_6F_3NH]^-$	5.32
6c	$M^- + C_6F_5NH_2 \rightarrow M + [C_6F_5NH_2]^- \rightarrow F_2 + H + [C_6F_3NH]^-$	9.80
6d	$M^- + C_6F_5NH_2 \rightarrow MFHF + [C_6F_3NH]^-$	-0.83
6e	$M^- + C_6F_5NH_2 \rightarrow MFH + F + [C_6F_3NH]^-$	5.53
6f	$M^- + C_6F_5NH_2 \rightarrow MF + HF + [C_6F_3NH]^-$	0.37
6g	$M^- + C_6F_5NH_2 \rightarrow MF_2 + H + [C_6F_3NH]^-$	5.94
6h	$M^- + C_6F_5NH_2 \rightarrow MH + F_2 + [C_6F_3NH]^-$	8.09

4.5 Loss of 2 HF from PFA

There are many potential reaction channels that could result in $[PFA-2(HF)]^-$ (Table 9, reactions 7a-7h). The lowest energy pathway, based on relative energies involves electron transfer to PFA followed by the sequential loss of 2 HF molecules. Ommarson et. al. also observed the loss of two HF molecules from PFA in their electron attachment experiments, further suggesting that this fragment anion is the result of the sequential loss of two HF molecules.[79]

Table 9. Relative energies (in eV) of potential reaction channels of, Rb^- and Cs^- (using K^- as a stand-in) with PFP and PFA calculated using CBS-4M methods in Gaussian 09. See computational methods for details.

#	Reaction	K^-
7a	$M^- + C_6F_5NH_2 \rightarrow 2HF + [C_6F_3N]^-$	2.74
7b	$M^- + C_6F_5NH_2 \rightarrow 2H + 2F + [C_6F_3N]^-$	7.29
7c	$M^- + C_6F_5NH_2 \rightarrow FHF + H + [C_6F_3N]^-$	8.70
7d	$M^- + C_6F_5NH_2 \rightarrow 2\ M\text{-}HF + [C_6F_3N]^-$	9.06
7e	$M^- + C_6F_5NH_2 \rightarrow M\text{-}FHF + H + [C_6F_3N]^-$	3.85
7f	$M^- + C_6F_5NH_2 \rightarrow M\text{-}FHF + H + [C_6F_3N]^-$	8.70
7g	$M^- + C_6F_5NH_2 \rightarrow M\text{-}F_2 + H_2 + [C_6F_3N]^-$	13.13
7h	$M^- + C_6F_5NH_2 \rightarrow 2\ M\text{-}H + 2\ M\text{-}F + [C_6F_3N]^-$	3.26

4.6 Conclusions

Table 10 displays a summary of the resultant anions and neutral products of collisions between gaseous Cs^-/Rb^- and Fe^- with neutral PFA/ PFP.Global similarities in the fragmentation products of PFP and PFA from collisions with Cs^-, Rb^- and Fe^- in comparison to those observed by Omarsson et al. is a strong indication that dissociative electron transfer is occurring.[78,79] The strongest evidence comes from reactions of Cs^- with PFP and PFA. The high flux of Cs^- allowed all of the fragment anions observed via electron attachment to PFP/PFA by Omarsson et al. to also be observed in the spectrums produced by Cs^- and PFP/PFA (Figures 18-20). The trend observed within this data set suggests that a positive temperature dependence exists in the formation of product anions as a result of dissociative electron transfer. The data suggests that no positive temperature dependence occurs in the production of fragment anions resulting from reactions where the metal anion plays a direct role, such as H,F or FHF loss. Contrasting the electron affinities of PFP (0.25 eV), PFA (0.05 eV) and the test metal anion K (0.68), as well as the knowledge that a positive temperature dependence denotes an internal energy barrier to electron transfer, [65-68] the statement can be made that 1) dissociative electron transfer from Cs^- and Rb^- is thermodynamically controlled and that 2) significant geometric rearrangement is required to form some of the dissociative product anions, due to their positive temperature dependence (Figure 18 E-F, Figure 20 B-F). Furthermore, the data demonstrates that dissociative electron transfer can occur without an internal energy barrier for strongly exothermic channels, demonstrated by the high intensity of HF loss from PFP and the 0 eV onset energy required (Figure 18/19 C). The ease of its formation is likely to due to strong hydrogen bonding between the F and H atoms which maintain a geometry closely close to that $C_6F_4O^-$,

resulting in little to no energy barrier for this reaction. Strong hydrogen bonding was also suggested to play a significant role in the high relative intensities of $C_6F_4O^-$ noted by Omarsson et al. in their electron attachment studies.[78,79] However, the loss of HF from PFA shows a positive temperature dependency, suggesting there is significant geometric rearrangement required for electron transfer and subsequent loss of HF (Figure 20/21). This corresponds well to the attachment energy observed by Omarsson et al. who found the highest cross sections of HF loss from PFA required an electron of ~1.5 eV.[78,79] This agrees with the observation that extra internal energy acquired by increasing the centre of mass collision energy of Cs^- with PFA is required for dissociative electron transfer to occur. Different from the reactions of NO, NO_2 and SO_2, is the tendency of PFP and PFA to dissociate into various fragments. The relative energies of these dissociation pathways suggest that they are thermodynamically accessible given the internal energies of the initial PFP and PFA neutral molecules, while those of NO, NO_2 and SO_2 are not. Thus, dissociative electron transfer, similar to dissociative electron attachment, is thermodynamically and kinetically controlled depending on molecular geometry and relative electron affinities.

Table 10. Calculated (CBS-4M) Relative Reaction Energies for the most likely reaction pathways of Fe^- and K^-. K^- was used as a stand-in for calculations regarding Cs^- and Rb^- due to limitations within the computational method chosen.

Reaction Number	Incident Anion	Collision Partner	Neutral Product	Product Anion	m/z	Relative Energy
	Fe^-	**C_6F_5OH**				
1			Fe	$[C_6F_5OH]^-$	184	-0.14
1c			FeH	$[C_6F_5O]^-$	183	-1.63
3a			Fe + HF	$[C_6F_4OH]^-$	164	0.16
	K^-	**C_6F_5OH**				
1			K	$[C_6F_5OH]^-$	184	0.43
1c			KH	$[C_6F_5O]^-$	183	-0.63
1d			KF	$[C_6F_4OH]^-$	165	-2.33
3a			K + HF	$[C_6F_4O]^-$	164	0.72
3c			KHF	$[C_6F_4O]^-$	164	0.94
5d			KFHF	$[C_6F_3O]^-$	145	-2.32
5f			KF + HF	$[C_6F_3O]^-$	145	-1.13
	K^-	**$C_6F_5NH_2$**				
2			K	$[C_6F_5NH_2]^-$	183	0.63
2c			KH	$[C_6F_5NH]^-$	182	0.46
2d			KF	$[C_6F_4NH_2]^-$	164	-1.97
4a			K + HF	$[C_6F_4NH]^-$	163	0.61
4c			KHF	$[C_6F_4NH]^-$	163	0.82
6d			KFHF	$[C_6F_3NH]^-$	144	-0.83
6f			KF + HF	$[C_6F_3NH]^-$	144	0.37
7a			K + 2HF	$[C_6F_3N]^-$	143	2.74

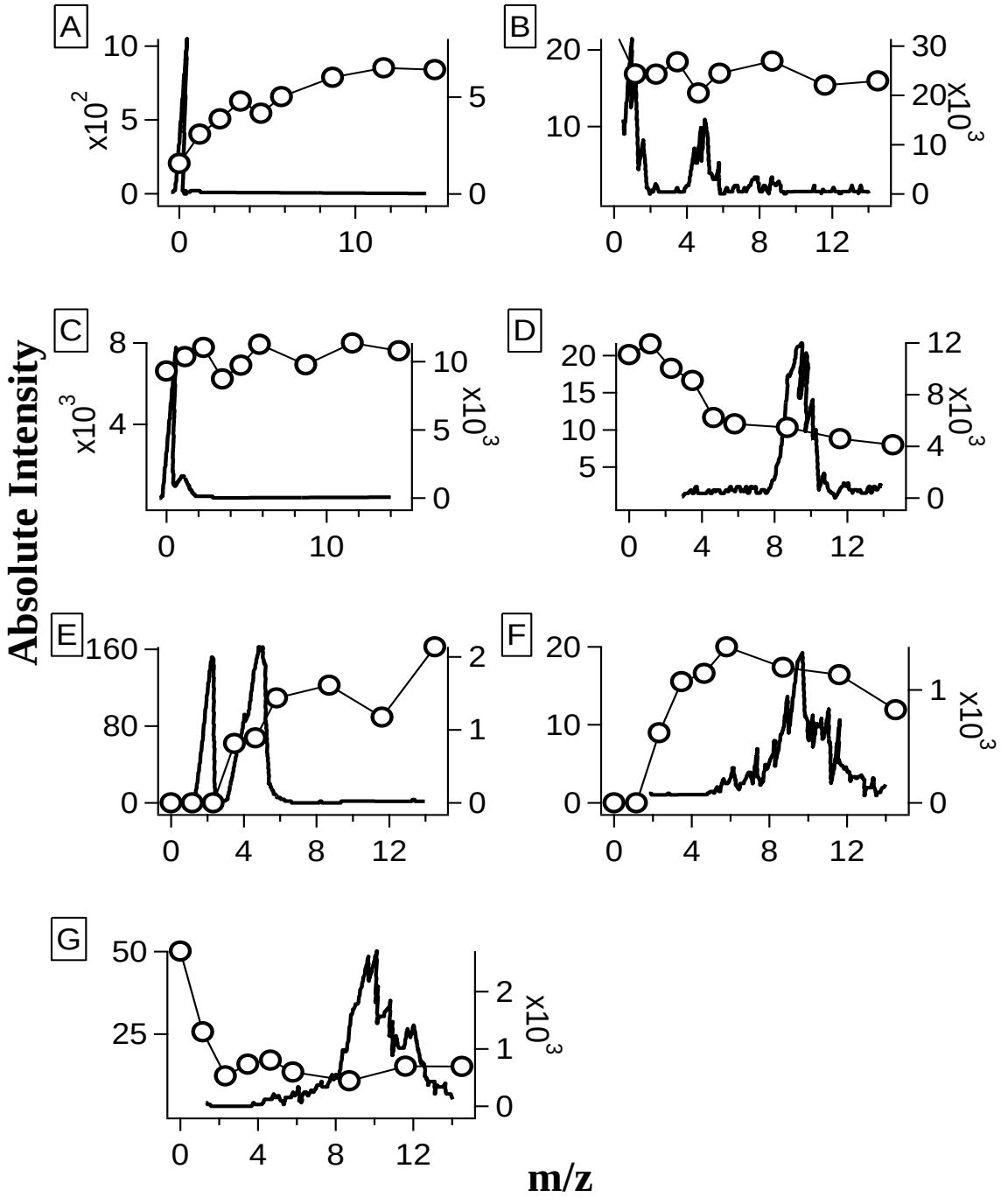

Figure 18. Intensity (left/right axis) vs. energy (eV) of the product anions from electron attachment (naked line, left axis) and electron transfer from Cs^- (line with circles, right axis) to pentafluorophenol (PFP). A) m/z 184, denoting $C_6F_5OH^-$ B) m/z 183, denoting $C_6F_5O^-$ C) m/z 164, denoting $C_6F_4O^-$ D) m/z 145, denoting $C_6F_3O^-$ E) m/z 136, denoting $C_6F_4O^-$ F) m/z 117, denoting $C_6F_3O^-$ G) m/z 19, denoting F^-. Pressure of gaseous PFP was set to 1.8 x 10^{-4} torr.

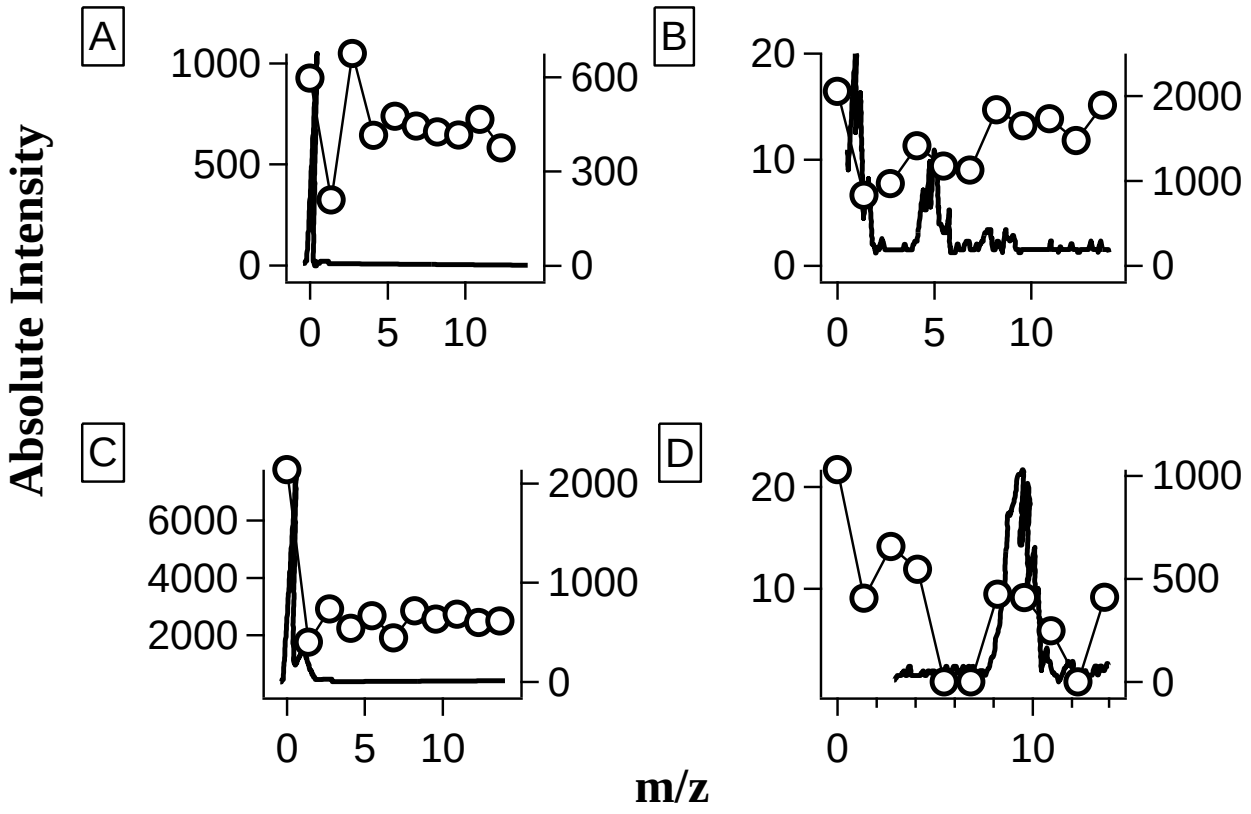

Figure 19. Intensity (left/right axis) vs. energy (eV) of the product anions from electron attachment (naked line, left axis) and electron transfer from Rb^- (line with circles, right axis) to pentafluorophenol (PFP). A) m/z 184, denoting $C_6F_5OH^-$ B) m/z 183, denoting $C_6F_5O^-$ C) m/z 164, denoting $C_6F_4O^-$ D) m/z 145, denoting $C_6F_3O^-$. Pressure of gaseous PFP was set to 1.1 x 10^{-4} torr.

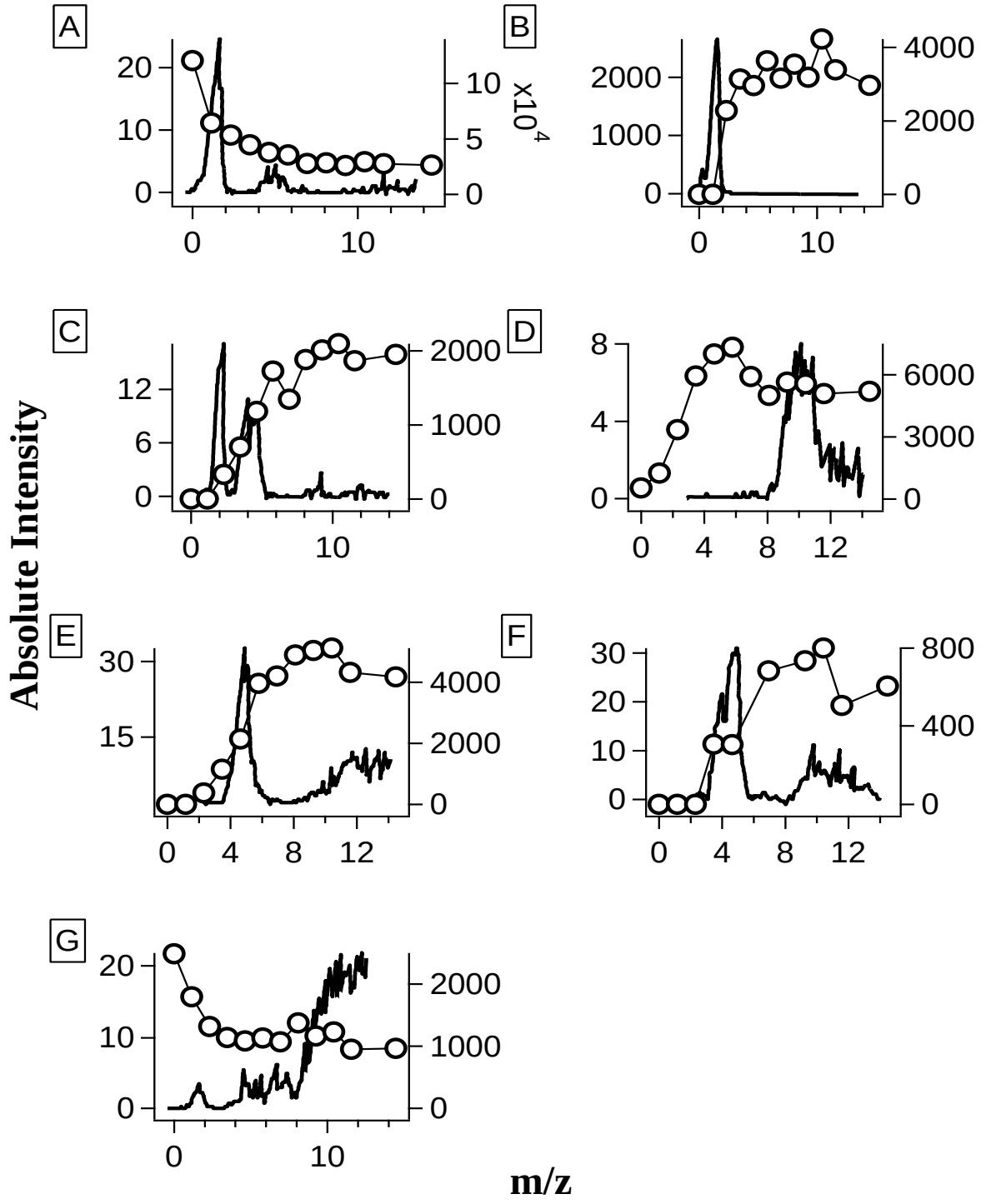

Figure 20. Intensity (left/right axis) vs. energy (eV) of the product anions from electron attachment (naked line, left axis) and electron transfer from Cs^- (line with circles, right axis) to pentafluoraniline (PFA). A) m/z 183, denoting $C_6F_5NH^-$ B) m/z 163, denoting $C_6F_4NH^-$ C) m/z 143, denoting $C_4F_3N^-$ D) m/z 124, denoting C_4F_4 E) m/z 74, denoting $C_3F_2^-$ F) m/z 26, denoting CN^- G) m/z 19, denoting F^-. Pressure of gaseous PFA was 2.2 x 10^{-4} torr.

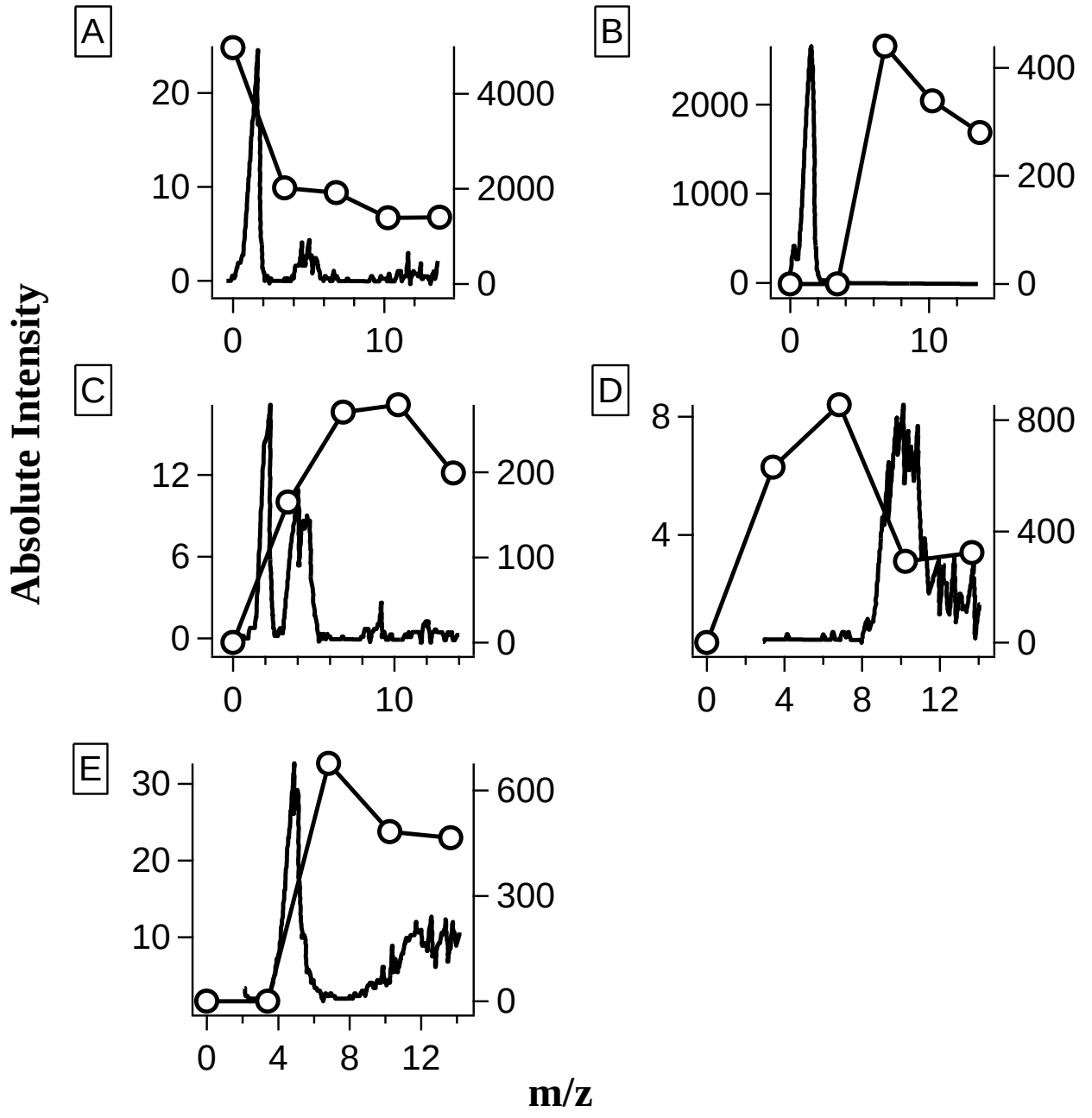

Figure 21. Intensity (left/right axis) vs. energy (eV) of the product anions from electron attachment (naked line, left axis) and electron transfer from Rb^- (line with circles, right axis) to pentafluoraniline (PFA). A) m/z 183, denoting $C_6F_5NH^-$ B) m/z 163, denoting $C_6F_4NH^-$ C) m/z 143, denoting $C_4F_3N^-$ D) m/z 124, denoting C_4F_4 E) m/z 74, denoting $C_3F_2^-$. Pressure of gaseous PFA was 2.2 x 10^{-4} torr.

Chapter 5 – Reactions of Fe^-, Cs^- and Cu^- with perfluorinated compounds

5.1 Pentafluoroaniline

Observations of FeF_3^- and CuF_2^- from collisions of Fe^-/Cu^- with pentafluoroaniline were the first indications that Cu^- and Fe^- react to produce metal adduct molecular anions (Figure 22). It is curious that Fe^- did not produce any electron transfer products with pentafluoroaniline (PFA), but did with pentafluorophenol (PFP). This may be a result of the much higher absolute intensity of fragment anions produced via electron transfer and electron attachment with PFP compared with PFA (Figures 18-21).[78,79]

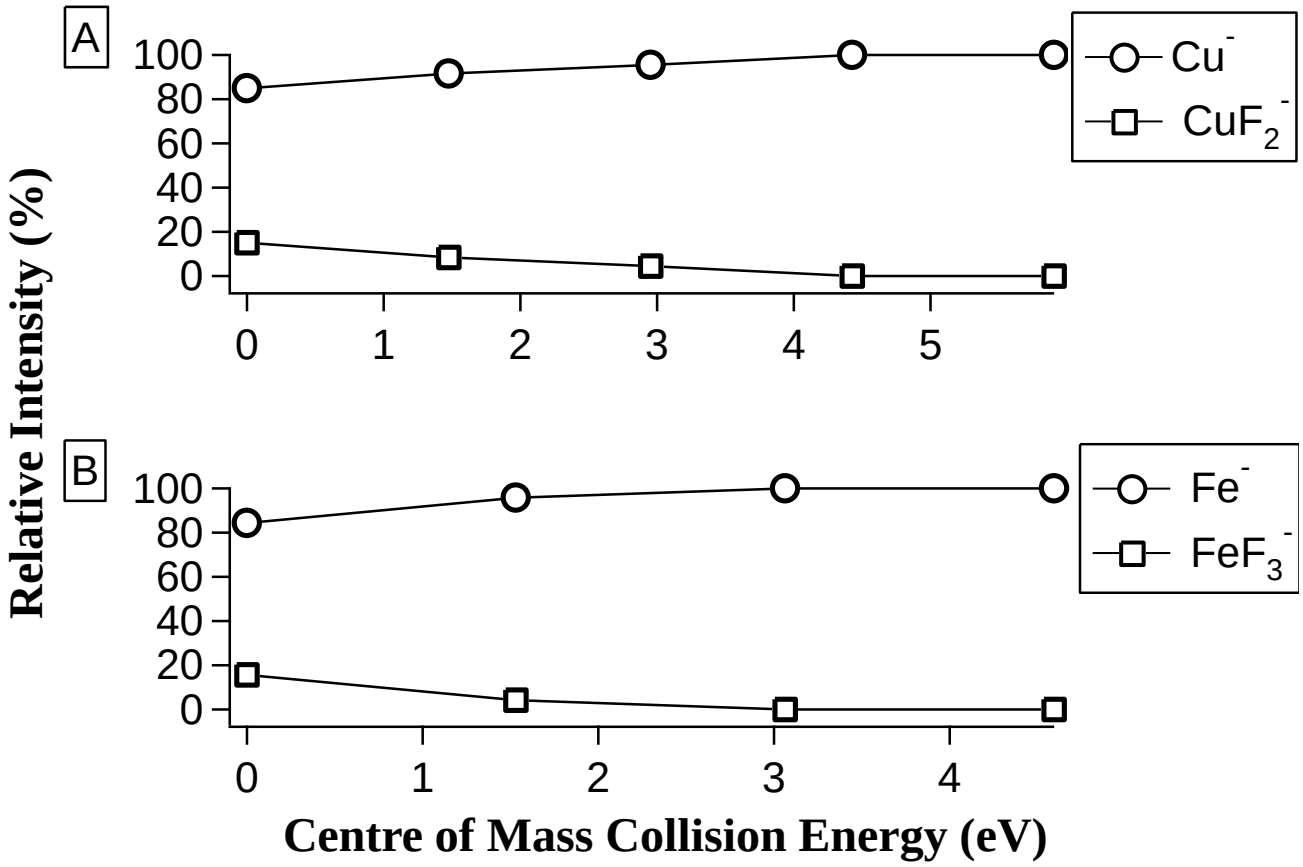

Figure 22. Reactions of A) Cu^- and B) Fe^- with pentafluoroaniline. The Y axis corresponds to relative intensity (%) while the X-axis corresponds to centre of mass collision energy. Pressure of gaseous PFA was A) 1.7 x 10^{-4} and B) 1.1 x 10^{-4} torr.

5.2 Hexaflurobenzene

Electron attachment to neutral C_6F_6 produces intact $C_6F_6^-$.[80] Therefore, given the quenching nature of electron transfer from atomic anions, electron transfer should also produce the intact anion.[8] Fe^- was observed to produce $C_6F_6^-$, while Cu^- was not. The electron affinity of C_6F_6 is 0.7 eV as measured via LPES, thus it is not surprising that Fe^- (EA 0.15 eV) is able to transfer its electron, while Cu^- (EA 1.2 eV) is not.[7,81] Furthermore, the high relative intensity of CuF_2^- (~50%) suggests this reaction channel would dominate the potential energy surface (Figure 23). Given that C_6F_6 does not produce F^- from electron attachment,[81] the formation of $C_6F_5^-$ is likely due to fluorine abstraction to form neutral CuF and FeF (Figure 23). No electron affinity information is available for CuF or FeF, however $C_6F_5^-$ possesses an electron affinity ranging from 2.48-3.18 eV depending on the author/method.[82-84] Given that only neutral CuF and FeF are the likely reaction partners of $C_6F_5^-$, it can be stated that the upper limit on the electron affinities of these molecules is less 3.18 eV. Increasing centre of mass collision energy favours the formation of CuF and FeF as well as electron transfer from Fe^- to C_6F_6 while decreasing the relative intensity of CuF_2^- and FeF_3^- (Figure 23). The positive temperature dependence of electron transfer from Fe^- to C_6F_6 suggests the presence of an internal energy barrier with regard to electron transfer. [65-68] The reactions forming FeF/FeF_3^- both have onsets of 0 eV, suggesting that both are thermodynamically accessible. Increasing centre of mass collision energy favours the formation of CuF over CuF_2^-. The formation CuF_2^- is favoured over F abstraction forming $C_6F_5^-$/CuF as demonstrated by its high relative intensity (~50%) at 0 eV (Figure 23 B).

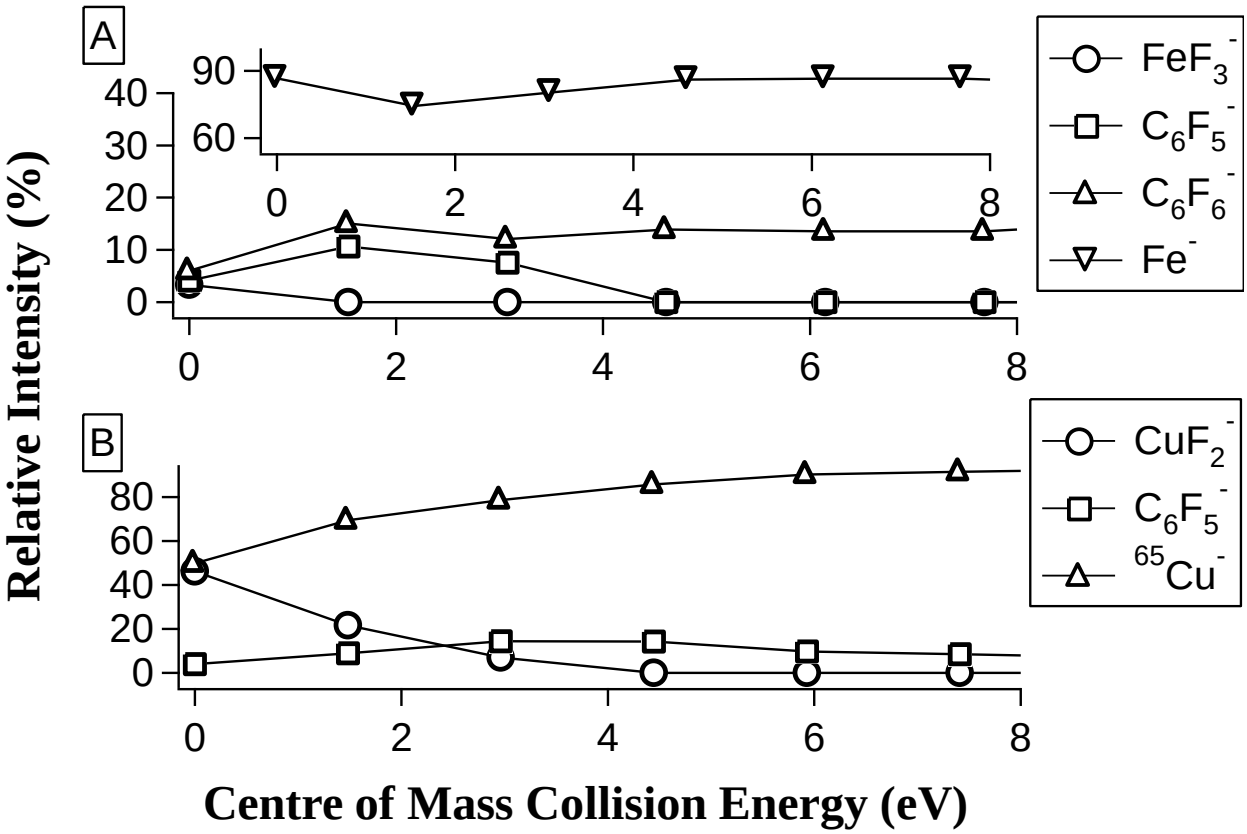

Figure 23. Reactions of A) Fe^- and B) Cu^- with hexafluorobenzene. The Y axis corresponds to relative intensity (%) while the X-axis corresponds to centre of mass collision energy. Pressure of gaseous hexafluorobenzene was A) 1.1 x 10^{-4} and B) 3.0 x 10^{-4} torr.

5.3 Trans-octafluoro-butene

Fe^- reacts with trans-2-octafluorobutene to produce $C_4F_8^-$, FeF_3^- and FeF^- (Figure 24 B). The production of FeF_3^- and FeF^- occur at 0 eV with the highest relative intensities and decrease with additional energy. The relative intensity of $C_4F_8^-$ increases with increasing centre of mass collision energy suggesting an internal energy barrier for the electron transfer from Fe^- to C_4F_8. The presence of FeF^- demonstrates that fluorine abstraction via Fe^- is a viable reaction pathway. Taking into account that gaseous Fe^- and C_6F_6 results in the formation of FeF and $C_6F_5^-$, the formation of FeF^- suggests that the electron affinity of C_4F_7

is below both C_6F_5 and FeF (EA 3.18-2.48 eV for C_6F_5 > EA FeF > EA C_4F_7). No electron affinity data for C_4F_7 is currently available, thus this reaction is able to provide an upper limit for this value.

Cu^- reacts with trans-2-octafluorobutene to produce $C_4F_8^-$, $C_4F_7^-$, F^-, CuF_2^- and CuF^- (Figure 24 A). The production of CuF_2^-occurs at high relative intensity at 0 eV and decreases with additional centre of mass collision energy. The production of $C_4F_8^-$, $C_4F_7^-$, F^- and CuF^- increase with additional centre of mass collision energy, but remain at very low relative intensities. The presence of both $C_4F_7^-$ and CuF^- suggests a charge competition between these two molecules and place the electron binding energy of both below that of FeF^- when taking into account the known electron affinity of C_6F_5 and the assumed production of neutral FeF via fluorine abstraction (Figure 23 A). The increase in relative intensity of $C_4F_8^-$ with increasing centre of mass collision energy suggests an internal energy barrier for the electron transfer from Cu^- to C_4F_8.

Electron attachment of electrons, < 8 eV in energy, to 2-C_4F_8 produced $C_4F_8^-$, $C_4F_7^-$, $C_4F_6^-$, $C_3F_5^-$, $C_3F_3^-$, $C_2F_3^-$, CF_3^- and F^- fragments.[85] $C_4F_8^-$ was the only product observed at significant intensities at 0 eV,[85] while all others occurred at > 3 eV, thus it is not surprising that they were not observed from electron transfer. The production of F^- was observed during collisions of Cu^- and C_4F_8. That it does not occur with collisions Fe^- and C_4F_8 and suggests a reaction mechanism specific to Cu^-.

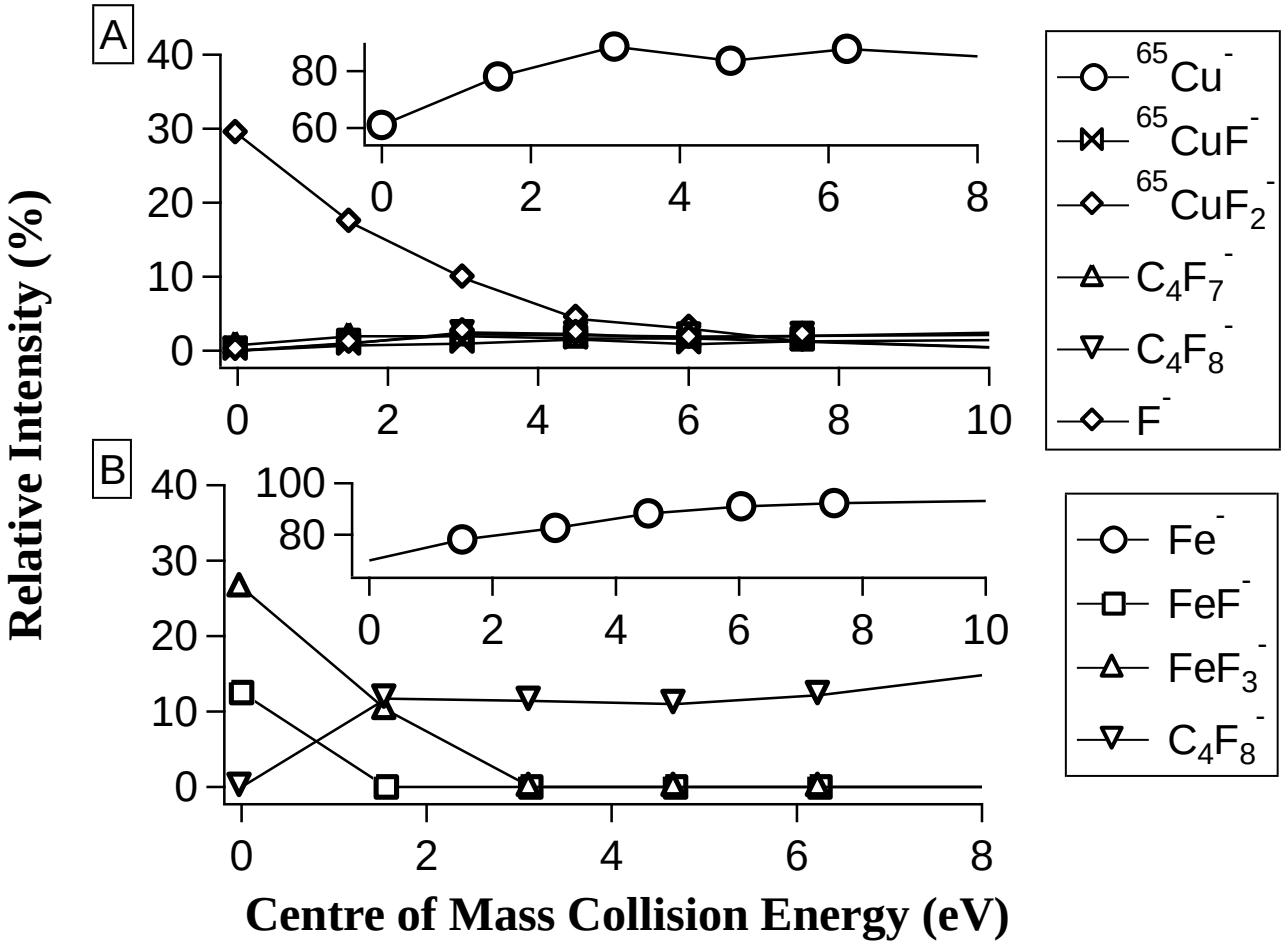

Figure 24. Reactions of A) Fe^- and B) Cu^- with trans-2-fluorobutene. The Y axis corresponds to relative intensity (%) while the X-axis corresponds to centre of mass collision energy. Pressure of gaseous octafluorobutene was A) 3.2×10^{-4} and B) 4.6×10^{-4} torr.

5.4 (1,2,3) (1,2,4) and (1,3,5)-trifluorobenzene

Fe^-, Cu^- and Cs^- were reacted with (1,2,3), (1,2,4) and (1,3,5) trifluorobenzene with a view to explore if positional identity played a role in the formation of adducts anions. The metal anions were able to generate many of the same fragment anions generated from electron transfer. Novel products involving the metal anions were also observed. Cu^- and Cs^- were not reacted with 1,2,3 trifluorobenzene due to a limited quantity of the reactant available.

5.4.1 Fe^-

The reactions of Fe^- are difficult to deduce due to the isobaric nature of the potential fragment identities. For example, m/z 113 could be FeF_3^- or $C_6F_2H_3^-$, m/z 94 could be FeF_2^- or $C_6H_3F^-$ and m/z 75 could be FeF^- or $C_6H_3^-$. M/z 75 and 94 are novel to reactions involving Fe^- (unobserved from reactions with Cu^- and Cs^-), therefore it is likely that these are FeF^- and FeF_2^- respectively. However, m/z 113 is present in all other reactions, making the assignment of m/z 113 to that of FeF_3^- or $C_6FH_3^-$ difficult. Based on the low relative intensity of FeF produced via reactions of Fe^- with C_6F_6, the low intensity of FeF^- observed with E-octafluoro-butene and the lack of any single F abstraction products observed with PFP/PFA, it is likely that m/z 113 is a result of the formation of FeF_3^- and rather than $C_6F_2H_3^-$.

Fe^- was reacted with all three variants (Figures 25-27). Comparison of the relative intensities suggests that the position of the fluorine atoms does play a role in the formation of FeF_2^- and FeF_3^-. Comparison of the 1,3,5 and 1,2,4 trifluorobenzene (Figures 26 and 27) gives initial clues as to how these reactions take place. The intensity of both FeF_2^- and FeF_3^-

increased when two fluorine atoms were side by side in 1,2,4 $C_6F_3H_3$ relative to 1,3,5, $C_6F_3H_3$, producing FeF_2^- at 30/36% relative intensity and FeF_3^- at 6%/9% relative intensity at 0 eV. Contrasting this with the reactions of Fe^- and 1,2,3 $C_6F_3H_3$ (Figure 25) we find that Fe^- reactions with this molecule produced FeF_2^- (13%) relative to FeF_3^- (31%). This result suggests that having all three fluorine atoms side by side (as in the case of 1,2,3 trifluorobenzene) enables FeF_3^- formation much more readily, suggesting positional identity is important in these reaction channels and the formation of FeF_3^-.

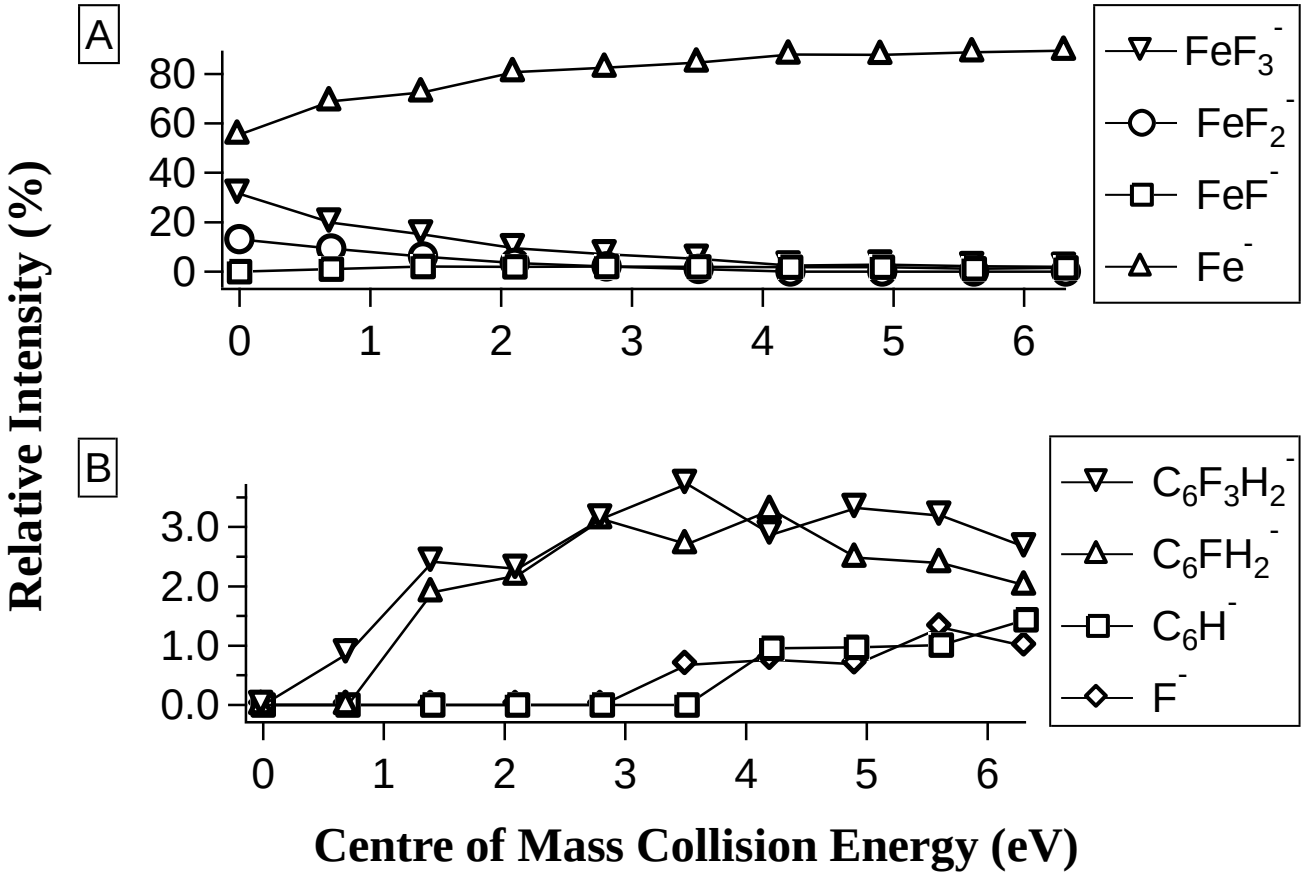

Figure 25. Reactions of Fe^- with 1,2,3 trifluorobenzene. Panel A) showcases charged metal-based species observed while B) showcases all other charged fragments. The Y axis corresponds to relative intensity (%) while the X-axis corresponds to centre of mass collision energy. Pressure of gaseous 1,2,3 trifluorobenzene was 3.9 x 10^{-4} torr.

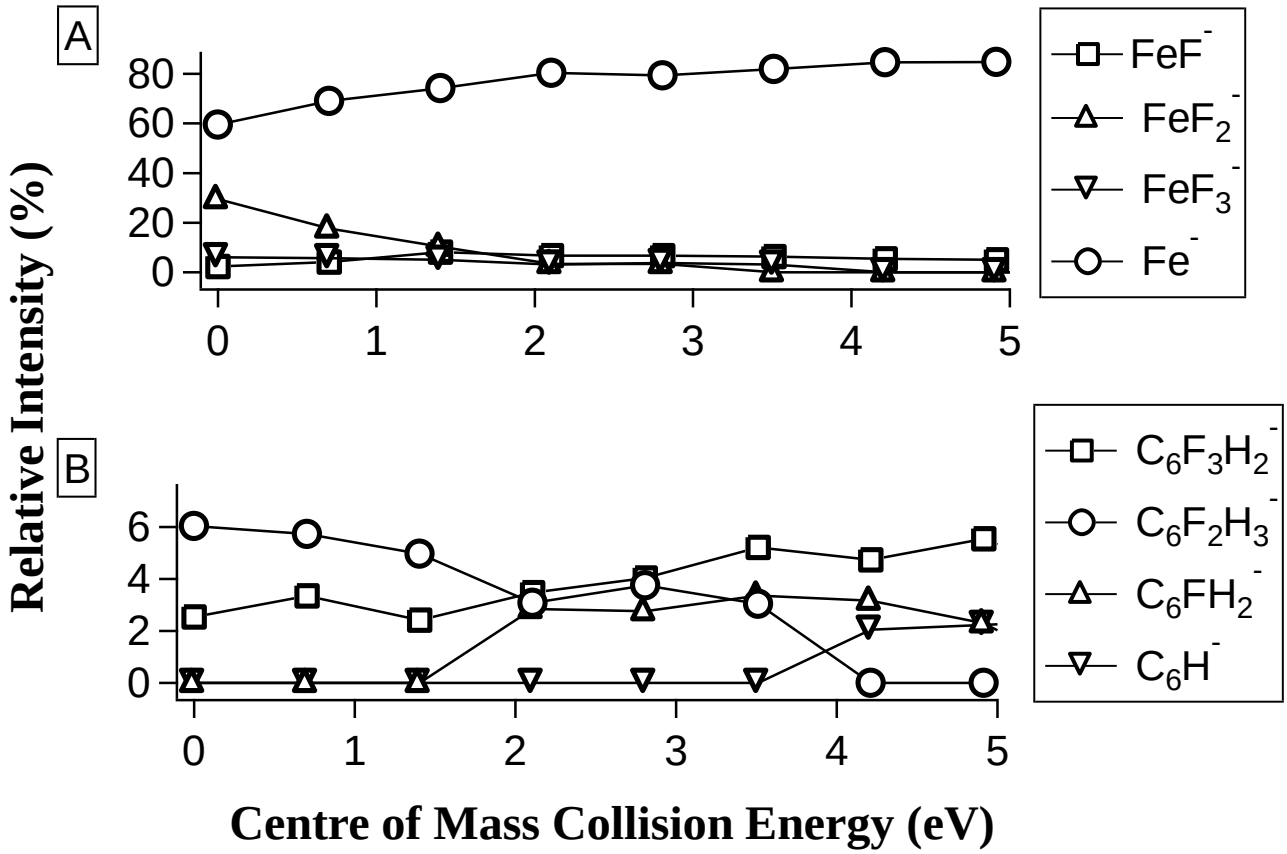

Figure 26. Reactions of Fe^- with 1,3,5 trifluorobenzene. Panel A) showcases charged metal-based species observed while B) showcases all other charged fragments. The Y axis corresponds to relative intensity (%) while the X-axis corresponds to centre of mass collision energy. Pressure of gaseous 1,3,5 trifluorobenzene was 4.5 x 10^{-4} torr.

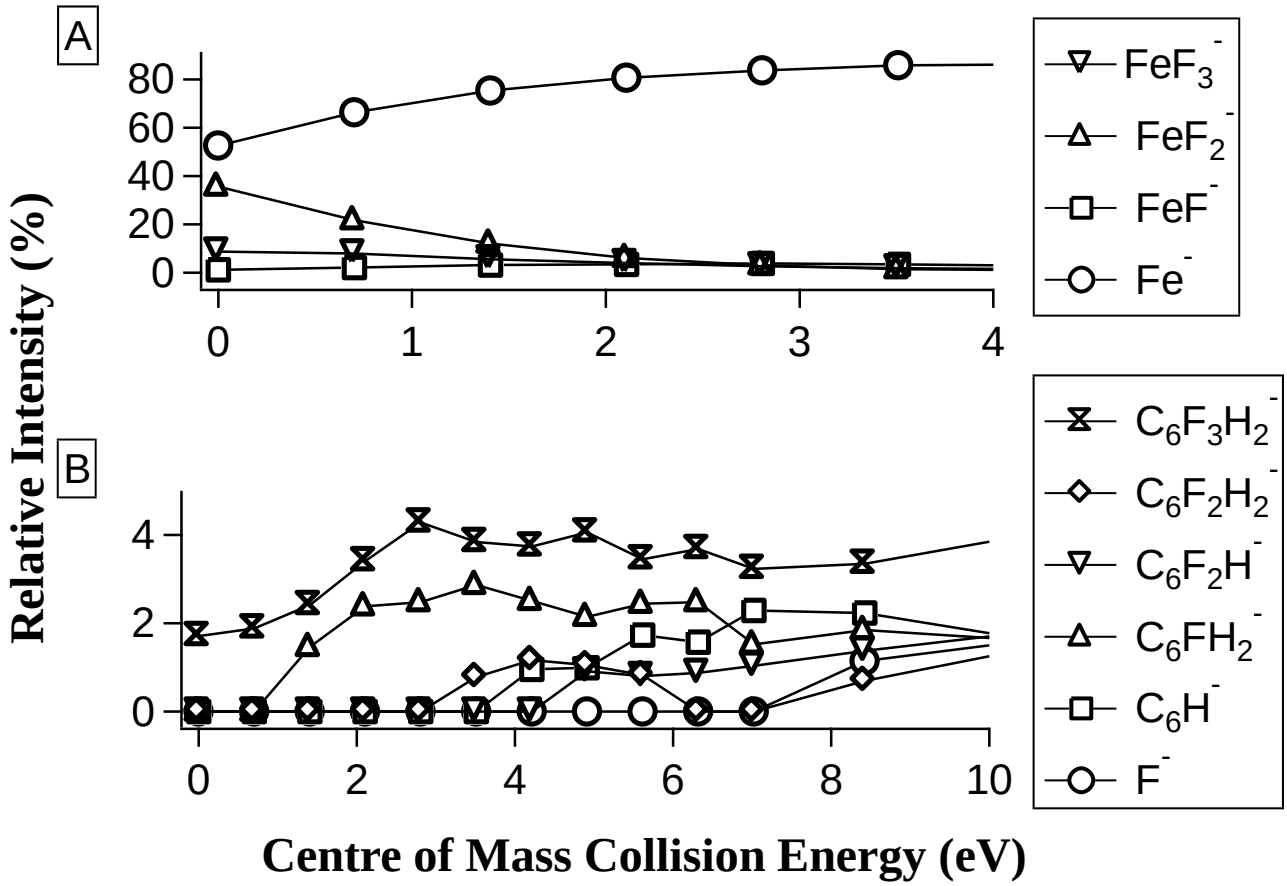

Figure 27. Reactions of Fe^- with 1,2,4 trifluorobenzene. Panel A) showcases charged metal-based species observed while B) showcases all other charged fragments. The Y axis corresponds to relative intensity (%) while the X-axis corresponds to centre of mass collision energy. Pressure of gaseous 1,2,4 trifluorobenzene was 3.9×10^{-4} torr.

5.4.2 Cu^-

Reactions of Cu^- with 1,3,5 and 1,2,4 trifluorobenzene show the formation of CuF^- and CuF_2^-at low relative intensities. Fragment anions $C_6F_3H_2^-$ and $C_6F_2H_3^-$ suggest the formation of neutral CuH as well as CuF. As observed from previous experiments with perfluorinated compounds, the formation of CuF_2^- is thermodynamically favoured, while the formation of CuF^- is favoured at higher centre of mass collision energies (Figures 28-29). There is apparent charge competition between the formation of CuF^- and $C_6F_2H_3^-$ (Figures 28-29).

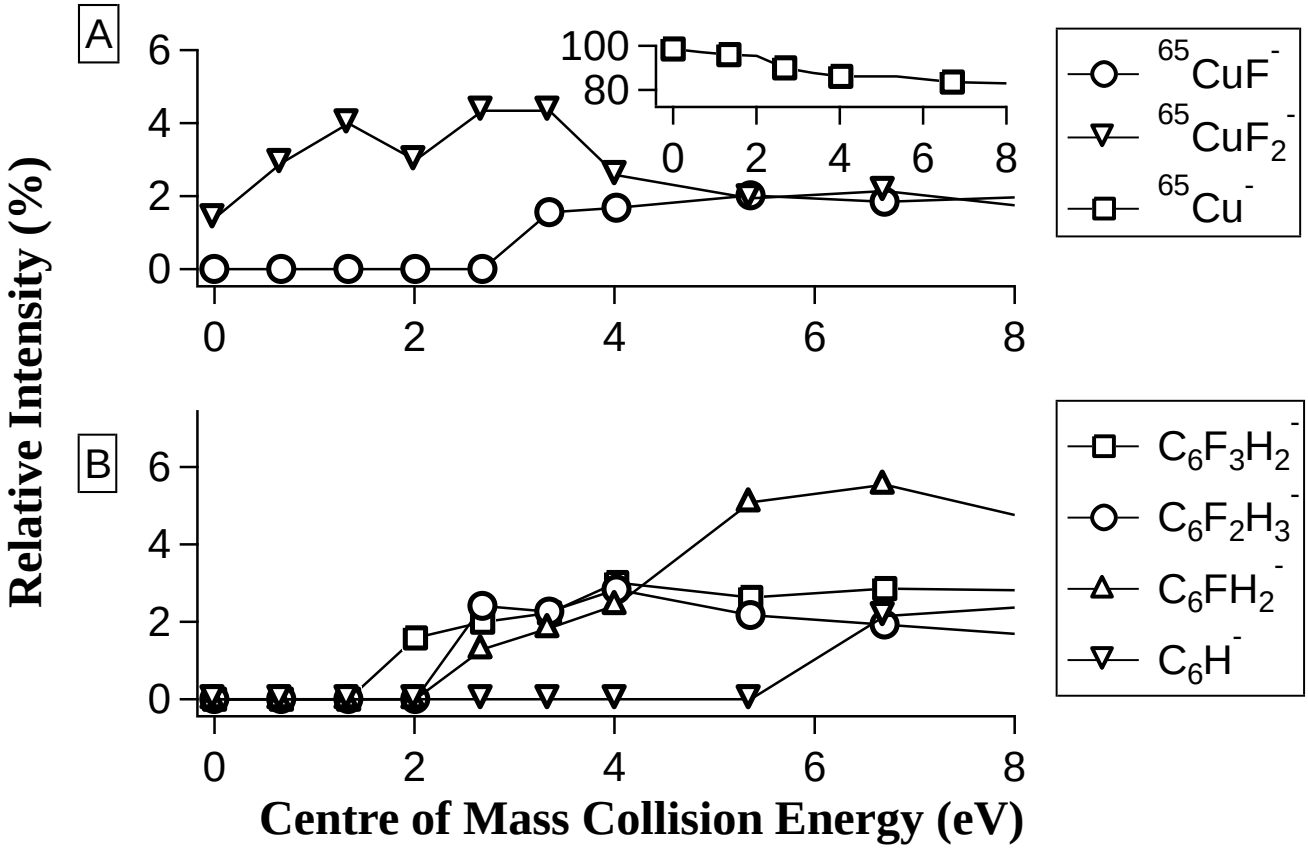

Figure 28. Reactions of Cu^- with 1,3,5 trifluorobenzene. Panel A) showcases charged metal-based species observed while B) showcases all other charged fragments. The Y axis corresponds to relative intensity (%) while the X-axis corresponds to centre of mass collision energy. Pressure of gaseous 1,3,5 trifluorobenzene was 5.0 x 10^{-4} torr.

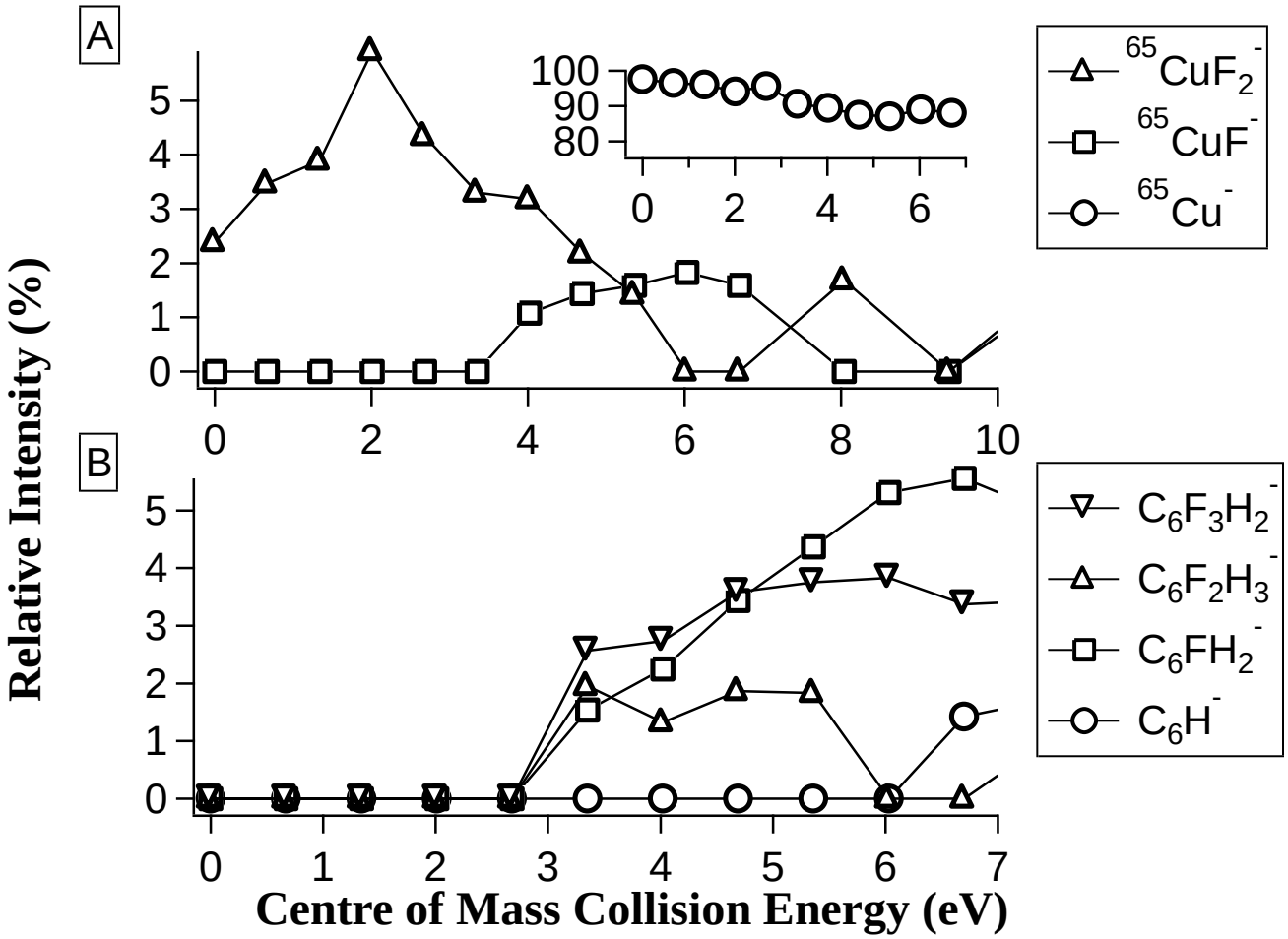

Figure 29. Reactions of Cu^- with 1,2,4 trifluorobenzene. Panel A) showcases charged metal-based species observed while B) showcases all other charged fragments. The Y axis corresponds to relative intensity (%) while the X-axis corresponds to centre of mass collision energy. Pressure of gaseous 1,2,4 trifluorobenzene was 5.0 x 10^{-4} torr.

5.4.3 Cs^-

Cs^- was also reacted with 1,3,5 and 1,2,4 trifluorbenzene. Products anions $C_6F_3H_2^-$ and $C_6F_2H_3$- suggest the formation of neutral CsH and CsF. Fragments of m/z 93 and 73 corresponding to $C_6FH_2^-$ and C_6H^- were also observed. The most interesting products observed were CsF^- as well as CsF_2^-; CsF_2^-could be either $[F\text{-}Cs\text{-}F]^-$ or $[Cs\text{-}F\text{-}F]^-$. Both Cu^- and Cs^- possess highest occupied molecular orbitals of $4s^2$ and $6s^2$.[1,6] Thus it would appear that the formation of these difluoride anions is related to the orbital configurations of these two metal anions.

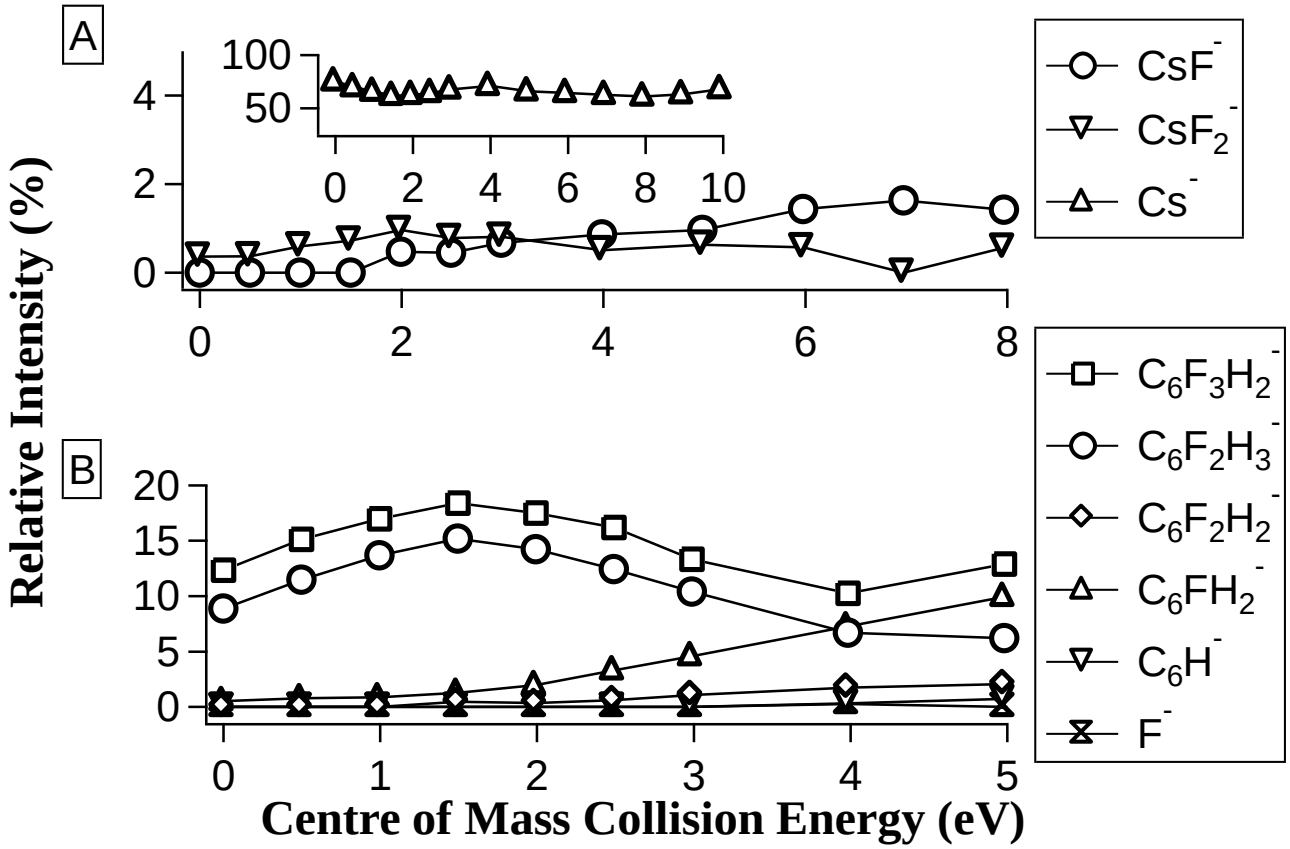

Figure 30. Reactions of Cs^- with 1,3,5 trifluorobenzene. Panel A) showcases charged metal-based species observed while B) showcases all other charged fragments. The Y axis corresponds to relative intensity (%) while the X-axis corresponds to centre of mass collision energy. Pressure of gaseous 1,3,5 trifluorobenzene was 4.8 x 10^{-4} torr.

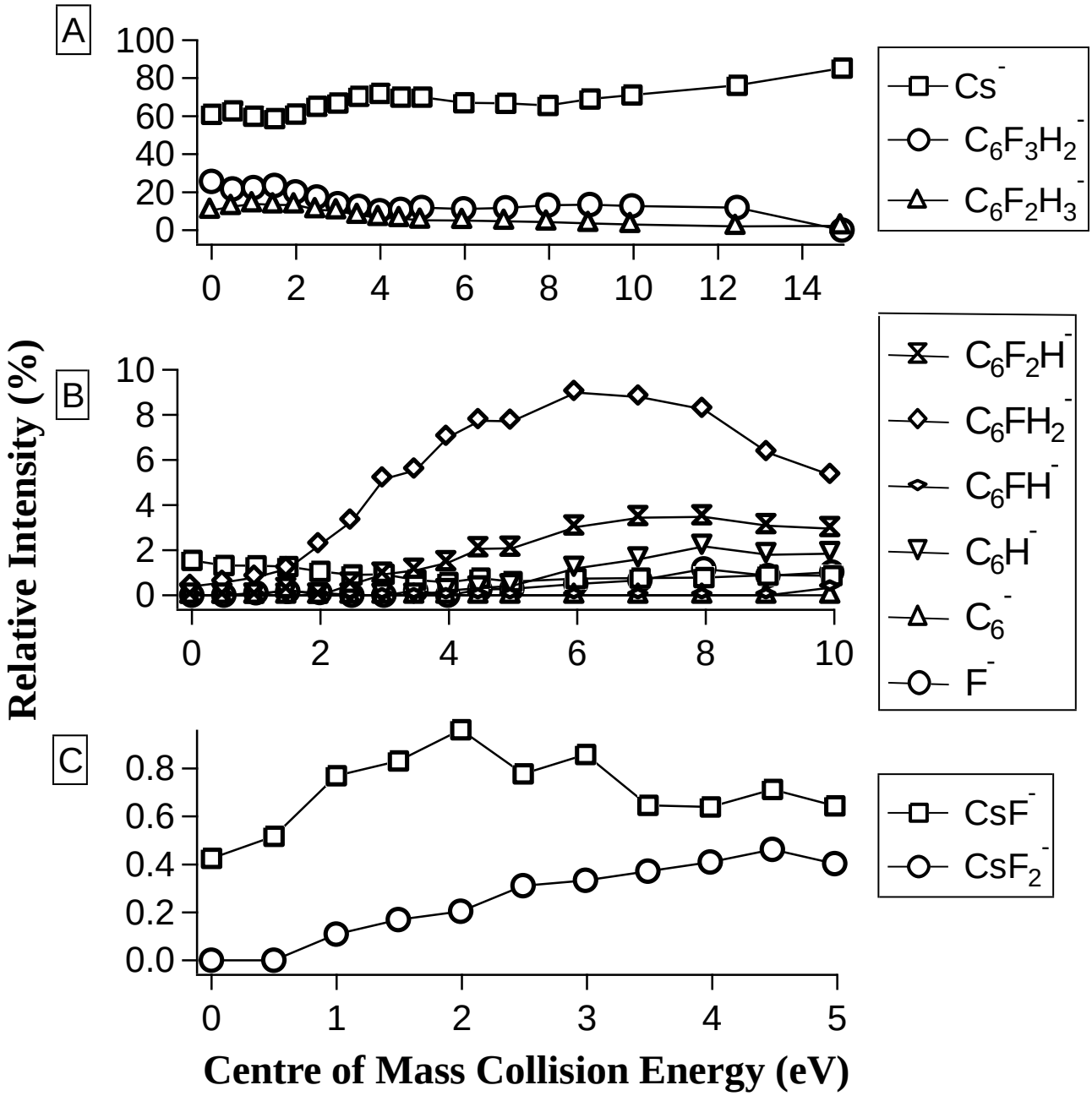

Figure 31. Reactions of Cs^- with 1,2,4 trifluorobenzene. Panel A) showcases charged metal-based species observed while B) showcases all other charged fragments. The Y axis corresponds to relative intensity (%) while the X-axis corresponds to centre of mass collision energy. Pressure of gaseous 1,2,4 trifluorobenzene was 4.9 x 10^{-4} torr.

5.4.4 Fragment Anions

Reactions of Fe^-, Cs^- and Cu^- with each variant produced the same fragment anions, $C_6F_3H_2^-$, $C_6F_2H_3^-$, $C_6F_2H_2^-$, $C_6FH_2^-$ as well as C_6H^-. The production of $C_6F_3H_2^-$ and $C_6F_2H_3^-$ are due to the formation of neutral MH and MF molecules. $C_6FH_2^-$ is likely due to the neutral loss of F_2. The formation of C_6H^- is also observed.

5.5 Conclusions

In the review by Kiplinger et al., the authors state that while transition metals are employed as catalysts for the hydrogenation, hydroformylation and polymerization of olefins, there exists no such processes for fluorocarbons.[86] Additionally, as stated by Armentrout, 'the active agents and key intermediates in these systems are coordinately unsaturated transition metal-ligand complexes where one or more ligands have fallen off the stable complex. Active agents and intermediates in catalysis are typically 'unsaturated' systems that are transient, unstable and reactive'.[87] With a view to explore their potential reactivity, the reactions of the most unsaturated form of metal centres, atomic metal anions (Fe^-, Cu^- and Cs^-) and perfluorinated compounds were explored and the results presented in the previous sections.

The reactions of Rb^- and Cs^- with PFP/PFA as well as Cs^- with 1,2,4 and 1,3,5 trifluorobenzene demonstrated that these anions have a tendency to form ionic salts such as CsH and CsF. This reactivity is not surprising, as noted by Kiplinger et al., there exists a tendency of the alkali earth metals for form ionic salts with fluoride, making them unsuitable for use in catalytic cycles.[86] The formation of CsF^- and CsF_2^- have not been observed prior to

this study. The formation of CsF_2^- may be of the form $[F\text{-}Cs\text{-}F]^-$ or that of a 'side bonded' $[CsF_2]^-$. Without additional studies to determine the vibrational modes of these anions, the existence of either form cannot be directly confirmed.

The formation of FeF^-, FeF_2^-, FeF_3^-, CuF^- and CuF_2^- is remarkable. The high relative intensities with which FeF^-, FeF_2^-, FeF_3^-, CuF^- and CuF_2^- (Figures 22-29) are formed demonstrates the substantial reactivity with which these metal anions exhibit towards the activation of the C-F bond. The formation of FeF^-, FeF_2^-, FeF_3^-, CuF^- and CuF_2^- may be related to electron affinities. The formation of FeO^-, FeO_2^-,FeO_3^-,CuO^- and CuO_2^- from collisions of Fe^-/Cu^- with NO_2 was linked to the increasing relative electron affinities of the metal adduct anions as each oxygen atom was added (see section 3.6 'Adduct Formation of Cu^- and Fe^-' for further details). The highly substituted FeO_3^- and CuO_2^- adduct anions were observed at non-statistical relative intensities compared to FeO_2^-/FeO^- and CuO^-. The formation of FeF_3^- and CuF_2^- are also observed at non-statistical relative intensities compared to the relative intensity of FeF^-/FeF_2^- and CuF^- respectively. Therefore, increasing electron affinity of the metal adduct anion with each additional F atom could play a role in the observed formation of FeF_3^- and CuF_2^- at non-statistical relative intensities in the reactions of gaseous Fe^-/Cu^- with fluorinated compounds. Additional experimental data determining the electron affinities of these fluorinated metal adduct anions would greatly aid in the formation of a more coherent mechanistic explanation and represents a future research opportunity. While no mechanistic details of these reactions can be confirmed, the existence of these reactions by atomic metal anions and could be of potential use as a proof of concept with which to justify the exploration of more stable organometallic complexes capable of forming reactive 'odd electron' species.

Chapter 6 – Contributions to Knowledge

6.1 Electron transfer from Atomic Metal Anions to Small molecules

The reactions of AMAs with small neutral molecules (NO, SO_2 and NO_2) possessing electron affinities approximately below (NO)/similar to (SO_2)/well above (NO_2) the metal anions demonstrate that AMAs are able to transfer electrons to neutral molecules at high relative intensities relative to other anions possessing higher electron affinities. A manuscript outlining these results is in preparation for submission to Chemical Physics Letters.

6.2 Dissociative Electron Transfer Reactions of Atomic Metal Anions and Small molecules

The reactions of AMAs with pentafluorophenol and pentafluoroaniline, specifically Cs^- and Rb^- demonstrate that alkali atomic metal anions are able to transfer electrons to these molecules producing dissociation products nearly identical to those produced via electron attachment. Specifically for the case of Cs^-, all product anions observed via electron attachment were observed in the mass spectrum. Furthermore, there is clear thermodynamic effects associated with the relative intensities of these fragments in that the local hydrogen bonding between the H atom of the hydroxyl group and local F atoms of pentafluorophenol produced the loss of HF at much higher intensities than which other product anions were observed. A manuscript outlining these results is in preparation for submission to Chemical Physics Letters.

6.3 C-F bond activation via Atomic Metal Anions

The reactions of metal anions, specifically those of Cu^- and Fe^- demonstrate significant reactivity. This reactivity is manifested via the activation of the C-F bonds in saturated and unsaturated fluorinated species resulting in the formation of FeF^-, FeF_2^-, FeF_3^-, CuF^- and CuF_2^-. These results suggest that if similar reaction environments were recreated in more stable organocomplexes, anionic transition metals could possess significant C-F activation. The reactions of Cs^- resulted in the production of CsF^- and CsF_2^-, the first observation of such chemical species.

Chapter 7 – References

(1) Andersen, T. *Physics Reports* **2004**, *394*, 157.

(2) Buckman, S. J.; Clark, C. W. *Reviews of Modern Physics* **1994**, *66*, 539.

(3) H. S. W. Massey, F. R. S. *Negative Ions*; 2 ed.; The Syndics of the Cambridge University Press: London, 1950.

(4) Bardsley, J. N.; Mandl, F. *Reports on Progress in Physics* **1968**, *31*, 471.

(5) Bilodeau, R. C.; Haugen, H. K. *Physical Review Letters* **2000**, *85*, 534.

(6) Andersen, T.; Haugen, H. K.; Hotop, H. *Journal of Physical and Chemical Reference Data* **1999**, *28*, 1511.

(7) Hotop, H.; Lineberger, W. C. *Journal of Physical and Chemical Reference Data* **1975**, *4*, 539.

(8) Smirnov, B. M. *Negative Ions*; McGraw-Hill Inc. , 1982.

(9) Kebarle, P.; Chowdhury, S. *Chemical Reviews* **1987**, *87*, 513.

(10) Dawton, R. H. V. M. *Nuclear Science, IEEE Transactions on* **1972**, *19*, 231.

(11) Middleton, R. *Nuclear Science, IEEE Transactions on* **1976**, *23*, 1098.

(12) Squires, R. R. *Journal of the American Chemical Society* **1985**, *107*, 4385.

(13) Kaiser, H. J.; Heinicke, E.; Baumann, H.; Bethge, K. *Z. Physik* **1971**, *243*, 46.

(14) Patterson, T. A.; Hotop, H.; Kasdan, A.; Norcross, D. W.; Lineberger, W. C. *Physical Review Letters* **1974**, *32*, 189.

(15) Slater, J.; Read, F. H.; Novick, S. E.; Lineberger, W. C. *Physical Review A* **1978**, *17*, 201.

(16) Scheer, M.; Thøgersen, J.; Bilodeau, R. C.; Brodie, C. A.; Haugen, H. K.; Andersen, H. H.; Kristensen, P.; Andersen, T. *Physical Review Letters* **1998**, *80*, 684.

(17) Bartschat, K. *Journal of Physics B: Atomic, Molecular and Optical Physics* **1993**, *26*, 3595.

(18) Khuskivadze, A. A.; Fabrikant, I. I.; Thumm, U. *Physical Review A* **2003**, *68*, 063405.

(19) Scheibner, K. F.; Hazi, A. U.; Henry, R. J. W. *Physical Review A* **1987**, *35*, 4869.

(20) Balling, P.; Brink, C.; Andersen, T.; Haugen, H. K. *Journal of Physics B: Atomic, Molecular and Optical Physics* **1992**, *25*, L565.

(21) Ivanov, V. K. *Journal of Physics B: Atomic, Molecular and Optical Physics* **1999**, *32*, R67.

(22) Amusia, M. Y.; Gribakin, G. F.; Ivanov, V. K.; Chernysheva, L. V. *Journal of Physics B: Atomic, Molecular and Optical Physics* **1990**, *23*, 385.

(23) Sallans, L.; Lane, K.; Squires, R. R.; Freiser, B. S. *Journal of the American Chemical Society* **1983**, *105*, 6352.

(24) Sallans, L.; Lane, K. R.; Squires, R. R.; Freiser, B. S. *Journal of the American Chemical Society* **1985**, *107*, 4379.

(25) Curtis, S.; Renaud, J.; Holmes, J.; Mayer, P. *J Am Soc Mass Spectrom* **2010**, *21*, 1944.

(26) Knapp, M.; Echt, O.; Kreisle, D.; Märk, T. D.; Recknagel, E. *Chemical Physics Letters* **1986**, *126*.

(27) Kahwa, I. A.; Mulokozi, A. M. *Journal of Thermal Analysis* **1981**, *22*, 61.

(28) Attygalle, A. B.; Axe, F. U.; Weisbecker, C. S. *Rapid Communications in Mass Spectrometry* **2011**, *25*, 681.
(29) Burnier, R. C.; Cody, R. B.; Freiser, B. S. *Journal of the American Chemical Society* **1982**, *104*, 7436.
(30) Sallans, L.; Lane, K. R.; Freiser, B. S. *Journal of the American Chemical Society* **1989**, *111*, 865.
(31) Stevens Miller, A. E.; Miller, T. M.; Morris, R. A.; Viggiano, A. A.; Van Doren, J. M.; Paulson, J. F. *International Journal of Mass Spectrometry and Ion Processes* **1993**, *123*, 205.
(32) Viggiano, A. A.; Morris, R. A.; Dale, F.; Paulson, J. F.; Giles, K.; Smith, D.; Su, T. *The Journal of Chemical Physics* **1990**, *93*, 1149.
(33) Stevens Miller, A. E.; Miller, T. M.; Viggiano, A. A.; Morris, R. A.; Paulson, J. F. *International Journal of Mass Spectrometry* **2000**, *195–196*, 341.
(34) Curtis, S.; DiMuzio, J.; Mungham, A.; Roy, J.; Hassan, D.; Renaud, J.; Mayer, P. M. *The Journal of Physical Chemistry A* **2011**, *115*, 14006.
(35) Fenn, J. B. *Angewandte Chemie International Edition* **2003**, *42*, 3871.
(36) Dole, M.; Mack, L. L.; Hines, R. L.; Mobley, R. C.; Ferguson, L. D.; Alice, M. B. *The Journal of Chemical Physics* **1968**, *49*, 2240.
(37) Nobelprize.org; Nobel Media AB 2013: 2013.
(38) Rayleigh, L. *The London, Edinburgh, and Dublin Philosophical Magazine and Journal of Science* **1882**, *14*, 184.
(39) Zeleny, J. *Physical Review* **1917**, *10*, 1.
(40) Taylor, G. *Proceedings of the Royal Society of London. Series A. Mathematical and Physical Sciences* **1964**, *280*, 383.
(41) Iribarne, J. V.; Thomson, B. A. *The Journal of Chemical Physics* **1976**, *64*, 2287.
(42) Nguyen, S.; Fenn, J. B. *Proceedings of the National Academy of Sciences* **2007**, *104*, 1111.
(43) de Hoffmann, E. In *Kirk-Othmer Encyclopedia of Chemical Technology*; John Wiley & Sons, Inc.: 2000.
(44) Douglas, D. J. *Mass Spectrometry Reviews* **2009**, *28*, 937.
(45) Cech, N. B.; Enke, C. G. *Mass Spectrometry Reviews* **2001**, *20*, 362.
(46) Ochterski, J. W.; Petersson, G. A.; Montgomery, J. J. A. *The Journal of Chemical Physics* **1996**, *104*, 2598.
(47) Montgomery, J. J. A.; Frisch, M. J.; Ochterski, J. W.; Petersson, G. A. *The Journal of Chemical Physics* **2000**, *112*, 6532.
(48) Frisch, M. J.; Trucks, G. W.; Schlegel, H. B.; Scuseria, G. E.; Robb, M. A.; Cheeseman, J. R.; Scalmani, G.; Barone, V.; Mennucci, B.; Petersson, G. A.; Nakatsuji, H.; Caricato, M.; Li, X.; Hratchian, H. P.; Izmaylov, A. F.; Bloino, J.; Zheng, G.; Sonnenberg, J. L.; Hada, M.; Ehara, M.; Toyota, K.; Fukuda, R.; Hasegawa, J.; Ishida, M.; Nakajima, T.; Honda, Y.; Kitao, O.; Nakai, H.; Vreven, T.; Montgomery, J. A.; Peralta, J. E.; Ogliaro, F.; Bearpark, M.; Heyd, J. J.; Brothers, E.; Kudin, K. N.; Staroverov, V. N.; Kobayashi, R.; Normand, J.; Raghavachari, K.; Rendell, A.; Burant, J. C.; Iyengar, S. S.; Tomasi, J.; Cossi, M.; Rega, N.; Millam, J. M.; Klene, M.; Knox, J. E.; Cross, J. B.; Bakken, V.; Adamo, C.; Jaramillo, J.; Gomperts, R.; Stratmann, R. E.; Yazyev, O.; Austin, A. J.; Cammi, R.; Pomelli, C.; Ochterski, J. W.; Martin, R. L.; Morokuma, K.; Zakrzewski, V. G.; Voth, G. A.;

Salvador, P.; Dannenberg, J. J.; Dapprich, S.; Daniels, A. D.; Farkas; Foresman, J. B.; Ortiz, J. V.; Cioslowski, J.; Fox, D. J. Wallingford CT, 2009.

(49) Christophorou, L. G. *Beiträge aus der Plasmaphysik* **1987**, *27*, 237.

(50) Massey, H. S. W. In *Advances in Atomic and Molecular Physics*; David, R. B., Benjamin, B., Eds.; Academic Press: 1979; Vol. Volume 15, p 1.

(51) Tate, J. T.; Smith, P. T. *Physical Review* **1932**, *39*, 270.

(52) Sambe, H.; Ramaker, D. E. *The Journal of Chemical Physics* **1991**, *94*, 2548.

(53) Chantry, P. J. *Physical Review* **1968**, *172*, 125.

(54) Rangwala, S. A.; Krishnakumar, E.; Kumar, S. V. K. *Physical Review A* **2003**, *68*, 052710.

(55) Abouaf, R.; Paineau, R.; Fiquet-Fayard, F. *Journal of Physics B: Atomic and Molecular Physics* **1976**, *9*, 303.

(56) Spyrou, S. M.; Sauers, I.; Christophorou, L. G. *The Journal of Chemical Physics* **1986**, *84*, 239.

(57) Cadez, I. M.; Pejcev, V. M.; Kurepa, M. V. *Journal of Physics D: Applied Physics* **1983**, *16*, 305.

(58) Orient, O. J.; Srivastava, S. K. *The Journal of Chemical Physics* **1983**, *78*, 2949.

(59) Franck, J.; Dymond, E. G. *Transactions of the Faraday Society* **1926**, *21*, 536.

(60) Condon, E. U. *Physical Review* **1928**, *32*, 858.

(61) Sharma, D. K. S.; Kebarle, P. *Journal of the American Chemical Society* **1982**, *104*, 19.

(62) Marcus, R. A. *The Journal of Chemical Physics* **1956**, *24*, 966.

(63) Gioumousis, G.; Stevenson, D. P. *The Journal of Chemical Physics* **1958**, *29*, 294.

(64) Bass, L.; Su, T.; Chesnavich, W. J.; Bowers, M. T. *Chemical Physics Letters* **1975**, *34*, 119.

(65) Farneth, W. E.; Brauman, J. I. *Journal of the American Chemical Society* **1976**, *98*, 7891.

(66) Olmstead, W. N.; Brauman, J. I. *Journal of the American Chemical Society* **1977**, *99*, 4219.

(67) Streit, G. E. *The Journal of Chemical Physics* **1982**, *77*, 826.

(68) Babcock, L. M.; Streit, G. E. *The Journal of Chemical Physics* **1981**, *75*, 3864.

(69) Hughes, B. M.; Lifshitz, C.; Tiernan, T. O. *The Journal of Chemical Physics* **1973**, *59*, 3162.

(70) Berkowitz, J.; Chupka, W. A.; Gutman, D. *The Journal of Chemical Physics* **1971**, *55*, 2733.

(71) Wu, H.; Desai, S. R.; Wang, L.-S. *Journal of the American Chemical Society* **1996**, *118*, 5296.

(72) Blyholder, G.; Head, J.; Ruette, F. *Inorganic Chemistry* **1982**, *21*, 1539.

(73) Fan, J.; Wang, L.-S. *The Journal of Chemical Physics* **1995**, *102*, 8714.

(74) Andrews, L.; Chertihin, G. V.; Ricca, A.; Bauschlicher, C. W. *Journal of the American Chemical Society* **1996**, *118*, 467.

(75) Wu, H.; Desai, S. R.; Wang, L.-S. *The Journal of Chemical Physics* **1995**, *103*, 4363.
(76) Polak, M. L.; Gilles, M. K.; Ho, J.; Lineberger, W. C. *The Journal of Physical Chemistry* **1991**, *95*, 3460.
(77) Douglas, D. J. *J Am Soc Mass Spectrom* **1998**, *9*, 101.
(78) Ómarsson, B.; Bjarnason, E. H.; Ingólfsson, O.; Haughey, S.; Field, T. A. *Chemical Physics Letters* **2012**, *539–540*, 7.
(79) Omarsson, B.; Bjarnason, E. H.; Haughey, S. A.; Field, T. A.; Abramov, A.; Klupfel, P.; Jonsson, H.; Ingolfsson, O. *Physical Chemistry Chemical Physics* **2013**, *15*, 4754.
(80) Gant, K. S.; Christophorou, L. G. **1976**.
(81) Schneider, H.; Vogelhuber, K. M.; Weber, J. M. *The Journal of Chemical Physics* **2007**, *127*, 114311.
(82) Compton, R. N.; Reinhardt, P. W. *Chemical Physics Letters* **1982**, *91*, 268.
(83) Büker, H. H.; Nibbering, N. M. M.; Espinosa, D.; Mongin, F.; Schlosser, M. *Tetrahedron Letters* **1997**, *38*, 8519.
(84) Herd, C. R.; Adams, N. G.; Smith, D. **1989**.
(85) Sauers, I.; Christophorou, L. G.; Carter, J. G. **1979**.
(86) Kiplinger, J. L.; Richmond, T. G.; Osterberg, C. E. Y. **1994**.
(87) Armentrout, P. B. *Accounts of Chemical Research* **1995**, *28*, 430.